(12) INTERNATIONAL APPLICATION PUBLISHED UNDER THE PATENT COOPERATION TREATY (PCT)

(19) World Intellectual Property Organization
International Bureau

(43) International Publication Date
13 April 2017 (13.04.2017)

WIPO | PCT

(10) International Publication Number
WO 2017/062882 A1

(51) International Patent Classification:
A61B 5/055 (2006.01) *G01R 33/385* (2006.01)
G01R 33/48 (2006.01) *G01R 33/54* (2006.01)

(21) International Application Number:
PCT/US2016/056147

(22) International Filing Date:
7 October 2016 (07.10.2016)

(25) Filing Language: English

(26) Publication Language: English

(30) Priority Data:

62/238,121	7 October 2015 (07.10.2015)	US
62/302,577	2 March 2016 (02.03.2016)	US
15/167,828	27 May 2016 (27.05.2016)	US
62/382,695	1 September 2016 (01.09.2016)	US

(71) Applicant: **BIOPROTONICS LLC** [US/US]; P O Box 1029, Santa Ynez, CA 93460 (US).

(72) Inventors: **CHASE, David, R.**; C/O BIOPROTONICS LLC, P O Box 1029, Santa Ynez, CA 93460 (US). **JAMES, Timothy, W.**; C/O BIOPROTONICS LLC, P O Box 1029, Santa Ynez, CA 93460 (US). **JAMES, Kristin, E.**; C/O BIOPROTONICS LLC, P O Box 1029, Santa Ynez, CA 93460 (US).

(74) Agent: **FISCHER, Felix, L.**; 1607 Mission Drive, Suite 204, Solvang, CA 93463 (US).

(81) Designated States *(unless otherwise indicated, for every kind of national protection available)*: AE, AG, AL, AM, AO, AT, AU, AZ, BA, BB, BG, BH, BN, BR, BW, BY, BZ, CA, CH, CL, CN, CO, CR, CU, CZ, DE, DJ, DK, DM, DO, DZ, EC, EE, EG, ES, FI, GB, GD, GE, GH, GM, GT, HN, HR, HU, ID, IL, IN, IR, IS, JP, KE, KG, KN, KP, KR, KW, KZ, LA, LC, LK, LR, LS, LU, LY, MA, MD, ME, MG, MK, MN, MW, MX, MY, MZ, NA, NG, NI, NO, NZ, OM, PA, PE, PG, PH, PL, PT, QA, RO, RS, RU, RW, SA, SC, SD, SE, SG, SK, SL, SM, ST, SV, SY, TH, TJ, TM, TN, TR, TT, TZ, UA, UG, US, UZ, VC, VN, ZA, ZM, ZW.

(84) Designated States *(unless otherwise indicated, for every kind of regional protection available)*: ARIPO (BW, GH, GM, KE, LR, LS, MW, MZ, NA, RW, SD, SL, ST, SZ, TZ, UG, ZM, ZW), Eurasian (AM, AZ, BY, KG, KZ, RU, TJ, TM), European (AL, AT, BE, BG, CH, CY, CZ, DE, DK, EE, ES, FI, FR, GB, GR, HR, HU, IE, IS, IT, LT, LU, LV, MC, MK, MT, NL, NO, PL, PT, RO, RS, SE, SI, SK, SM, TR), OAPI (BF, BJ, CF, CG, CI, CM, GA, GN, GQ, GW, KM, ML, MR, NE, SN, TD, TG).

Published:

— *with international search report (Art. 21(3))*

(54) **Title**: SELECTIVE SAMPLING FOR ASSESSING STRUCTURAL SPATIAL FREQUENCIES WITH SPECIFIC CONTRAST MECHANISMS

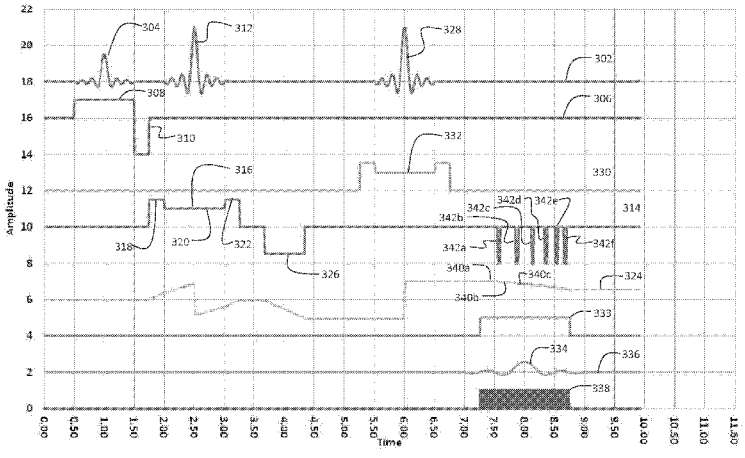

FIG. 3

(57) **Abstract**: The disclosed embodiments provide a method for acquiring MR data at resolutions down to tens of microns for application in in-vivo diagnosis and monitoring of pathology for which changes in fine tissue textures can be used as markers of disease onset and progression. Bone diseases, tumors, neurologic diseases, and diseases involving fibrotic growth and/or destruction are all target pathologies. Further the technique can be used in any biologic or physical system for which very high-resolution characterization of fine scale morphology is needed. The method provides rapid acquisition of selected values in k-space, with multiple successive acquisitions of individual k- values taken on a time scale on the order of microseconds, within a defined tissue volume, and subsequent combination of the multiple measurements in such a way as to maximize SNR. The reduced acquisition volume, and acquisition of only select values in k-space along selected directions, enables much higher in- vivo resolution than is obtainable with current MRI techniques.

WO 2017/062882 A1

SELECTIVE SAMPLING FOR ASSESSING STRUCTURAL SPATIAL FREQUENCIES WITH SPECIFIC CONTRAST MECHANISMS

REFERENCE TO RELATED APPLICATIONS

[PARA 1] The present application relies on the priority of provisional application serial no. 62/238,121 filed on 10/07/2015 entitled SELECTIVE SAMPLING MAGNETIC RESONANCE-BASED METHOD FOR ASSESSING STRUCTURAL SPATIAL FREQUENCIES A and provisional application serial no. 62/382,695 filed on 09/01/2016 entitled SELECTIVE SAMPLING FOR ASSESSING STRUCTURAL SPATIAL FREQUENCIES WITH SPECIFIC CONTRAST MECHANISMS. This application additionally relies on the priority of application serial no. 15/167,828 filed on 05/27/2016 which is a continuation in part of application serial no. 14/840,327 filed on 08/31/2015 now US Patent no. 9366738. Application 14/840,327 relies on the priority of US provisional applications serial no. 62/044,321 filed on 09/01/2014 entitled SELECTIVE SAMPLING MAGNETIC RESONANCE-BASED METHOD FOR ASSESSING STRUCTURAL SPATIAL FREQUENCIES, serial no. 62/064,206 filed on 10/15/2014 having the same title and serial no. 62/107,465 filed on 01/25/2015 entitled MICRO-TEXTURE CHARACTERIZATION BY MRI, the disclosures of which are incorporate herein by reference. Application 15/167,828 additionally relies on the priority of provisional application serial no. 62/302,577 filed on 03/02/2016 entitled METHOD FOR ASSESSING STRUCTURAL SPATIAL FREQUENCIES USING HYBRID SAMPLING WITH LOW OR INCREASED GRADIENT FOR ENHANCEMENT OF VERY LOW NOISE SELECTIVE SAMPLING WITH NO GRADIENT. The referenced applications all have a common assignee with the present application and the disclosures thereof are incorporated herein by reference.

BACKGROUND

Field Of The Invention

[PARA 2] The herein claimed method relates to the field of diagnostic assessment of fine textures in biological systems for pathology assessment and disease diagnosis, and in material and structural evaluation in industry and in engineering research. More

specifically, the invention employs a method for repeat measurement of k-values associated with the spatial organization of biologic tissue texture, with the MRI machine gradients turned off and for k-values in an narrowly associated neighborhood with a low gradient. This allows assessment of tissue texture on a time-scale on the order of a msec, whereby the problem of patient motion becomes negligible. The method enables in vivo assessment, towards diagnosis and monitoring, of disease and therapy-induced textural changes in tissue. Representative targets of the technique are: 1) for assessment of changes to trabecular architecture caused by bone disease, allowing assessment of bone health and fracture risk, 2) evaluation of fibrotic development in soft tissue diseases such as, for example, liver, lung, and heart disease, and 3) changes to fine structures in neurologic diseases, such as the various forms of dementia, or in cases of brain injury and downstream neuro-pathology as in, for example, Traumatic Brain Injury (TBI) and Chronic Traumatic Encephalopathy (CTE), or for characterization and monitoring of abnormal neurologic conditions such as autism and schizophrenia. Other pathology applications include assessment of vascular changes such as in in the vessel network surrounding tumors or associated with development of CVD (Cerebrovascular Disease), and of changes in mammary ducting in response to tumor growth. The invention also has applications in assessment of fine structures for a range of industrial purposes such as measurement of material properties in manufacturing or in geology to characterize various types of rock, as well as other uses for which measurement of fine structures/textures is needed.

Description Of The Related Art

[PARA 3] Though fine textural changes in tissue have long been recognized as the earliest markers in a wide range of diseases, robust clinical assessment of fine texture remains elusive, the main difficulty arising from blurring caused by subject motion over the time required for data acquisition.

[PARA 4] Early and accurate diagnosis is key to successful disease management. Though clinical imaging provides much information on pathology, many of the tissue changes that occur as a result of disease onset and progression, or as a result of therapy, are on an extremely fine scale, often down to tens of microns. Changes in fine tissue texture have been recognized for many years by diagnosticians, including radiologists and pathologists as the earliest harbinger of a large range of diseases, but in vivo assessment and

measurement of fine texture has remained outside the capabilities of current imaging technologies. For instance, differential diagnosis of obstructive lung disease relies on a textural presentation in the lung parenchyma, but the robustness of the Computed Tomography (CT) measure of early stage disease is limited. Trabecular bone microarchitecture, the determinant of fracture risk in aging bone, has also remained elusive due to image blurring from patient motion during Magnetic Resonance (MR) imaging scans. Post processing analysis of MR-images is sometimes used to try to differentiate surface textures in structures such as tumors and white matter. (DRABYCZ, S., et al.; "Image texture characterization using the discrete orthogonal S-transform"; Journal of Digital Imaging, Vol. 22, No 6, 2009. KHIDER, M., et al.; "Classification of trabecular bone texture from MRI and CT scan images by multi-resolution analysis"; 29th Annual International Conference of the IEEE Engineering in Medicine and Biology Society, EMBS 2007.) But post processing analysis is limited in effect as it doesn't deal with the underlying problem that prevents high resolution acquisition of textural information, i.e. subject motion. (MACLAREN, J. et al.; "Measurement and correction of microscopic head motion during magnetic resonance imaging of the brain", PLOS/ONE, Nov. 7, 2012. MACLARAN, J. et al.; "Prospective motion correction in brain imaging: a review; Magnetic Resonance in Medicine, Vol. 69, 2013.)

[PARA 5] The main sources of motion affecting MR imaging are cardiac pulsatile motion, respiratory-induced motion and twitching. The first two are quasi-cyclic, the usual approach to which is gating at the slowest phase of motion. However, even with gating, there is sufficient variation between acquisitions to cause loss of spatial phase coherence at the high k-values of interest for texture measurements. This problem is exacerbated by the fact that motion may not be perfectly cyclic, and often originates from combined sources. Twitching is rapid, inducing random displacements, and hence it is not possible to maintain coherence at the high k-values of interest when measuring texture.

[PARA 6] While Positron Emission Tomography (PET) provides valuable diagnostic information, it is not capable of resolution below about 5mm and relies on the use of radioactive tracers for imaging as well as x-ray beams for positioning, raising dose concerns, especially if repeat scanning is needed. (BERRINGTON DE GONZALEZ, A. et al.; "Projected cancer risks from Computed Tomographic scans performed in the United

States in 2007"; JAMA Internal Medicine, Vol. 169, No. 22, Dec 2009.) Further, PET imaging is extremely costly, requiring a nearby cyclotron. CT resolution down to 0.7 mm is possible in theory, though this is obtained at high radiation dose and is subject to reduction by patient motion over the few minute scan time. The non-negligible risk from the associated radiation dose makes CT problematic for longitudinal imaging and limits available resolution. Along with serious dose concerns, digital x-ray resolution is limited because the 2-dimensional image obtained is a composite of the absorption through the entire thickness of tissue presented to the beam. Current clinical diagnostics for the diseases that are the target of the method claimed herein are fraught with difficulties in obtaining sufficient in vivo resolution, or accuracy. In some cases, no definitive diagnostic exists currently. In other pathologies, particularly in breast and liver, diagnosis is dependent on biopsy, with its non-negligible risk of morbidity and even mortality, and which is prone to high read and sampling errors. (WELLER, C; "Cancer detection with MRI as effective as PET-CT scan but with zero radiation risks"; Medical Daily, Feb. 18, 2014.)

[PARA 7] Bone health is compromised by ageing, by bone cancer, as a side effect of cancer treatments, diabetes, rheumatoid arthritis, and as a result of inadequate nutrition, among other causes. Bone disease affects over ten million people annually in the US alone, adversely affecting their quality of life and reducing life expectancy. For assessment of bone health, the current diagnostic standard is Bone Mineral Density (BMD), as measured by the Dual Energy X-ray Absorptiometry (DEXA) projection technique. This modality yields an areal bone density integrating the attenuation from both cortical and trabecular bone, similar to the imaging mechanism of standard x-ray, but provides only limited information on trabecular architecture within the bone, which is the marker linked most closely to bone strength. (KANIS, J. AND GLUER, C.; "An update on the diagnosis and assessment of osteoporosis with densitometry"; Osteoporosis International, Vol. 11, issue 3, 2000. LEGRAND, E. et al.; "Trabecular bone microarchitecture, bone mineral density, and vertebral fractures in male osteoporosis"; JBMR, Vol. 15, issue 1, 2000.) BMD correlates only loosely with fracture risk. A post-processing technique, TBS (Trabecular Bone Score) attempts to correlate the pixel gray-level variations in the DEXA image, to yield information on bone microarchitecture. A comparison study determined that BMD at hip remains a better predictor of fracture. But, though TBS does not yield a detailed assessment

of trabecular architecture. (BOUSSON, V., et al.; "Trabecular Bone Score (TBS): available knowledge, clinical relevance, and future prospects"; Osteoporosis International, Vol. 23, 2012. DEL RIO, et al.; "Is bone microarchitecture status of the spine assessed by TBS related to femoral neck fracture? A Spanish case-control study": Osteoporosis International, Vol. 24, 2013.) TBS is a relatively new technique and is still being evaluated.

[PARA 8] Measurement of bone microarchitecture, specifically trabecular spacing and trabecular element thickness, requires resolution on the order of tenths of a millimeter. MRI, ultrasound imaging, CT, and microCT have all been applied to this problem. In MRI, though high contrast between bone and marrow is readily obtained, resolution is limited by patient motion over the long time needed to acquire an image with sufficient resolution to characterize the trabecular network. The finer the texture size of this network, the greater the blurring from motion. An attempt to mitigate the effects of patient motion by looking only at the skeletal extremities, removed from the source of cardiac and respiratory motion sources, has been tried using both MRI and microCT. However, the correlation between bone microarchitecture in the extremities and that in central sites in not known. Further, a large data matrix, hence long acquisition time, is still required to obtain sufficient image information to determine trabecular spacing and element thickness. This long acquisition time results in varying levels of motion-induced blurring, depending on patient compliance—twitching is still a serious problem even when measuring extremities. A proposed MR-based technique, fineSA (JAMES, T., CHASE, D.; "Magnetic field gradient structure characteristic assessment using one dimensional (1D) spatial-frequency distribution analysis" ; US patent No. 7,932,720 7; April 26, 2011.), attempts to circumvent the problem of patient motion by acquiring a much smaller data matrix of successive, finely-sampled, one-dimensional, frequency-encoded acquisitions which are subsequently combined to reduce noise. Imaging in this case is reduced to one dimension, reducing the size of the data matrix acquired and, hence, the acquisition time. However, as the gradient encoded echoes, are very low Signal to Noise (SNR), noise averaging is required. Though some resolution advantage is gained by this method relative to 2 and 3-d imaging, the need to acquire many repeat spatially-encoded echoes over several response times (TRs) for signal averaging results in an acquisition time on the order of minutes—too long to provide motion immunity. Thus, resolution improvement obtainable by the technique is limited.

[PARA 9] What is needed is an accurate, robust, non-invasive, in vivo measure of trabecular spacing and trabecular element thickness capable of assessing bones in the central skeleton, as these are the key markers for assessing bone health and predicting fracture risk. Until now, no clinical technique has been able to provide this capability.

[PARA 10] Fibrotic diseases occur in response to a wide range of biological insults and injury in internal organs, the development of collagen fibers being the body's healing response. The more advanced a fibrotic disease, the higher the density of fibers in the diseased organ. Fibrotic pathology occurs in a large number of diseases, from lung and liver fibrosis, to cardiac and cystic fibrosis, pancreatic fibrosis, muscular dystrophy, bladder and heart diseases, and myelofibrosis, in which fibrotic structures replace bone marrow. Fibrotic development is attendant in several cancers, such as breast cancer. A different pathology development is seen in prostate cancer, where the disease destroys healthy organized fibrous tissue. In all cases, textural spacings highlighted in the tissue change in response to disease progression, as collagen fibers form along underlying tissue structures. In liver disease, the textural wavelength changes as the healthy tissue texture in the liver is replaced by a longer wavelength texture originating from the collagen "decoration" of the lobular structure in the organ. In other organs/diseases, textural change reflects the upset in healthy tissue with development of texture indicative of fibrotic intervention.

[PARA 11] To span the range of disease progression in most fibrotic pathologies, evaluation of textural changes from fibrotic development requires resolution on the scale of tenths of a mm. One of the most prevalent of such pathologies, liver disease, is representative of the difficulty of assessing fibrotic structure. Currently, the gold standard for pathology assessment is tissue biopsy—a highly invasive and often painful procedure with a non-negligible morbidity—and mortality—risk (patients need to stay at the hospital for post-biopsy observation for hours to overnight), and one that is prone to sampling errors and large reading variation. (REGEV, A.; "Sampling error and intraobserver variation in liver biopsy in patients with chronic HCV infection" ; American Journal of Gastroenterology; 97, 2002. BEDOSSA, P. et al.; "Sampling variability of liver fibrosis in chronic hepatitis C"; Hepatology, Vol. 38, issue 6, 2004. VAN THIEL, D. et al.; "Liver biopsy: Its safety and complications as seen at a liver transplant center"; Transplantation, May 1993.) Ultrasound, another modality often used to assess tissue damage in liver

disease, is only able to provide adequate assessment in the later stages of the disease—it is used to diagnose cirrhosis. Magnetic Resonance-based Elastography (MRE), which has been under development for some time for use in assessment of liver disease, is not capable of early-stage assessment—the read errors are too large prior to significant fibrotic invasion (advanced disease). Further, this technique requires expensive additional hardware, the presence of a skilled technician, and takes as much as 20 minutes total set up and scanning time, making it a very costly procedure. The ability to image fibrotic texture directly by MR imaging is compromised both by patient motion over the time necessary to acquire data and by lack of contrast between the fibers and the surrounding tissue. Even acquisition during a single breath hold is severely compromised by cardiac pulsatile motion and noncompliance to breath hold, which results in significant motion at many organs, such as liver and lungs. And SNR is low enough that motion correction by combining reregistered MR-intensity profiles obtained from successive echoes is extremely problematic. Similarly, assessment of the amount of cardiac fibrosis in early stage disease using MRI is seriously hampered by cardiac pulsation over the time of the measurement. As motion is, unlike Gaussian noise, a non-linear effect, it can't be averaged out—there must be sufficient signal level to allow reregistration before averaging for electronic noise-reduction. A more sensitive (higher SNR), non-invasive technique, capable of assessing textural changes throughout the range of fibrotic development, from onset to advanced pathology, is needed to enable diagnosis and monitoring of therapy response.

[PARA 12] Onset and progression of a large number of neurologic diseases are associated with changes in repetitive fine neuronal and vascular structures/textures. However, ability to assess such changes in the brain is only available post mortem. Currently, definitive diagnosis of Alzheimer's Disease (AD) is by post mortem histology of brain tissue. AD and other forms of dementia such as Dementia with Lewy Bodies, motor diseases such as Amyotrophic Lateral Sclerosis (ALS), Parkinson's disease, conditions precipitated by Traumatic Brain Injury (TBI) such as Chronic Traumatic Encephalopathy (CTE), as well as those caused by other pathologies or trauma, or conditions that involve damage to brain structures such as Multiple Sclerosis (MS), Cerebrovascular Disease (CVD), and other neurologic diseases, are often only diagnosable in advanced stages by behavioral and memory changes, precluding the ability for early stage intervention. Further,

conditions such as epilepsy and autism have been associated with abnormal variations in fine neuronal structures, which, if clinically diagnosable, would allow targeted selection for testing therapy response.

[PARA 13] Various in vivo diagnostic techniques are available for AD and other dementias, but none of them are definitive. These techniques range from written diagnostic tests, which are prone to large assessment errors, to PET imaging to assess amyloid plaque density or glucose metabolism (FDG PET). As discussed previously, PET imaging is extremely expensive, cannot provide high resolution, and relies on use of radioisotopes and positioning x-ray beams, complicating approval for longitudinal use due to dose concerns. Further, neither amyloid imaging nor FDG PET has been shown to provide a definitive indication of AD. (MOGHBEL, M. et al. "Amyloid Beta imaging with PET in Alzheimer's disease: is it feasible with current radiotracers and technologies?"; Eur. J. Nucl. Med. Mol. Imaging.)

[PARA 14] Use of CSF biomarkers for dementia diagnosis is painful and highly invasive and cannot differentiate signal levels by anatomic position in the brain, as is possible with imaging biomarkers. As various forms of dementia are found to have different spatial/temporal progression through the brain, this is a serious drawback to use of liquid biopsy. Another disease associated with various forms of dementia is CVD (Cerebrovascular Disease), which induces cognitive impairment as a result of reduced blood flow through blocked vessels leading to brain tissue. Something capable of high-resolution assessment of pathology-induced changes in micro-vessels is needed here.

[PARA 15] Tissue shrinkage due to atrophy in many forms of dementia including AD is measurable with careful registration of longitudinally-acquired data in MRI, but the disease is advanced by the time this shrinkage is measureable. Early stages of disease are indicated in post mortem histology by degradation in the columnar ordering of cortical neurons, the normal spacing for these columns being on the order of 100 microns in most cortical regions. (CHANCE, S. et al.; "Microanatomical correlates of cognitive ability and decline: normal ageing, MCI, and Alzheimer's disease"; Cerebral Cortex, August 2011. E. DI ROSA et al.; "Axon bundle spacing in the anterior cingulate cortex of the human brain"; Journal of Clinical Neuroscience, 15, 2008.) This textural size, and the fact that the cortex is extremely thin, makes speed of acquisition paramount, as even tiny patient motion will make data

collection impossible. Assessment of textural changes on the order of tens of microns microns is extremely problematic in vivo, but would, if possible, enable targeting a range of fine textural changes in neuronal disease diagnosis and monitoring, and would play an important role in therapy development.

[PARA 16] Another possible neurologic application for the claimed method is to, in vivo, determine the boundaries of the various control regions of the cerebral cortex or the different Brodmann's areas of which these are comprised. Such ability would greatly aid data interpretation in brain function studies, such as those performed using, for example, FMRI (Functional Magnetic Resonance Imaging).

[PARA 17] The three classes of diseases listed above, bone disease, fibrotic diseases, and neurologic diseases are not an all-inclusive list. Other disease states in which pathology-induced changes of fine structures occur, for instance angiogenic growth of vasculature surrounding a tumor, or fibrotic development and changes in vasculature and mammary gland ducting in response to breast tumor development, also are pathologies wherein the ability to resolve fine tissue textures would enable early detection of disease, and monitoring of response to therapy.

[PARA 18] The ability to measure changes in fine textures would be of great value for disease diagnosis. Non-invasive techniques that do not rely on use of ionizing radiation or radioactive tracers allow the most leeway for early diagnosis and repeat measurement to monitor disease progression and response to therapy. Magnetic Resonance Imaging (MRI), which provides tunable tissue contrast, is just such a non-invasive technique, with no radiation dose concerns. However, in order to circumvent the problem of signal degradation due to patient motion, data must be taken on a time scale not previously possible.

SUMMARY OF THE INVENTION

[PARA 19] A method for selective sampling to assess tissue texture using magnetic resonance (MR) is accomplished by applying a contrast mechanism enhancing the contrast between the component tissue types in a multiphase biologic sample being measured. A volume of interest (VOI) is then selectively excited employing a plurality of time varying radio frequency signals and applied gradients. An encoding gradient pulse is applied to induce phase wrap to create a spatial encode for a specific k-value and orientation, the

specific k-value determined based on texture within the VOI. A time varying series of acquisition gradients is initiated to produce a time varying trajectory through 3D k-space of k-value encodes, a resulting k-value set being a subset of that required to produce an image of the VOI. Multiple sequential samples of the NMR RF signal encoded with the k-value set are simultaneously recorded. The recorded NMR signal samples are then post-processed to produce a data set of signal vs k-values for k-values in the k-value set determined by the trajectory, to characterize the tissue in the VOI.

BRIEF DESCRIPTION OF THE DRAWINGS

[PARA 20] The features and advantages of embodiments disclosed herein will be better understood by reference to the following detailed description when considered in connection with the accompanying drawings wherein:

[PARA 21] FIG. 1 is a simulation showing the number of data samples required for averaging to achieve an output SNR $\geq$ 20dB as a function of input SNR;

[PARA 22] FIG. 2 is a simulation showing the number of data samples needed for averaging to achieve a SNR $\geq$ 20db as a function of location in k-space;

[PARA 23] FIG. 3 is an example timing diagram of a pulse sequence for the claimed method showing the timing of a single TR;

[PARA 24] FIG. 4 is a close-up of the example timing diagram of FIG. 3;

[PARA 25] FIG. 5 is an example of a timing diagram for the claimed method, designed to acquire multiple measures of a select set of k-values, with a different number of samples acquired at each k-value to counteract the decrease in energy density at increasing k-value;

[PARA 26] FIG. 6 is a simulation showing that the ability provided by the claimed method to acquire many repeats of a targeted k-value within a single TR enables robust signal averaging to boost SNR;

[PARA 27] FIG. 7 is a simulation showing the results of attempting to acquire 90 samples for averaging using the conventional frequency-encoded echo approach, wherein acquisition of only a small number of repeats of a particular k-value are possible in each TR due to the long record time for each echo;

[PARA 28] FIG. 8 is an example timing diagram for the claimed method designed to provide data acquisition over multiple refocused echoes within a single TR; and,

[PARA 29] FIGs. 9 and 10 are a depiction of two possible shapes for the acquisition volume of interest (VOI);

[PARA 30] FIG. 11 is an example timing diagram of a pulse sequence for the claimed hybrid method showing the timing of a single TR;

[PARA 31] FIG. 12 is a detailed view of the hybrid elements of the method at an expanded scale;

[PARA 32] FIG. 13 is a further detailed view of the very-low SNR acquisition mode portion of FIG. 12;

[PARA 33] FIG. 14 is a further detailed view of the low SNR acquisition portion of FIG. 12;

[PARA 34] FIG. 15 is a further detailed view of the high SNR acquisition portion of FIG. 12;

[PARA 35] FIG. 16 is an example timing diagram of a pulse sequence for the claimed hybrid method showing data acquisition in a single echo;

[PARA 36] FIG. 17 is a further detailed view of the very-low SNR, low SNR and high SNR acquisition portions of FIG. 16;

[PARA 37] FIG. 18 is a an example timing diagram of a pulse sequence for a low SNR acquisition;.

[PARA 38] FIG. 19 is a further detailed view of the low SNR acquisition mode of FIG. 18;

[PARA 39] FIG. 20 is an example timing diagram of a pulse sequence for high SNR acquisition;

[PARA 40] FIG. 21 is a further detailed view of the high SNR acquisition mode of FIG. 20;

[PARA 41] FIGs. 22A and 22B are pictorial representations of healthy an osteoporitic bone structure;

[PARA 42] FIG. 23 is a pictorial representation of fibrotic tissue in a liver;

[PARA 43] FIG. 24 is an example timing diagram of a pulse sequence implementing a first diffusion contrast;

[PARA 44] FIG. 25 timing diagram of a pulse sequence implementing a seconed diffusion contrast;

[PARA 45] FIG. 26 is a pictorial representation of VOIs dispers3ed in fibrotic tissue;

[PARA 46] FIG. 27 is a pictorial representation of cortical minicolumns in the brain;

[PARA 47] FIG. 28 is a pictorial representation of VOI placement in the brain;

[PARA 48] FIGs. 29A -29C are representations of three histology images showing progressive pathology with AD advancement; and,

[PARA 49] FIG. 30 is exemplary representation of placement of a VOI in the brain cortex and application of gradients for k-value .

DETAILED DESCRIPTION OF THE INVENTION

[PARA 50] The following definition of terms as used herein is provided:

180^0 inversion pulse RF pulse that inverts the spins in a tissue region to allow refocusing of the MR signal.

180^0 pulse An RF pulse that tips the net magnetic field vector antiparallel to B_0

90^0 pulse An RF pulse that tips the net magnetic field vector into the transverse plane relative to B_0

3T 3 Tesla

A/D Analog to digital converter

AD Alzheimer's Disease

ADC Average diffusion coefficient measured in Diffusion Weighted Imaging

Adiabatic pulse excitation Adiabatic pulses are a class of amplitude- and frequency-modulated RF-pulses that are relatively insensitive to 6 inhomogeneity and frequency offset effects.

AWGN Additive White Gaussian Noise Additive white Gaussian noise (AWGN) is a basic noise model used in Information theory to mimic the effect of many random processes that occur in nature.

Biopsy A biopsy is a sample of tissue extracted from the body in order to examine it more closely.

C/N Contrast to Noise, a measure of image quality based on signal differences between structural elements rather than on overall signal level

CAWGN Complex-valued, additive white Gaussian noise

CBF Cerebral Blood Flow

Chemical shift Small variations in MR resonant frequency due to the different molecular environments of the nuclei contributing to an MR signal.

CJD Creutzfeld-Jakob Disease

Crusher gradients Gradients applied on either side of a 180^0 RF refocussing slice selection pulse to reduce spurious signals generated by imperfections in the pulse.

CSF Cerebrospinal fluid

DEXA Dual Energy X-ray Absorptiometry is a means of measuring bone mineral density using two different energy x-ray beams.

DSC Dynamic susceptibility contrast

DTI Diffusion Tensor Imaging

DWI Diffusion Weighted Imaging

Echo The RF pulse sequence where a 90° excitation pulse is followed by a 180° refocusing pulse to eliminate field inhomogeneity and chemical shift effects at the echo.

Frequency encodes Frequency-encoding of spatial position in MRI is accomplished through the use of supplemental magnetic fields induced by the machine gradient coils

Gaussian noise Gaussian noise is statistical noise having a probability density function (PDF) equal to that of the normal distribution, which is also known as the Gaussian distribution.

Gradient pulse a pulsing of the machine magnetic field gradients to alter the k-value encode

Gradient set the set of coils around the bore of an MR scanner used primarily to spatially encode signal or to set a particular phase wrap in a selected direction

GRE Gradient Recalled Echo

Interleaved acquisition Signal acquisition from a multiplicity of VOIs, successively excited within a single TR

Isochromat A microscopic group of spins that resonate at the same frequency.

k-space The 2D or 3D Fourier transform of the MR image.

k-value coefficient The coefficient in a Fourier series or transform reflecting the relative weight of each specific k-value in the series.

k-space The 2D or 3D Fourier transform of the MR image.

k-value One of the points in k-space reflecting the spacing of structural elements in a texture field.

k-value selection pulse The gradient pulse used to select a specific k-value encode along the sampled direction

Library of k-space values the net collection of k-space coefficients acquired in a particular region of tissue for tissue characterization

Machine gradients the magnetic field gradients imposable through use of the set of gradient coils in an MR scanner

MRE Magnetic Resonance Elastography—an imaging technique that measures the stiffness of soft tissues using acoustic shear waves and imaging their propagation using MRI.

MRI Magnetic Resonance Imaging

MS Multiple Sclerosis

Noise floor In signal theory, the noise floor is the measure of the signal created from the sum of all the noise sources and unwanted signals within a measurement system

NMR Nuclear Magnetic Resonance

PET Positron Emission Tomography is a functional imaging technique that produces a three-dimensional image of functional processes in the body using a positron-emitting radiotracer.

Phase coherence (spatial) When referring to multiple measurements within a common VOI of a or multiple k-values indicates that the sample has the same position relative to the measurement frame of reference

Phase encode A phase encode is used to impart a specific phase angle to a transverse magnetization vector. The specific phase angle depends on the location of the transverse magnetization vector within the phase encoding gradient, the magnitude of the gradient, and the duration of the gradient application.

Phase wrap The helical precession of the phase of the transverse magnetization along a phase encoded sample

Pitch with reference to the pitch of a screw, the tightness of the phase wrap along the direction of k-value encode

Profile A one dimensional plot of signal intensity

RF Radio Frequency electromagnetic signal

Semi-crystalline texture a texture exhibiting regular spacing along one or more directions

slice (slab) Used interchangeably to indicate a non-zero thickness planar section of the

Slice-selective refocusing Refocussing of spins through combination of a slice selective gradient and an RF pulse such that the bandwidth of the RF pulse selects a thickness along the direction of the gradient, and the RF pulse tips the net magnetization vector away from its equilibrium position Only those spins processing at the same frequency as the RF pulse will be affected.

SE Spin Echo

SNR Signal to Noise Ratio

Spoiler gradients see crusher gradients

T2 Defined as a time constant for the decay of transverse magnetization arising from natural interactions at the atomic or molecular levels.

T2* In any real NMR experiment, the transverse magnetization decays much faster than would be predicted by natural atomic and molecular mechanisms; this rate is denoted T2* (**"T2-star"**). T2* can be considered an "observed" or "effective" T2, whereas the first T2 can be considered the "natural" or "true" T2 of the tissue being imaged. T2* is always less than or equal to T2.

TBS Trabecular Bone Score is a technique that looks for texture patterns in the DEXA signal for correlation with bone microarchitecture for assessing bone health

TbTh trabecular thickness for bone measurement.

TbSp trabecular spacing for bone measurement.

TbN trabecular number for bone measurement.

TE Spin Echo sequences have two parameters: Echo Time (TE) is the time between the 90° RF pulse and MR signal sampling, corresponding to maximum of echo. The 180° RF pulse is applied at time TE/2. Repetition Time is the time between 2 excitations pulses (time between two 90° RF pulses).

Textural frequency the number of texture wavelength repeats per unit length in a texture

Texture wavelength the characteristic spacing between structural elements in a texture

TR Spin Echo sequences have two parameters: Echo Time (TE) is the time between the 90° RF pulse and MR signal sampling, corresponding to maximum of echo. The 180° RF pulse is applied at time TE/2. Repetition Time is the time between 2 excitations pulses (time between two 90° RF pulses).**Vector combination gradient** A magnetic gradient resulting from any vector combination of the gradient coil set

VOI Volume of Interest

Windowing function In signal processing, a window function (also known as an apodization function or tapering function) is a mathematical function that is zero-valued outside of some chosen interval

x-ray diffraction X-ray diffraction is a tool used for identifying the atomic and molecular structure of a crystal

[PARA 51] The embodiments disclosed herein provide an MR-based technique that enables in vivo, non-invasive, high-resolution measurement and assessment of fine biologic textures, enabling monitoring of texture formation and/or change in response to disease onset and progression in a range of pathologies. This same method can be applied to fine-texture characterization in other biologic and physical systems. It enables MR-based resolution of fine textures to a size scale previously unattainable in in vivo imaging. The method, while described herein with respect to biological systems for examination of tissue, is equally applicable for assessment of fine structures in a range of industrial purposes such as measurement of material properties in manufacturing or in geology to characterize various types of rock, as well as other uses for which measurement of fine structures/textures is needed.

[PARA 52] The method claimed herein achieves this significant improvement in in vivo resolution of fine texture by acquiring the requisite data fast enough that the effect of subject motion, the factor that limits MRI resolution, becomes negligible. This fast acquisition is achieved by acquiring data incrementally--at a single location, orientation and at one, or a select set, of k-values at a time—within one TR. After applying an encoding gradient to select the k-value of interest, data is acquired with the gradient switched off, allowing multiple acquisition repeats of the encoded k-value for subsequent averaging to reduce electronic noise, thus enabling robust measure of individual k-values before motion blurring can occur. To build up measurements on a larger set of selected k-values present

within the tissue, or towards development of a continuous spectrum of textural spacings within the tissue, the acquisition TR can be repeated as many times as necessary, changing the encode as needed to span the desired extent of real and of k-space required. The set of one or more k-values output from each TR are now high SNR due to the ability to average repeats without motion effects, and since the measure of interest is textural spacing, and not development of an image, the lack of phase coherence between TRs is of no concern.

[PARA 53] In its simplest form the method claimed herein consists of acquiring MR signal from within an inner volume to encompass a specific tissue region of interest, such as a lesion, an organ, a location in an organ, a specific region of bone, or a number of regions in a diseased organ for sampling. This inner volume may be excited by one of a number of methods, including but not limited to: intersecting slice-selective refocusing, selective excitation using phased-array transmit in combination with appropriate gradients, adiabatic pulse excitation to scramble signal from the tissue outside the region of interest, outer volume suppression sequences, and other methods of selectively exciting spins in an internal volume including physically isolating the tissue of interest, to name a few,

[PARA 54] After definition of a volume of interest (VOI), the gradient is turned off, and multiple samples of signal centered at a specific k-value, the spread of which is defined by receiver BW and sampling length, are acquired. This measurement is repeated only in specified directions within the VOI rather than trying to map all of k-space, as is required to generate an image. One or more samples of a particular k-value are acquired within an acquisition block during a single TR and the k-value subsequently incremented or decremented, allowing further multiple samples of other k-values as desired during the same TR. This method allows multiple sampling of each k-value of interest over a time period of milliseconds, providing immunity to subject motion. The process can then be repeated in further TRs, the requirement on motion between k-value acquisitions being only that the VOI remain within the tissue region of interest. Build up of a magnitude spectrum of spatial frequencies may be accomplished without the need to acquire it in a spatially coherent manner. Because the quantities of interest are the relative intensities of the various k-values (textural spacings) present in the sample volume, as long as the acquisition volume remains within a representative sample of tissue, any motion between the blocks does not compromise the measurement. In the case where motion of sufficiently large magnitude that

the internally excited volume could move into other tissue volumes over the course of building up a spectrum of k-values contained in the tissue, use of fairly robust, real-time piloting and acquisition algorithms can be used for gross repositioning of the internal selectively excited volume and for rejecting data sets that have failed to stay in the proper tissue.

[PARA 55] Repositioning the VOI to allow sampling of texture at multiple positions within or across an organ or anatomy allows determination of the variation in pathology through the organ. The data acquired can, with reference to positioning images, be mapped spatially. Either the VOI can be moved in successive TRs or interleaved acquisition done within a single TR by exciting additional volumes during the time that the signal is recovering in advance of the next TR. The requirement is that successive VOIs be excited in new tissue, that does not overlap the previous slice selects. Spatial variation of pathology can be determined by this method. This can also be used to monitor temporal progression of a pathology through an organ if the measure is repeated longitudinally.

[PARA 56] Tailoring the pulse sequence to pre-wind phase in the sample volume positions the highest k-values of interest at the echo peak where the signal is strongest, providing best SNR measurement.

[PARA 57] Sampling of k-values along multiple directions at varying angles and along varying paths, either rectilinear or curved, within the volume under study can yield important information on texture, especially textures with semi-ordered structure in specific directions, such as neuronal minicolumns. Measurement of the k-values associated with columnar spacing is extremely sensitive to alignment of the sampling path, as slight variations in sampling direction on either side of perpendicular show a rapid drop off in signal for that k-value. Rocking the acquisition path on either side of the signal maximum can yield a measure of pathology-induced randomness which is indicated by the width of the peak.

[PARA 58] With the gradient switched off for data acquisition, tuning the bandwidth to particular chemical species can enhance structural information when the chemical composition of the structure under study is known.

[PARA 59] The method claimed herein can be used in conjunction with time-dependent contrast schemes that target blood flow. Some of these contrast techniques are Blood

Oxygenation Level Dependent (BOLD) imaging, Arterial Spin Labeling (ASL) imaging, and Dynamic Susceptibility Contrast (DSC) imaging. As these methods use various techniques to highlight vasculature, changes in the texture of the vasculature associated with many pathologies, including CVD (cerebrovascular disease) and tumor growth can be measured.

[PARA 60] The method claimed herein can also be used in conjunction with other MR-based measurement techniques, including DWI and DTI, to provide front end information toward parameter selection for the diffusion techniques as well as correlation with their measurements of tissue health.

[PARA 61] The rapid repeat measurement of a single k-value, with the total time to acquire a block being on the order of a msec, reduces patient and machine motion-induced blurring to a negligible level, enabling robust assessment of fine textures previously not accessible in vivo. (For comparison, standard MR image acquisition times are much longer in duration over which patients are asked to remain completely stationary.) The SNR of each k-value measured is significantly improved through combination of the individual samples at each k-value within a block; this averaging can now can be done without concern for subject motion, which is eliminated due to the rapid sequential acquisition of the individual samples in the block.

[PARA 62] This significant improvement in SNR is made possible because the method claimed herein focuses on acquiring only the k-values of interest for determination of fine texture pathology signatures rather than on acquisition of the large number of entire spatially-encoded echoes required for image formation. The significantly reduced data matrix enables the increased number of repeats at the targeted k-values, and hence significant improvement in SNR.

[PARA 63] Energy density within a range of textural spacings is proportional to textural wavelength, or inversely to k-value—i.e. the higher the k-value, the lower the associated signal intensity. The fast acquisition enabled through use of the method claimed herein, enables tailoring the number of acquisition repetitions at a particular k-value to acquire k-values for which there is low signal first, before T_2 and T_2* effects have degraded signal amplitude. In this way, the SNR of each repeat to be averaged for noise cancellation (or spatial-phase-corrected before combining it with the measurements of k-value from

subsequent TRs) will be above this threshold. It does not matter that there is motion between acquisition cycles at different k-values as long as each acquisition lies within the tissue volume of interest (VOI). As the claimed method targets only assessment of pathology-induced changes in tissue texture, there is no requirement for phase coherence over an entire cycle of data acquisition, as is required in imaging.

[PARA 64] Several benefits result from acquiring data after the gradient is switched off for single-k-value sampling in a reduced volume (the VOI). By proper pulse sequencing, the echo record window can be designed such that recording begins with the highest k-values of interest, as signal level is highest at the echo peak. This enables recording of fine structures currently unachievable with in vivo MR imaging.

[PARA 65] Additionally, T2* is longer with the gradient off, so SNR is improved by the longer acquisition times possible This allows acquisition of an increased number of samples, N.

[PARA 66] Coil combination is also simplified by having higher SNR for each k-value, hence providing a significant improvement in overall SNR. This is especially beneficial as the trend in MRI is towards coil arrays composed of many small element coils. As the acquisition volumes targeted in the method claimed herein are small, correction for phase across the sample volume is not needed. Only one phase and gain value for each coil is needed for combining the multiple element channels. These can be combined using the Maximal Ratio Combining (MRC) method, which weights the coil with the highest SNR most heavily, or other multi-signal combination methods. (Phase and gain for the elements of a given coil array can be determined once from a phantom and applied to patient data.)

[PARA 67] Signal acquisition and data sampling in a standard MRI scan is done by acquiring complex-valued samples of multiple echoes, while applying a gradient sequence concurrently, as well as in sequence with the echoes. Imaging relies on frequency encode for one of the dimensions because this allows a line in k-space to be acquired with each phase encode rather than a single point. For 3-dimensional imaging, two dimensions in k-space normally rely on phase encode to generate the targeted filling of k-space, with the third dimension frequency-encoded. Phase encode acquisition in imaging usually entails acquisition of on the order of 256 k-values in each of the phase-encode directions, hence is is a relatively slow process. Clinical MRI scans take on the order of 10-15 minutes to

generate an image. The aim in image construction is to acquire sufficient k-space coverage to fill out all the coefficients in the 2 or 3-dimensional Fourier series, which is why in standard MR resolution is limited by subject motion.

[PARA 68] The method claimed herein is in direct contrast to standard MR data acquisition, with its focus on image generation. Image formation is plagued by blurring resulting from subject motion over the long time necessary to acquire the large data matrix required. Since the target of the method claimed herein is texture rather than image, the only requirement on subject motion is that the sampled volume remain within a region of similar tissue properties over the course of acquiring data. This is a much less stringent and easy to achieve target than the requirement of structural phase coherence, as the scale of the allowable motion is then large enough, and of a temporal order, to be easily correctable by real-time motion assessment and correction techniques. The speed of acquisition for the method claimed herein is such that, in most cases, real-time motion correction may not be necessary at all. While other methods have focused on post-processing of images to try to extract textural measures, the method claimed herein eliminates the need for image generation, focusing instead on directly measuring texture, hence enabling a more sensitive and robust measure.

[PARA 69] Frequently, k-space sampling is considered synonymous with sampling of an echo in the presence of a gradient set. In the method claimed herein, the approach to k-space filling is to acquire only the set of k-values needed for texture evaluation in the targeted pathology, with data acquired after the gradient is switched off. This method enables such rapid acquisition of single-k-value repeats for averaging for noise reduction that subject motion does not degrade the data.

[PARA 70] Along with the huge improvement in SNR that arises from sampling k-values individually, with many repeats of a select set of k-values acquired in a single TR, acquisition after the gradient is switched off allows further significant improvement in SNR and hence, increase in measurement robustness. This is explained in the following discussion.

[PARA 71] MR echo sampling provides specific samples vs. time of a time-dependent echo. The echo is comprised by the gradients applied concurrently (for the frequency-encode axis) and prior to (for a phase encode axis), but also contains the isochromats

associated with the different chemical species of the sample, as well as the envelope (T2 & T2*) associated with spin-spin interactions.

[PARA 72] Conventional frequency-encoded spin acquisitions impose a time-varying gradient upon the sample, which effectively travels in k-space along a pre-defined path. For rectilinear sampling, the path is along a straight line.

[PARA 73] Frequency encodes generate only one measurement at a given k-value—at a given point in time, the acquired sample of the echo represents the one value which corresponds to the Fourier coefficient at a specific k-space location. The next echo sample represents the value at a different k-space location, the next k-value dependent on the slope of the gradient applied concurrently. As long as there is sufficient signal at the corresponding k-value, this approach works well. However, in cases where the signal of interest is near or even below the noise floor, usually additional samples and subsequent post-processing will be required.

[PARA 74] One way to reduce the noise floor in a frequency-encoded gradient read-out is to reduce the gradient strength and lower the receiver bandwidth. Decreasing the receiver bandwidth will indeed decrease the noise level, and improve lower signal level detection (proportional to the term k_BTB, with $k_B$corresponding to Boltzmann's constant, T corresponding to Temperature in Kelvin, and B is the receiver bandwidth in Hz.) However, this comes at the expense of larger chemical shift artifacts.

[PARA 75] Chemical shift artifacts arise as a consequence of the different isochromats associated with different chemical species within the biological sample. In a frequency-encoded k-space read-out, those chemical species which resonate at a slightly higher frequency will appear to be displaced from their actual location in image space towards the direction of increasing frequency. If the spatial frequency encoding gradient is shallow, the apparent displacement can be quite large.

[PARA 76] As such, to minimize chemical shift artifacts, the gradient slope is typically made as steep as possible to minimize the apparent shift to within a narrow range (i.e. within 1 or two pixels in the image domain). However, this then requires a larger receiver bandwidth to accommodate the larger frequency range. This in turn increases the overall noise floor at a level proportional to the receive bandwidth.

[PARA 77] The conclusion is that frequency readouts generally force a trade-off between gradient strength, noise level, and chemical shift artifacts.

[PARA 78] A common technique for noise reduction in signal acquisition is through repeat sampling of a signal and subsequent combination of the multiple measurements. For linear noise sources, such as Gaussian noise, this technique improves SNR through cancellation of the random noise on the signal, the cancellation effect increasing with the number of samples, N.

[PARA 79] Noise reduction by this cancellation technique works for static subjects. However, motion-induced blurring is a non-linear effect, so signal combining for which the individual measurements have shifted through large spatial phase angles (relative to the textural/structural wavelengths under study) does not lead to an improved SNR. A fairly standard technique to correct for motion is to look at the MR intensity data in real space and reregister successive traces/images to each other to maximize overlap. It is assumed that, as with the reduction in white noise, linear combination of these reregistered signals will result in reduction of the blurring caused by the motion. However, this only works if the SNR on each individual acquisition is high enough. Reregistering low SNR samples results in a high variance in the estimated position. Threshold theory defines that combining reregistered signals with non-linear blurring, when the original signals are below a certain noise threshold, only increases signal error.

[PARA 80] The nonlinearity introduced by subject motion increases at higher k-values, since the motion-induced textural phase shift increases with k—i.e. as the size of the structures of interest decrease, the adverse consequence of motion become more acute. This implies that the multiple samples to be combined need to be derived from the same acquisition sequence, acquired in a sufficiently short time span, to ensure there is negligible motion between samples.

[PARA 81] The Cramér-Rao Lower Bound provides insight into the number of samples that are required for a lower bound on the residual variance of an estimate, i.e. the SNR vs. number of samples, in Additive White Gaussian Noise (AWGN). For low source SNRs in AWGN, one needs a large number of samples to average in order to obtain a usable SNR. The primary assumption is that multiple acquisitions can be taken, then averaged to achieve the higher SNR. (CRAMÉR, H.; “Mathematical Methods of Statistics”; Princeton

University Press, 1946. RAO, C.R., "Information and the accuracy attainable in the estimation of statistical parameters"; Bulletin of the Calcutta Mathematical Society 37, 1945.)

[PARA 82] Referring to the drawings, the graph in FIG. 1 comparing output SNR shown in trace 102 with number of samples required shown in trace 104 demonstrates that, for high input SNRs, a single sample is sufficient to yield a low noise measure. For lower SNRs, multiple samples are required to "average out" the noise contribution. The ability to combine the samples explicitly assumes that the underlying signal of interest is relatively constant during the multiple sample acquisition process (i.e. the only component which changes is the noise).

[PARA 83] The graph in FIG. 2 is a simulation with signal model, trace 202, providing an input SNR, trace 204, showing number of samples of k-value, trace 206, needed to yield a SNR of 20dB as a function of location in k-space, given an input noise level of 3mV rms. Since spectral energy density is generally proportional to k^{-1}, to maintain adequate SNR a larger number of input samples is required at higher spatial frequencies (higher k-values). The noise level for the simulation is adjusted for ~10dB SNR at k = 2 cycles/mm (λ=500μm).

[PARA 84] As pointed out above, this type of averaging is possible for purely static samples with no displacement or deformation of the targeted tissue occurring over the temporal span of data acquisition. However, for in vivo applications, natural motion occurs even if the patient is compliant. As the texture spacing of interest decreases, the adverse consequences of motion become more acute. More to the point, this type of averaging is based upon the assumption that the underlying signal is the same across acquisitions, and that only the zero-mean, complex-valued, additive, white Gaussian noise (CAWGN) changes. If the signal itself changes, the result will be an average, not only of the noise, but also of the N different versions of the underlying signal, which really doesn't improve SNR.

[PARA 85] Using low SNR samples to estimate and correct for motion will result in a high variance of the estimated position. This in turn yields a large variance in the "corrected" acquisitions and does not yield the anticipated increase in SNR when these acquisitions are averaged. This implies that the multiple samples need to be derived from

the same acquisition sequence, where motion between samples is extremely small. This is enabled by the method claimed herein.

[PARA 86] The issue becomes more acute with shorter structural wavelengths. Consider two acquisitions, noise-free for the moment, one of which has been displaced by an amount d. For a given k-value, an attempt to average them produces:

$$Y(2\pi k) := S(2\pi k)\left[1+e^{-j2\pi kd}\right]/2 \quad (0.1)$$

Where $S(2\pi k)$ is the complex-valued signal, and $Y(2\pi k)$ represents the average of the two acquisitions.

[PARA 87] This can be expressed as:

$$Y(2\pi k) := S(2\pi k)e^{-j\pi kd}\cos(\pi kd) \quad (0.2)$$

Which shows both a magnitude attenuation and phase shift, due to the displacement d. Limiting the magnitude attenuation to a floor value a, where $0 < a < 1$, limits d to:

$$|d| \le \frac{\cos^{-1}(a)}{\pi k} \quad (0.3)$$

[PARA 88] This shows that, for a given magnitude error, the allowable displacement decreases with increasing values of k. This is because, the smaller the textural spacing of interest, the less motion can be tolerated over the course of data acquisition.

[PARA 89] To deal with this problem, an alternate approach is taken in the method claimed herein, which is to dispense with the frequency-encoded readout and to sample specific k-space points, acquiring one or multiple measurements at each k-value of interest at a single spatial location and orientation at a time.

[PARA 90] Within a given acquisition in standard MR practice, there are M samples which are acquired of the echo. Instead of acquiring a sample at each k-value, $N \le M$ of those samples could be used for estimation of the (complex-valued) underlying signal value at a specific k-value. Multiple samples within an acquisition can be combined with much less concern of movement than across acquisitions because they are much closer in time.

[PARA 91] If the entire echo is used to measure one k-value, the receive bandwidth can be adjusted so as to pass the most abundant resonant peaks in the underlying NMR spectrum, and attenuate frequencies above them.

[PARA 92] Taking a straight MRS spectrum (no structural phase encodes), would yield a spectrum consisting primarily of peaks corresponding to H_2O (with a chemical shift of δ=4.7ppm), as well as Carbon-Hydrogen bonds which occur in fat (e.g. CH3, CH2, CH=CH, etc.), each with a different chemical shift ranging from 0.9-5.7ppm, with the most abundant resonance coming from CH2 in the aliphatic chain which occurs at δ=1.3ppm.

[PARA 93] Assuming use of a 3T machine, since the Gyromagnetic ratio of Hydrogen is γ=42.576MHz/T, the chemical shift values are in the range of 166Hz (for CH2) to 600.3Hz (for H2O). As long as a (single sided) receiver bandwidth in excess of 600.3Hz is used, the H2O peak will pass. Assuming baseband sampling, this implies a sampling rate >1.2kHz (note, if complex base-band sampling is used, this could theoretically be reduced by about ½.) The point here is that a narrow bandwidth can be used by this method, and sample rates on the order of 800μs. Noise on the signal is thereby reduced and multiple repeats of the k-value acquisition data are acquired in milliseconds, thereby making the acquired data immune to patient motion. For comparison, a *single* imaging acquisition is made with a TE of ~30ms, and TR on the order of 500ms-2000ms. To acquire the repeats necessary for signal averaging can take minutes—a temporal range wherein respiratory, cardiac, and twitching motion limits resolution through motion-induced blurring. The claimed method enables acquisition of values in regions of k-space which have very low signal levels, such as would be found for higher k-values (shorter textural-wavelengths) —the fine texture range that has hitherto remained elusive.

[PARA 94] To maximize the signal, the non-zero frequencies of abundance are selected. In general, this does not correspond to a mere averaging of all of the samples acquired. Instead it is akin to a matched filter which is "tuned" to the frequency of interest, corresponding to the specific chemical species of interest.

[PARA 95] As a side note, the full NMR spectrum may be extracted (without any phase encoding gradients: just volume selection) to obtain a baseline of the underlying signal strength (and associated frequencies), which in turn will be spatially modulated, providing insight into textural wavelengths through knowledge of the chemical species expected in the textural elements under study.

[PARA 96] The isochromats of interest can be extracted by acquiring N samples of the echo, then taking the Fourier transform. Since the echo is being played out with no

gradient, the strength of the resulting signal at the Isochromat of interest will correspond to the (complex-valued) k-value coefficient of interest.

[PARA 97] Given the goal is to extract the relative magnitude of textural wavelengths, just the magnitude vs. textural wavelength measurement is the required information. However, in order to extract sufficient signal strength and differentiate it from the underlying noise floor, the complex phasor values must be preserved until the end.

[PARA 98] The relationship between the noise floor, the signal strength (at a specific isochromat where there is an abundance of chemical species), the number of samples required, and the max tolerated error can be approximated as

$$N \geq \frac{\sigma^2}{|A|^2 \varepsilon^2} \quad (0.4)$$

Where σ^2 represents the noise variance, $|A|^2$ represents the squared magnitude of the isochromat(s) of interest, and $0 < \varepsilon < 1$ represents the allowable error of the estimate. Further assuming that the noise is mostly sourced from the biological sample, this can be further approximated as:

$$N \geq \frac{NF_{eff} \cdot k_B TB}{|A|^2 \varepsilon^2} \quad (0.5)$$

Where NF_{eff} is the effective noise figure of the receiver, k_B is Boltzmann's constant, T is the temperature in Kelvin of the biological sample, and B is the receiver bandwidth. In this case, N can be used as a guide to the number of samples that need to be acquired within a given acquisition in order to create a reasonable estimate.

[PARA 99] If the number of samples required exceeds the number available in one acquisition, combination of measurements from a single acquisition may be needed to maximize the signal, prior to spatial reregistration between acquisitions. A reasonable estimate and displacement correction between the two or more acquisition sets is needed. Combination of measurements at a single k-value from a single TR block can now be used to boost the SNR such that reregistration between successive TRs has a much greater chance of success.

[PARA 100] While the entire set of samples acquired in an echo or entire TR could be allocated to the estimate of one coefficient in k-space, if acceptable values can be estimated

using fewer than the maximum number of echo samples, it opens up the possibility of being able to acquire more than one coefficient in k-space within a specific echo or TR.

[PARA 101] FIG. 3 shows an example timing diagram for a pulse sequence for data acquisition using the method claimed herein. RF pulses included in trace 302 are employed to excite selected volumes of the tissue under investigation, as in typical MR imaging. A first RF pulse, 304, is transmitted coincidentally with a gradient pulse 308 on the a first magnetic field gradient, represented in trace 306 . This excites a single slice, or slab, of tissue the positioning of which is dependent on the orientation and magnitude of the first gradient, and the frequencies contained in the RF pulse. The negative gradient pulse, pulse 310, rephases the excitation within the defined thickness of the slice or slab.

[PARA 102] A second RF pulse 312, at twice the magnitude of first RF pulse 304, is transmitted coincidentally with gradient pulse 316, on a second gradient, represented in trace 314, exciting a slice-selective refocus of spins, this second tissue slice intersecting with the first. (As this second RF pulse 312 tips the net magnetic vector to antiparallel to B_0, it results in inversion of spins and subsequent refocusing, thus leading to a signal echo at a time after the 180 degree RF pulse equivalent to the time between the 90° and 180° RF pulses.) An initial higher value gradient pulse, 318, at the start of gradient pulse 316 is a crusher, or "spoiler" gradient, designed to induce a large phase wrap across the tissue volume. A similar gradient pulse, 322, at the trailing end of pulse 316, as it comes after the 180 degree RF inversion pulse, unwinds this phase wrap. In this way, any excitation that is not present prior to the 180 degree RF pulse, such as excitations from imperfections in the 180 pulse itself, will not have this pre-encode so will not be refocused by the second crusher, hence will not contribute to the signal. In summary, the second RF pulse, in combination with the applied second gradient, provides slice selective refocusing of the signal in a region defined by the intersection of the first slice and the second slice set by this second gradient.

[PARA 103] An encoding gradient pulse 326, on trace 314, sets an initial phase wrap, hence k-value encode, along the direction of gradient pulse 326. In general, the k-value encode can be oriented in any direction, by vector combination of the machine gradients but for ease of visualization is represented as on the second gradient.

[PARA 104] A refocusing third RF pulse 328, applied in combination with gradient pulse 332 on a third gradient, represented by trace 330, defines a third intersecting slice selective refocus to define the VOI. Gradient pulse 332 again employs crusher gradients.

[PARA 105] The negative prephasing gradient pulse 326 winds up phase such that, at the signal echo following the second 180° RF pulse, signal acquisition starts at high k-value, which may then be subsequently decremented (or incremented or varied in orientation) for further acquisitions, as will be described below. As energy density in the signal is generally proportional to k^{-1}, this method ensures k-values with lower SNR are acquired first, before T_2 effects have caused much overall signal reduction.

[PARA 106] With all gradients off, a receive gate 333 is opened to receive the RF signal, which is shown in FIG. 3 as pulse 334 on trace 336. The RF signal in trace 336 is a representation showing only the signal present in the receive gate window without showing the actual details of the RF signal outside the window. Sampling occurs as represented by trace 338 beginning with the initial k-value, 340a, seen on trace 324. Note that, at the scale of the drawing, the sampling rate is high enough that the individual triggers of the analog to digital converter (A/D) have merged together in trace 338. (The expanded time scale in FIG. 4 described below shows the individual A/D triggers.)

[PARA 107] In regions of k-space where the corresponding coefficients are sufficiently large that they can be well-estimated using a small subset of the samples of one echo, acquisition of another k-value, obtained by applying a gradient pulse 342a shown on trace 314, to select a new k-value, during the time the echo is being recorded, is accomplished. After a suitable settling time, another set of samples of the echo (now derived from the new k-value coefficient) can be collected. This process can be repeated, acquiring multiple samples at each of a select set of k-values within one TR. A plurality of samples are taken at the initial k-value 340a. A k-value selection gradient pulse 342a is then applied and the resultant k-value 340b is sampled. (Though shown in the figure as a negative pulse on the second gradient, decrementing the k-value, in practice this pulse and subsequent k-value gradient pulses can be designed through any vector combination of gradients to select any k-value or orientation.) Similarly, the k-value selection gradient pulse 342b, selects a third k-value 340c which is sampled by the A/D. Each gradient pulse changes the phase wrap, selecting a new k-value. Application of a k-value selection gradient pulse (342c – 342f)

followed by multiple sampling of the resultant k-value coefficient is repeated as many times as desired. While data is being acquired throughout, the samples of interest are acquired when all gradients are off. The gradient orientations for slice and k-value select may be coincident with the machine gradients, which are aligned to lie coincident or orthogonal to the B_0 field. Alternatively, the acquisition directions and k-value encodes may be selected using gradients that are a vector combination of all three machine-gradient axes.

[PARA 108] In the circumstance where it is desired to measure a low SNR k-value the prewinding encoding gradient pulse can be set such that the fist k-value to be measured is the desired low SNR k-value. Alternatively, the prewinding gradient pulse can be set to zero so that the first k-value measured is k0. A measurement of k0 may be desired for the purpose of determining the systems receiver sensitivity to the particular VOI, determining the relative prevalence of isochromats (e.g., water vs. lipids) irrespective of texture in the VOI, or for the purpose of establishing a reference value for normalization of the other k-values measured in a VOI or for comparison with k-values from other VOI. Furthermore a strategy for gathering a specified set of k-values for a VOI may include measuring the low SNR k-values (typically the higher k-values) in a first set of multiple TR and then measuring k0 and other higher SNR k-values in other TRs while remaining in the same VOI.

[PARA 109] As is shown diagrammatically in FIG. 3, the signal reaches a maximum at the time of the spin echo. It is also shown diagrammatically that the signal is varying throughout the acquisition of the multiple RF measurements of a k-value and more so between successive blocks of measurements of k-values. Alignment in time of the measurement of the low SNR k-values with the highest echo signal enhances the SNR of the k-value measurement, alternatively alignment of higher SNR k-values with lower echo signal allows gathering additional useful k-value acquisitions during the echo.

[PARA 110] FIG. 4 shows a close-up of the pulse sequence of FIG. 3 during the initial portion of the RF sampling window 338 between 7.25 and 8.00 msec. Multiple samples of the same k-value, taken in rapid succession with all gradients off, provide the input for signal averaging to reduce AWGN when SNR is low. In a first block 344a of the sampling window 338, multiple samples 346a are taken of the first k-value 340a. During application of the k-value selection gradient pulse 342a, transition samples 348a are taken. When the k-

value selection gradient is switched off, multiple samples 346b are taken at the second k-value 340b. Application of k-value selection gradient pulse 342b then occurs with associated transition samples 348b, and subsequent acquisition of samples 346c of the third k-value 340c after the gradients are switched off. The underlying signal is minimally impacted by motion due to the very short time window used to acquire data at each given k-value. Since the data is acquired with gradients off, there is no issue with chemical shift and the effective T_2^* is longer, boosting the signal value.

[PARA 111] The sampled values of the echo, acquired while the k-value selection gradient pulse is ramped up, held steady, and then ramped down to zero, will necessarily be influenced by the applied gradient. These transition samples may provide other interesting information, but are not used in the consideration of a straight measurement of the k-value coefficient; only those samples which are recorded when there is no gradient currently active are used for this.

[PARA 112] A consistent number of samples at each k-value can be acquired, or an alternative sequence may be employed where, as k-values decrease, hence increasing in signal amplitude, fewer samples are acquired. A pulse sequence designed for this type of acquisition is illustrated in FIG. 5. Multiple samples of each k-value targeted in the acquisition are acquired in rapid succession, with all gradients off. These repeats provide the input for signal averaging in low SNR signals. As with the pulse sequence, depicted in FIGs. 3 and 4, the underlying signal is minimally impacted by motion due to the very short time window in which data is acquired for a given k-value.

[PARA 113] Samples within the portions of the sample window 344a – 344g outlined on FIG. 5 correspond to the number of samples acquired for a given k-value 340a – 340g each induced by an unwinding pulse 342a – 342f of the k-value selection gradient. N_k, the number of samples associated with a given k-value, can be selected based upon expected SNR, tissue contrast, contrast to noise, pathology, texture size, and/or texture bandwidth. For the example in FIG. 5 it can be seen that a decreasing number of samples are taken for progressively smaller k-values (larger textural features). This is because, as previously discussed, to first order signal amplitude increases with decreasing k-value—energy density is generally proportional to k^{-1}. For this same reason, larger k-values are acquired first in

this scheme, when T2 effects are least, the longer wavelength, higher signal strength, k-values being recorded later in the acquisition.

[PARA 114] Refocusing the echo, and/or a new TR can be used to build up a library of k-space samples. Acquisition of multiple k-values within one TR can be facilitated by application of multiple refocusing gradients and/or RF pulses, to increase the time over which the additional k-values can be sampled within a TR. These later echoes would presumably be used to acquire the coefficients of the lower k-values in the selected set, as their energy density in the continuum of values is generally higher so the effect of T_2 decay on overall signal will not affect them as severely as it would the higher k-values. In this way a larger portion of the required k-space filling can be accomplished over fewer TRs, allowing more rapid data acquisition, minimizing the need for repositioning the VOI.

[PARA 115] FIG. 8 shows an extension of the basic sequence of the method claimed herein, using spin-echo refocusing to extend the record time for the TR. Application of a refocusing RF pulse 802 with an associated gradient pulse 804 results in slice-selective refocusing. After an appropriate settling time, a second sampling window 806 is opened by the receive gate 808. Multiple k-value selection gradient pulses 810 are applied to increment the selected k-value and, after switching off each successive gradient pulse, multiple samples of the selected k-value are acquired in the sampling window. A second slice-selective refocusing RF pulse 812 with associated gradient pulse 814 again inverts the spins and, after application of each in the multiplicity of k-value selection gradient pulses 820, data is acquired in a third sampling window 816, opened by the receive gate 818. As shown in the drawing, an increasing number of k-values may be sampled with each refocusing. Refocusing can be repeated until the decrease in signal level from T2 and other effects makes further signal acquisition ineffective. Another method to extend the record time by exciting multiple signal echoes, is to use one, or a series of, gradient recalled echoes (GRE). GRE are different from the SE in that they cannot refocus the effects of stationary inhomogeneities, so T2* effects limit the number of repeats.

[PARA 116] In addition to the tissue contrast available, the k-values associated with particular pathology will be part of the determination of the number of samples needed for signal averaging, N_k. In liver fibrosis, the wavelength of pertinent textures is in the range of 400 microns, i.e. a k-value of 2.5 cycles/mm. This is similar to the textural spacings seen in

fibrotic development in many other diseases, such as cardiac fibrosis. The spacing of elements in trabecular bone varies a lot, but the *minimum* spacing of interest is the width of trabecular elements, which are approximately 80 microns, setting a maximum k-value of 12.5cycles/mm. In neuropathology, many of the textures of interest are very fine, on the scale of 50 microns, equivalent to a k-value of 20 cycles/mm.

[PARA 117] Each pathology will dictate what exactly is needed as quantitative data, i.e. what part of the continuum of k-values needs to be monitored, and with what resolution and sensitivity. In some pathologies, short (long) wavelength features increase at the expense of long (short) wavelength features (e.g. liver fibrosis). In other pathologies, an amplitude decrease and broadening of short wavelength features indicates disease progression—e.g. degradation of the ordered formation of cortical neuronal minicolumns (approximately 80-micron spacing) with advancing dementia. In bone, with increasing age, first the highest k-value features disappear in the structural spectrum. Next the major structural peaks shift slowly towards lower k-values with advancing osteoporosis, the pace of this shift accelerating as an increasing percentage of trabecular elements thin to the point that they break.

[PARA 118] The signal level obtainable will depend on anatomy to some extent. For instance, though the resolution needed is highest in brain, the proximity of the cortex to the surface of the head ensures that use of a surface coil will provide significant signal boost for cortical structures. Lower resolution is required in liver, as the structures of interest are on the order of several hundred, rather than tens of microns. But, the organ is deeper (further from the coil) reducing the measured signal. Using the in-table coil for spine data acquisition yields modest signal level and good stabilization. Also, bone is a high contrast target, so the SNR requirement is not as stringent. For all these reasons, the exact number of repeats needed for averaging depends on more than the k-value range targeted.

[PARA 119] FIG. 6 shows a simulation demonstrating that the ability provided by the claimed method to acquire many repeats of a targeted k-value within a single TR enables robust signal averaging to boost SNR. Assuming a subject displacement rate (which has in practice been measured clinically over the course of several scans) of 30μm/sec, and a sampling rate = 33.3kHz (ΔTsample = 30 μs), 90 repeat samples for averaging can be taken

rapidly enough that, even up to a k-value of 20 cycles/mm (texture wavelength = 50μm), the acquisition remains immune to motion effects.

[PARA 120] FIG. 7 shows that, for comparison, using the conventional approach of acquisition of a spatially encoded echo, even assuming a relatively fast gradient refocus sequence, which would provide a sampling rate of about 67Hz (ΔTsample = 15msec), subject motion over the time needed for 90 repeats would severely degrade the signal, and any ability to improve SNR by signal averaging. The situation is actually worse due to the fact that to acquire 90 repeats using conventional spatially-encoded echoes would require several TRs, making the acquisition time significantly longer, and the signal degradation due to motion much more severe. With the exception of the very lowest k-values, the potential SNR gain due to multiple sample combination has been nullified by the effects of motion.

[PARA 121] By acquisition of a large enough selected range of k-values, construction of a structural profile in one or more dimensions becomes a possibility. As discussed above, refocusing echoes within a single TR, or multiple TRs, can be used to build up a library of k-space samples. Phase coherence might not be maintained between different k-values if they are acquired in TRs separated temporally such that displacement has occurred between them. If our primary interest is in the relative strength of signals at particular k-values, this is not a problem. If creation of a profile or an image from this library of values is desired, the necessary post processing will have as input the high SNR measure obtained within each TR using the method claimed herein. These measures can then provide robust input for any required reregistration between echoes or TRs towards constructing a profile. As an example selection and measurement in a first TR of a set of selected k-values may be accomplished with at least one having a low k-value. In a subsequent TR, selection of the same set of k-values will allow re-registration of the data between the two TRs since even if significant motion has occurred the phase change in the low k-value phase shift will be less than for higher k-value textures and may be correlated between the two TRs. Basically, the higher the k-value, the greater the phase shift due to subject motion. Acquiring signal from successive encodes with a large difference in k-value enables a better estimate of phase shift by careful comparison of the apparent phase shift for each.

[PARA 122] This is very similar to x-ray diffraction, wherein the magnitude-only information (no phase) obtained presents the challenge of determining a best estimate of the corresponding structural profile based on this magnitude-only information. Algorithms exist towards solving the problem, the chance of success depending on the range of k-value coefficients obtained, the SNR of each averaged coefficient, and the width of values contained in a nominally single-valued acquisition of k-value. The chance of success in this effort is greatly increased using the claimed method due to its immunity to subject motion.

[PARA 123] The ability to reconstruct a profile from k-value data depends somewhat on the spectral broadness of each single-k-value acquisition. While this is influenced by the VOI (Volume of Interest) size and shape, it is also influenced by k-value and pathology, as degradation of tissue often tends to lead to more textural randomness within tissue.

[PARA 124] Selection of the VOI—shape, dimensions, orientation, and positioning within an organ/anatomy affects the data measured and its interpretation. The VOI shape can be chosen to maximize usefulness of the acquired data. Data can be acquired in different directions, and at different textural wavelengths (k-values) within a VOI enabling assessment of textural anisotropy. Texture can be sampled in multiple VOIs, either interleaved within a single TR, or in successive TRs, towards assessment of pathology variation across an organ. Standard interleaving processes for the VOI may be used within a TR to provide additional data by applying additional encoding pulses on vector combination gradients and associated k-value selection gradient pulses for k-values in the interleaved VOI. As previously described, additional excitation RF pulses with associated slice selection gradients may be repeated within the same TR by exciting a volume of interest with a gradient set in each repeat having at least a first gradient with an alternative orientation from the first gradient pulse 308 applied initially in the TR, to define an additional VOI for excitation in new tissue, that does not overlap any previous VOI in the TR (fourth, fifth and sixth gradients in a first repeat and succeeding incremental gradients in subsequent repeats). This response can be mapped, or the several measures taken and averaged, whatever is appropriate for the targeted pathology. This is similar to the multi-positioning of tissue biopsy. However, in the case of tissue biopsy, the number of repeats is limited due to the highly invasive nature of the technique. The minimum number of structural oscillations to be sampled at a specific k-value dictates a minimum VOI

dimension in the direction of sampling—the length required varying inversely with targeted k-value.

[PARA 125] To ensure adequate sampling of structure when targeting a range of k-values, the VOI dimension in the sampled direction can be held constant for all k-values in the targeted range, with the result that the number of structural oscillations sampled will vary with k-value. This is a simple solution, requiring the sampling dimension be set by the lowest k-value (longest wavelength structure). Using this approach, the sampling dimension of the VOI is larger than required for the highest k-value in the range, thus providing less localization within the tissue than would be otherwise possible.

[PARA 126] Alternatively, data at widely differing k-values can be acquired in successive TRs, using changing VOIs tailored to the specific k-value targeted. Or, the dimensions of the VOI can be selected such that acquisition in different directions within the VOI will be tailored to sampling in a specific textural frequency (k-value) range.

[PARA 127] Similarly, the VOI may be held constant and the vector combination gradient for the encoding and k-selection pulses may be altered from TR to TR for assessing feature size.

[PARA 128] In some instances, it is desired to localize tightly in the spatial domain, to broaden the localization in k-space. By defining a non-cubic acquisition volume, it would be possible to acquire data from differing k-values along the different (orthogonal or other) directions within the VOI, within one TR. The elliptical cross-section VOI 902 in FIG. 10 is one such possibility. Acquisition along any radial direction, as well as along the axis of the shape, would be possible within one TR.

[PARA 129] Additionally, one could use the flexibility of the method claimed herein to sample k-space in a linear or in a curved trajectory. For example, texture could be sampled along radial lines, or along an arc or a spiral, to extract information of textural sizes along different spatial directions. These methods can be used to determine the anisotropy of texture, or the sensitivity to alignment in structures that are semi-crystalline, such as cortical neuronal columns, or to more rapidly build up a library of k-values within a targeted extent of tissue in an organ.

[PARA 130] During one TR (i.e., one 90 degree excitation) k-value encodes can be applied in multiple directions by changing the applied vector combination gradients for

encoding and k-selection pulsing. The exact form of the VOI and sampling direction can be used to yield much textural information. For instance, the organization of cortical neuron fiber bundles is semi-crystalline, as the bundles in healthy tissue form in columns. Because of this, the measure of textural spacing perpendicular to the bundles is very sensitive to orientation. When the orientation is exactly normal to the columns, a very sharp signal maximum is expected, the signal falling off rapidly as the orientation varies on in either rotational direction away from this maximum. One way to measure the spacing and organizational integrity (a marker of pathology) would be to "rock" the acquisition axis around this maximum looking for a resonance in signal intensity. This approach of looking for "textural resonances" by looking for signal maxima can be applied in any tissue region. As pathology degrades the organizational integrity, the sharpness of this peak will degrade and the signal maximum will be reduced.

[PARA 131] Similarly, the randomness of the spacing in certain textures can be assessed by varying the length of tissue sampled in a specific, or in multiple directions, with subsequent change in acquisition length. The selected value for that length can be varied over multiple TRs to test the sensitivity of the measured coefficient to this parameter.

[PARA 132] The VOI can be selectively excited by a number of methods, for instance intersecting slice-selective refocusing, selective excitation using phased-array transmit in combination with appropriate gradients, adiabatic pulse excitation to scramble signal from the tissue outside the region of interest, as examples. Parameter selection for the various methods can be done with SNR optimization in mind. For instance, the VOI generated by a slice selective excitation and two additional mutually- orthogonal slice selective refocusing pulses, as by VOI 904 in FIG. 9. Through careful RF pulse design, the shape of the VOI can be designed so that the edges are smooth and more approximate a windowing function, as shown in FIG. 10. These windowing functions provide the volume selection without adverse impact on the spatial frequencies. Recall, in Fourier theory, each spectral line is smeared by the convolution of a Fourier transform of the window function. It is desirable to minimize this smearing of the underlying spectrum, as it decreases the energy spectral density, and adversely impacts SNR.

[PARA 133] Importantly, as has been discussed previously, the VOI can be moved from place to place within an organ or anatomy under study to measure the variation of

texture/pathology. This response can be mapped, or the several measures taken and averaged, as appropriate for the targeted pathology. This is similar to the multi-positioning of tissue biopsy. However, in the case of tissue biopsy, the number of repeats is limited due to the highly invasive nature of the technique.

[PARA 134] Different diseases and conditions affect tissue in different ways. Generally, pathology advancement entails: 1) a loss of energy density in specific regions of k-space, and/or 2) a shift in textural energy density from one part of k-space to another, both effects being accompanied by 3) changes in the width of existing peaks in the continuum of textural k-values. Using trabecular structure as an example—with decreasing bone health the average separation of trabecular elements widens (texture shifts to lower k-values) and becomes more amorphous (broader peaks in k-space), while in parallel the structural elements thin (a shift to higher k-values in a different part of the spectrum). Other tissues/organs are affected by diseases that have their own individual signatures in tissue texture.

[PARA 135] Using the method claimed herein, k-space is probed to reveal texture in such a way as to eliminate the loss of signal resolution that results from subject motion blurring. Instead of measuring the large continuum of k-values needed to create an image, the focus here is on acquisition of a select few k-values per TR, with sufficient repeats of each to yield high SNR. Each of the individual acquisitions is centered on a single k-value. While the spatial encode is, to first order, a single spatial frequency sinusoidal encode, there are a number of factors which have the effect of broadening the spatial frequency selectivity of the k-value measurement. One significant factor affecting the broadness, or bandwidth, of the k-value measurement is the length of the sampled tissue region. A longer sampling length encompasses more textural wavelengths along the sampled direction, which has the effect of narrowing the bandwidth of the k-value measurement. (This is the inverse relationship between extent of a measurement in real and in k-space.) Hence, an aspect of the claimed method is the ability to set the bandwidth of the k-value measurements by appropriate selection of the sampling length determined by the VOI dimensions or determined by the acquisition dimensions. Using this method, the bandwidth of the measurement can be set according to the desired k-space resolution appropriate to the tissue being evaluated. (Need both high k-values for good texture resolution, and high resolution

in k-space for sensitive monitoring of pathology-induced changes.) For highly ordered structures one could choose a set of narrow bandwidth measurements distributed over the expected range of texture wavelengths, whereas in a more randomly ordered structure, such as the development of fibrotic texture in liver disease, one could choose to use a single, or a few, broadband k-value measurements to monitor development of the fibrotic texture.

[PARA 136] A measure of both the relative intensities of the various textural k-values present in a tissue and the broadness of the peaks along the continuum of textural k-values present within the texture under study is needed. As such, data acquisition can be designed to probe specific region(s) of k-space, with parameter selection that will enable measurement of the relative width of peaks arising from the underlying tissue, rather than that resulting from experiment parameters. It is necessary to recognize the interaction of the two components, and design experiments to yield the best measure of pathology-induced tissue changes.

[PARA 137] It is desirable to obtain a good measure of texture by acquiring multiple measures of signal amplitude at specific k-values close in time before motion blurs the data, taking repeat measurements in minimal time to allow best inter-measure correlation for averaging. an alternative to acquiring many repeat measures at one point in 3D k-space, is to acquire data with a gradient on, such that the k-value is changing continuously across the acquisition, the extent in k-space being determined by the height of the gradient and its pulse width. In addition to varying the magnitude of the k-vector, its direction over the course of data acquisition can also be varied. Combination of direction and magnitude changes across an acquisition result in a curvilinear trajectory through k-space. If this deviation is small enough that the k-values remain correlated to some extent, they can be combined more effectively to increase SNR than if they were simply averaged. Gradient on acquisition can therefore be used to intentionally vary the direction and magnitude of the k-vector, for the purpose of smoothing signal speckle—which manifests as a time varying signal over the data acquisition, resulting from interference of the individual spin signals' varying phases and amplitudes. The selected variation in k-value direction and magnitude across the acquisition is chosen to provide sufficient combined measures to get an estimation of the representative power within a neighborhood of k-space.

[PARA 138] Varying the k-value to reduce speckle can be accomplished within a single, or multiple, echoes. For a sphere in k-space, defined by the magnitude of the k-value under study, the k-value can be varied by keeping the magnitude of k-constant but sweeping the vector over the surface of the sphere, or the same angular orientation may be maintained, and the magnitude of k varied, or both can be varied simultaneously

[PARA 139] For the purpose of reducing speckle effects, these variations would usually be small enough deviation from either the k-magnitude or direction that there is a meaningful correlation between the measurements for the particular tissue under investigation.

[PARA 140] The major components of the spatial frequency will be the same in all those measurements (they are correlated) unless the measured tissue is a highly crystalline texture. But the normal diffraction pattern for a micro-crystalline or amorphous structure has a lot of speckle. Consequently, by sampling a number of points in the same region of k-space they can be combined in various ways, selected to provide optimal smoothing to reduce the speckle-pattern. A better and more robust measure, from averaging out the fluctuations, is the result.

[PARA 141] A number of approaches to "dither" k-value to reduce speckle or to tailor width in k-space may be employed. A first approach employs constant k-magnitude plus sweeping through a range of angles by keeping gradients on during acquisition and combining the measures using correlative information to eliminate speckle. Alternatively, the same direction in k-space may be maintained but the magnitude varied by leaving gradient on during acquisition and combining the measures using expected correlation. As yet another alternative, both magnitude and direction may be varied simultaneously or over an acquisition series, essentially performing the other two alternatives simultaneously to both reduce noise and provide a better assessment of the representative k magnitude in a structure in a "small" region around a specific k-value, i.e., to reduce speckle.)

[PARA 142] For combining the measures at different k-magnitudes, for noise reduction averaging, there is a phase shift from one radius (magnitude) to the next from the gradient wind-up. Rephasing may be accomplished before averaging.

[PARA 143] Combining the different magnitude measures in an amorphous structure is more well-known than combining different angled measures. Now in addition to the scheme

of reducing thermal noise by rapid sampling the fluctuations due to speckle (which though real signal confounds good assessment of the spatial frequency) may be reduced.

[PARA 144] A dynamic k-space acquisition is therefore employed. The acquisition mode is dynamically chosen based upon the Signal to Noise Ratio (SNR) of the signal at various k-space locations. The gradient, applied during signal acquisition, post-acquisition receive bandwidth, and estimation algorithms used are dynamically adjusted based upon the expected SNR values in k-space to optimize acquisition time and post-processed SNR. In regions of high SNR, a single sample at a given k value may be a sufficient estimator. This requires a relatively wide receive bandwidth to accommodate the relatively rapid signal variations in the receive chain as k is changed rapidly (due to the large gradient).

[PARA 145] In regions of moderate-to-low SNR, the gradient magnitude is decreased so that, subsequent samples, while not taken at identical k values, are correlated, which in turn can be used to improve estimates of the underlying signal values within that range of k-values.

[PARA 146] Correlation may be introduced in k-space due to selected windowing in profile space. To enable combination of sequential samples from the ADC so as to improve SNR, correlation among successive samples will be increased by proper choice of windowing in profile space, a shorter window driving a greater correlation distance across sequential values in k-space and a longer window resulting in lower sample to sample correlation. Inducing correlation of neighboring points in k-space by windowing in profile-space is a mathematical tool that can, in many cases, help to measure the underlying texture in a low SNR environment. Basically, windowing blurs the data so that the k-value power spectrum is smeared out through k-space, so that sequential measures can be averaged/combined more easily to increase SNR.

[PARA 147] In a very high SNR environment as large a window as possible is used because is a measure of the actual textural power distribution across a range of k-space is desired. The longer the sampled region in real (profile) space the more accurate the measurement when measuring amorphous textures. Reducing the sampled region by windowing to induce correlation in k-space actually obscures the specific desired measurement point.

[PARA 148] However, while facilitating measurement, inducing correlation through windowing does blur to a greater or lesser degree the underlying relative power density profile in k-space arising from the underlying texture , which is the target of the measurement. As the sample-to-sample spacing (determined by the analog to digital converter speed and gradient height) in k-space decreases, there will be increased correlation, which can be used in post-acquisition processing to form better estimates. Additionally, the receive bandwidth in these regions can be decreased, which further decreases the noise floor.

[PARA 149] In regions of very low SNR, multiple acquisitions of the measured signal level at a specific k value can be taken, with zero (and/or non-zero) gradient during acquisition. The multiple acquisitions can then be optimally combined to provide an estimate for specific k values.

[PARA 150] An example Hybrid pulse sequence is shown in FIG. 11. This particular sequence is an example of a rapid acquisition with refocused echoes (RARE) type sequence wherein three different levels of gradient are used for acquisition as illustrated across three separate echoes. The shown pulse sequence for selecting the desired VOI and initial phase wrap for k is as described in FIG. 3 and is numbered consistently in FIG. 11. While this exemplary pulse sequence for establishing the VOI is employed in the various examples disclosed herein, the determination of VOI made be made by any of numerous approaches including, as an example, time varying RF pulses with commensurately time varying gradients applied. Similarly, during or after the pulse sequence employed for determining the VOI, the encoding gradient pulse may be applied for selection of the initial k-value. The data recording starts with acquiring values in regions where $|k|>>0$, given that the signals are smallest there and should be acquired first. The second echo samples values associated with $|k|>0$, but whose signal levels are still relatively small and require combination of multiple measures to provide robust SNR. The final echo samples values associated with $|k|$ in the neighborhood near $|k| \sim 0$ where the corresponding signals are largest. Note that this is just one example of how this hybrid approach, using both zero and non-zero gradient in one acquisition, could be used. Different amounts of k-value windup (as determined by the gradient height and pulse duration) can be acquired in one echo rather than in multiple echoes as will be described subsequently. Multiple combinations of the differing k-value

windup also can be acquired within one echo. Additionally, while refocusing is disclosed in the drawings as employing an RF pulse, gradient refocusing may also be employed.

[PARA 151] Details at expanded scale of the pulse sequence/signal acquisition are shown in FIG. 12. In this sequence, the first echo from RF pulse 328 with gradient pulse 332 uses the a pulse sequence similar to that previously described with regard to FIG.3 and acquisition of multiple samples with gradient = 0 and incrementing of k values with k value selection gradient pulses 1100a, 1100b and 1100c. This samples multiple values of a given location in k-space, which values are then optimally combined. This is appropriate for regions of k-space whose values are very small and therefore have very low SNR. This typically occurs in regions where |k| is large.

[PARA 152] The second echo from RF pulse 1102 with gradient pulse 1104 is acquired with a small non-zero gradient 1106 acting as a time dependent phase encode. A small gradient may be defined as a gradient inducing samples in k-space which will be sufficiently closely spaced so that the samples are highly correlated. These samples can then be post-processed by an estimator which takes advantage of the high inter-sample correlation to improve the resulting SNR. Quantitatively an exemplary "small" gradient might be up to 20% of the magnitude of the encoding gradient pulse. As seen in the figure samples of multiple values in a relatively small neighborhood, Δk, in k-space are obtained. The spacing of Δk can be chosen such that, due to the windowing of the VOI, there is high correlation between neighboring samples. The correlation is exploited in the estimation algorithm to generate an optimal estimate of the signal levels across a neighborhood in k-space. This is appropriate for regions of k-space which have low SNR, but whose values, because of the correlation induced by the windowing function, vary slowly across k-space in a small neighborhood.

[PARA 153] A third echo from RF pulse 1108 with gradient pulse 1110 is acquired with a relatively larger time dependent phase encode gradient 1112. The higher gradient employed herein creates sequential measurements in k-space which have a lower degree of correlation across the neighborhood of k-space under study. In this case, there is lower inter-sample correlation available for SNR improvement. A higher gradient may be employed for sampling k-space locations whose values have a high SNR to begin with (such as would be seen in lower textural frequency (low k-value) regions). As seen in the figure samples

relatively widely spaced across k-space, well outside the inter-sample correlation imposed by the window function, are generated over the entire pulse. This is appropriate for rapid acquisition of values in k-space whose signal levels are relatively high and enable high SNR recording. In this case, a single sample at a given point in k-space provides a high enough signal. However, in such higher SNR regions, the higher gradient may be employed and selected bursts of data samples may be rapidly recorded. Each of these bursts will have substantial inter-sample correlation within the burst and may allow computation of results similar to that described for the lower gradient acquisition discussed above. This may be viewed as transitioning along the K-space line with the higher gradient while sampling blocks of data at closely spaced k values to maintain correlation.

[PARA 154] Non-zero gradient acquisition allows sweeping across a curvilinear path in k-space. By a judicious choice of time increment, Δt, gradient magnitude, G, w(X), and the total number of samples acquired, N, the neighborhood of "high" correlation can be adjusted to be $M < N$. This in turn would allow estimation of a multiplicity of distinct values within k-space by using a subset of M samples for each output estimation. Textural data from within a tissue region defined by the VOI can be acquired with the non-zero gradient to enable determination of the local distribution of power density of k-values within a neighborhood in k-space. The extent of k-space sampled with a gradient pulse played out during acquisition is determined by the gradient height and the gradient pulse width (pulse duration). The spacing between signal samples in k-space is determined by the gradient height and the sampling rate (limited by the maximum speed of the analog to digital converter). The correlation between sequential samples in k-space is determined then by the spacing between samples, by subject motion, by the window used to bracket the acquisition in physical space, and by the underlying texture.

[PARA 155] A useful method for selecting the acquisition parameters is with reference to the degree of correlation needed within a set of values to be combined. The wavelength of a repeating structure (texture) is defined as the inverse of the k-value associated with that texture, $\lambda_{texture} = 1/k_{texture}$. To be able to combine a set of values [measurements] to yield improvement in SNR, the underlying textural signals must not be shifted in phase by a significant percentage of $\lambda_{texture}$ relative to each other. In exemplary embodiments, the phase shift across the set of samples to be combined should be no greater than 80% of 2π.

[PARA 156] Resolution in MR imaging is limited by subject motion during image acquisition. This limitation can be very severe with non-compliant patients. In addition to patient motion/compliance, the resolution achievable in MR imaging which is exemplary art comparable to the present invention, depends on several factors, such as tissue contrast, organ, coil type, proximity to coil. Robust imaging of structures below about 5mm in extent is problematic, and anything below about 1mm is outside the realm of routine clinical imaging. This is a clear shortcoming as many tissue textures in the range of about 5mm down to 10μm develop and change in response to pathology development, hence measurement of these textures can provide much diagnostic information—these tissue changes are most often the first harbinger of disease. It is this textural wavelength range, from about 5mm down to 10μm that is targeted with the presently disclosed method.

[PARA 157] To measure tissue texture, the range of wavelengths in real space which can be resolved, i.e. the wavelengths of the textures pertinent to the particular pathology, are in the range of several mm down to microns. This is the range made inaccessible (blurred) in imaging due to patient motion. As k is defined as 1/wavelength, a range of k-values from about 0.2 mm^{-1} to 100 mm^{-1} is employed in exemplary embodiments to define the textures of interest. This brackets the region of k-space of interest, and defines the gradient height and duration of the encoding gradient pulse to induce phase wrap to create a spatial encode for the specific k-value and orientation as well as for the non-zero gradients applied for measurement of the neighborhood around the initially selected k-value. The method of the embodiments herein for sample acquisition and post processing may all be conducted in k-space. The only localization in real space is the positioning of the VOI. Just enough of the neighborhood around a point in real-space is sampled to measure texture—i.e. to determine the power distribution within a neighborhood in k-space around the selected point in real space.

[PARA 158] The exact range needed varies with the targeted pathology. For example:

[PARA 159] Osteoporotic development in bone microarchitecture. As examples, the variation in average trabecular spacing (TbSp) from healthy to osteoporotic bone brackets a wavelength range of about 0.3mm to 3mm; the equivalent range of k-values is 0.34mm-1 to 3.4mm-1. With fibrotic liver disease monitoring change in liver tissue texture from the healthy collagen-highlighted vessel-to-vessel spacings to the diseased state in which the

lobule-to-lobule spacing becomes the prominent tissue texture. Vessel-to-vessel range is 0.4mm to 1.5mm translating to k-values of $0.67mm^{-1}$ to $2.5mm^{-1}$ while lobule-to-lobule spacing of approximately 1mm to 4mm, translating to k-values from $0.25mm^{-1}$to$1mm^{-1}$. Angiogenic vasculature development around a tumor site typically changes from the healthy vessel texture spacing of around 100μm; $k = 10mm^{-1}$. Due to its chaotic nature, the spacings in angiogenic vasculature cover a broad range from about 10μm to 1mm, or $1mm^{-1}$ to $100mm^{-1}$. Diagnostic assessment of dementia-related changes to the cortical neuronal spacing involves measuring high k-values, the healthy structure being about 100 μm spacing or $k = 10mm^{-1}$. Variations of about 10-20% of this value, with increasing randomness in structure, mark the disease.

[PARA 160] Therefore, the acquisition parameters can be chosen such that (1) the gradient height/duration generates a range of k-encodes spanning the neighborhood of k-space over which it is desired to inspect the power density present in the targeted tissue texture, (2) the samples to be combined must occur close enough in time that there is no significant blurring due to subject motion across the acquisition time of a block of samples to be combined, and (3) the tolerable amount of motion depends on the neighborhood of k-space under investigation (i.e., the wavelength).

[PARA 161] Acquisition of textural data from within a targeted VOI with the non-zero gradient enables determination of the local variation of power density of k-values within a neighborhood of the initial k-value in k-space. The extent of k-space sampled at each gradient pulse is determined by the gradient height and the pulse width. Spacing between the samples in k-space is determined by the gradient height and the sampling rate.

[PARA 162] These parameters are selected (1) to allow acquisition of sufficient data for combining toward significant SNR improvement, before subject motion can blur the data significantly relative to the texture to be measured, (2) to ensure sufficient correlation across the blocks of k-values from the acquisition to be combined to maintain a SNR $\geq$ 0.5dB, and (3) to set the extent of k-space over which the power density of k-values present in the texture is desired.

[PARA 163] Blocks of sequential signal samples to be recombined for SNR improvement can be non-overlapping, or overlapping by a selected number of points, or a sliding block used so as to combine, for example, measures 1-4, 2-5, 3-6 and so on as will be described

subsequently. Additionally, the number of samples in each block may be varied from block to block across the extent in k-space of the acquisition, this variation in number of samples to be combined being determined by the requirement for sufficient correlation to maintain SNR sufficient to provide a robust measurement. The approximate noise level can be determined independently by several methods well known to the industry including measuring noise in the absence of signal input.

[PARA 164] Acquiring data with different magnitude gradients within one echo, TR, or scan may be accomplished with the successive gradient heights being selected to enable best SNR of the combined signal at the various targeted regions of k-space. To enable combination of sequential samples from the ADC to improve SNR, correlation among successive samples can be increased by proper choice of windowing in profile space, a shorter window driving a greater correlation distance across sequential values in k-space and a longer window resulting in lower sample to sample correlation. The window width selected is defined by both the desire for correlation across many samples in k-space, which dictates a shorter window, and the need to sample a sufficient extent of texture in real space to provide robust measure, especially when measuring highly amorphous textures.

[PARA 165] Post-acquisition combination of the signals acquired in k-space in blocks, the number of samples to be combined determined by the requirement that the correlation between the individual signals to be combined be sufficient to achieve a SNR $\geq$ 0dB (the level of correlation is determined by subject motion, gradient height, sampling rate, window shape, and the underlying texture.)

[PARA 166] Use of non-zero gradient acquisition may be employed to intentionally vary the direction and magnitude of the k-vector over a range during data acquisition, for the purpose of smoothing signal speckle—which will manifest as a time varying signal during the data acquisition—that results from interference of the varying phases and amplitudes of the individual spin signals. The selected variation in k-value direction and magnitude during data acquisition is chosen to provide sufficient combined measures to get a an estimation of the representative power within a neighborhood of k-space, with a SNR of 0dB, where the neighborhood is within 20% of the 3D orientation and magnitude of the centroid of the neighborhood.

[PARA 167] Correction for change in k across a set neighborhood created by application of a non-zero gradient may be accomplished by employing proscribed k encodes for a specific set of k measurement. Additionally, correlation within a set of k measurements acquired within a time period and from a selected VOI can be induced by selecting the time period such that the biological motion is sufficiently small that the phase shift in the data induced by patient motion is less than 50% of the wavelength corresponding to the targeted textural k-value range. Alternatively, a windowing function may be selected such that there is sufficient correlation between individual measurements and the set estimate that a desired SNR can be achieved.

[PARA 168] Details of the very-low SNR acquisition mode at even further expanded scale are shown in FIG. 13. In this portion of the sequence, the k-value is constant at an initial value 1114a, a second value 1114b induced by k value selection gradient pulse 1100a, a third value 1114c induced by k value selection gradient pulse 1100b and a fourth value 1114d induced by k value selection gradient pulse 1100c in the region 1116 where the sample gate is open thereby producing samples 1118. This is the previously described pulse sequence where multiple repeats of signal at the same k value are rapidly sampled, all of which are then combined into one estimate.

[PARA 169] Details of the low SNR acquisition at the further expanded scale are shown in FIG. 14. In this portion of the sequence, notice that the k-values do change as shown by trace segment 1120, albeit slowly, due to the non-zero time-dependent phase-encode gradient 1106 present during the recording of the region 1122 when the sample gate is open. However, the range of samples1124 across k-space is a relatively compact neighborhood where the values are highly correlated due to the windowing function.

[PARA 170] Details of the high SNR acquisition at the further expanded scale are shown in FIG. 15. In this portion of the sequence, the k-values again change as shown by trace segment 1126, due to the non-zero time-dependent phase-encode gradient 1112 present during the opening of the sample gate in region 1128. The range of samples 1130 across K-space is still a relatively compact neighborhood, but outside the inter-sample correlation imposed by the window function.

[PARA 171] The low SNR and high SNR acquisition modes with non-zero gradient are distinct from a standard frequency-encoded MRI sequence as the applied gradient is not used to establish a position, i.e. frequency encoding, but as a time dependent phase encode to rapidly acquire a number of individual samples across a relatively broader neighborhood of k-space.

[PARA 172] As previously asserted, gradient acquisition can be acquired in one echo rather than in multiple echoes as seen FIG. 16. Again the illustrated pulse sequence for selecting the desired VOI and initial phase wrap for k is as described in FIG. 3 and is numbered consistently in FIG.16.

[PARA 173] As seen in FIG. 16 and at larger scale in FIG. 17, the k-value is constant at an initial value 1614a, a second value 1614b induced by k value selection gradient pulse 1600a and a third value 1614c induced by k value selection gradient pulse 1600b. Note that the k values are decremented as opposed to incremented in the example of FIG. 12. This is again the previously described pulse sequence where multiple repeats of signal at the same K value are rapidly sampled 1622a, 1622b and 1622c, all of which are then combined into one estimate.

[PARA 174] In a second portion of the sequence, within the same echo, the k-values do change as shown by trace segment 1620, albeit slowly, due to the non-zero time-dependent phase-encode gradient 1606 present during sampling. However, the range of samples1624 across k-space is a relatively compact neighborhood where the values are highly correlated.

[PARA 175] In a third portion of the sequence, again still within the same echo, high SNR acquisition is conducted. The k-values again change as shown by trace segment 1626, due to the non-zero time-dependent phase-encode gradient 1608 present during the opening of the sample gate. The range of 1628 across k-space is still a relatively compact neighborhood but outside the inter-sample correlation imposed by the window function.

[PARA 176] As seen in FIG. 18 (and in larger scale in FIG. 19), where the illustrated pulse sequence for selecting the desired VOI and initial phase wrap for k is as described in FIG. 3 and is numbered consistently in FIG. 18, a low non-zero magnitude gradienvast 1802 acting as a time dependent phase encode is applied and data samples 1804 are taken from an initial k-value 1806 for slowly time varying k-values, seen in trace segment 1808, having

high correlation as previously described. The initial phase wrap may be selected to provide an initial k-value with a magnitude corresponding to a low SNR region.

[PARA 177] Similarly, as seen in FIG. 20 (and in larger scale in FIG. 21), a pulse sequence for selecting the desired VOI and initial phase wrap to set the k-value region is illustrated and is as described in FIG. 3 and is numbered consistently in FIG. 20. A higher non-zero gradient 2002 acting as a time dependent phase encode is applied and data samples 2004 are taken from an initial k-value 2006 for more rapidly time varying k-values, seen in trace segment 2008. The initial phase wrap may be selected to provide an initial k-value with a magnitude corresponding to a higher SNR region. The encoding gradient 326 may be employed to wind up to the lowest or highest k-value in a targeted texture and the non-zero magnitude gradient pulse is imposed in the necessary direction (increasing or decreasing k) to reach the other limit in k-space to define the texture.

[PARA 178] The acquired samples may be outside the inter-sample correlation imposed by the window function. However, signal levels for the k-values are relatively large and have high SNR. Additionally as previously described, rapid acquisition of samples in subsets 2010a, 2010b, 2010c and 2010d as exemplary, may be accomplished in a manner that the samples within the subset may remain sufficiently correlated and may provide desired data in structures having predetermined or anticipated texture. One can combine however many sequential values are correlated enough to yield an improvement in SNR via the combination (averaging being one simple form of combining). Then, the set of combined data points is used to characterize the power distribution across the entire acquisition, to get a better measure of the underlying texture within the VOI.

[PARA 179] As previously discussed, rephrasing separate low and high k values based on low phase change in a second 90-180-180 excitation (TR). SNR is maximized with gradient ON acquisition by smart combination of successive k-value samples through reregistration of successive acquired signals. Data is acquired across a range of k-space for which the wavelengths are sufficiently long that subject motion can be easily corrected for by reregistration—i.e. the phase shift induced in the measure in this k range is much less than the textural wavelength. The low k-value signal is sampled in alternate refocusing sequences, or sequential excitations (TR), with the acquisition of the signal from the higher k-value range of interest. TE long wavelength measure is used to determine the motion-

induced phase shift across the measurements. That phase shift is then applied to the higher k-data prior to reregistration.

[PARA 180] A number of correlations are implied by spatial windowing.

[PARA 181] If g(x) corresponds to a 1D (real-valued) signal, the corresponding function in K-space is given by the Fourier transform as:

$$G(2\pi k) = \int_{-\infty}^{\infty} g(x)e^{-j2\pi xk}dx \qquad (1)$$

Which is frequently expressed as a Fourier pair as

$$g(x) \Leftrightarrow G(2\pi k) \qquad (2)$$

[PARA 182] Windowing is the process of limiting the extent of g(x) to a finite region of compact support, but doing it in such a way to minimize spectral artefacts due to discontinuities (artificially) introduced by the truncation.

[PARA 183] Despite the specific shape used of the window function, there is an inverse relationship between the width of the window, and its spectrum. This is due to the Fourier relationship

$$h(\alpha x) \Leftrightarrow \frac{1}{|\alpha|} H\left(\frac{2\pi k}{\alpha}\right) \qquad (3)$$

[PARA 184] Multiplying two functions has the effect of convolving their respective spectra, i.e.

$$f(x) := g(x)h(x) \Leftrightarrow F(2\pi k) = G(2\pi k) * H(2\pi k) \quad (4)$$

[PARA 185] The convolution can be thought of as a linear filtering of the spectrum as though the spectrum was the input signal

[PARA 186] The term $H\left(\frac{2\pi k}{\alpha}\right)$ acts like a low-pass filter to the $G(2\pi k)$ spectrum, which tends to smooth out the signal: the larger the value of α, the narrower the low-pass filter. This creates a significant correlation between adjacent values of $F(2\pi k)$.

[PARA 187] Estimators which observe noisy samples of a filtered input are well studied and can be applied to generate optimal estimates; Weiner filters, Kalman filters, etc.

[PARA 188] Dynamic acquisition modes may be employed wherein:

X corresponds to a 3D vector in image space,

g(X) corresponds to the value of the image at a given 3D spatial location,

K corresponds to the 3D vector,

G(**K**) corresponds to the value in k-space of the image g.

[PARA 189] For initial simplicity, the time-dependency of this signal is ignored which in turn depends upon T1, T2, $T2^*$, as well as signal contribution due to differing isochromats (different chemical species within the Volume) etc. In the sequel the effect of these is taken into account

[PARA 190] Basic Principles relied upon are:

Generally, SNR of G(K) is highest at $|\mathbf{k}|=0$, then decreases with increasing $|\mathbf{k}|$

The rate at which SNR decreases is typically expressed as SNR $\propto|\mathbf{k}|^{-\alpha}$ where α is in the range of 1-3.

The sampling rate, combined with the magnitude of the gradient will set the sample spacing (Δk) density in k-space for a given VOI.

As the gradient magnitude is decreased, the sample density increases (i.e. Δk decreases).

Depending upon the size of the windowing in image space, there is a corresponding correlation implied.

[PARA 191] For a generalized case the simplified MRI relationship between spatial coordinates and K-space given by

$$S(\mathbf{k}) = \iiint_{\mathbb{R}^3} I(\mathbf{r}) e^{-j2\pi \mathbf{k}\cdot\mathbf{r}} d\mathbf{r} \qquad (6)$$

Where

r represents the real valued 3-Dimensional spatial coordinates with units of meters (m).

I(**r**) represents the image which is a non-negative Real function of spatial coordinates **r**.

k represents the real valued 3-Dimensional k-space coordinates with units in cycles/meter (m^{-1})

S(**k**) represents the Fourier Transform of $I(\mathbf{r})$ and is generally a complex-valued function of **k**

And the integral is over the entire 3-Dimensional spatial plane.

[PARA 192] In words, S(**k**)represents the corresponding value in 3-dimensional k-space of the image function*I*(**r**).

[PARA 193] The k-space coordinates, in turn, are a function of time and have the general form

$$\mathbf{k}(t) = \gamma \int_{-\infty}^{t} \mathbf{g}(\tau) d\tau \qquad (7)$$

Where

γ is the proton gyromagnetic ratio with value 42.576MHz/T

g(t) is a real-valued 3-Dimensional function of time representing the gradient strength with units in T/m. This function, is a design input as part of the pulse sequence whose purpose is to manipulate the proton spins in some desired way.

[PARA 194] The integral in equation (7) indicates that the value of **k**(t) for a given value of *t*, is computed as the integral of all previous history of the gradient function. While technically correct, it is often more convenient to express this as

$$\mathbf{k}(t) = \gamma \int_{t_0}^{t} \mathbf{g}(\tau) d\tau + \mathbf{k}(t_0) \qquad (8)$$

[PARA 195] Where now t_0 represents a convenient starting time, $\mathbf{k}(t_0)$is the corresponding k-value at t_0, and the lower limit of the integral starts at t_0.

[PARA 196] Making the dependence on time more explicit, equation (6) can be expressed as

$$S(t) = \iiint_{\mathbb{R}^3} I(\mathbf{r}) e^{-j2\pi \mathbf{k}(t)\cdot\mathbf{r}} d\mathbf{r} \quad t \geq t_0 \qquad (9)$$

$S(t)$ represents the complex-valued baseband signal one might obtain during an MRI echo experiment which is played in conjunction with a gradient sequence encoded in**g**(t).

[PARA 197] Without loss of generality, **k**, **g** and **r** can be decomposed into Cartesian components as

$$\mathbf{k} = \begin{bmatrix} k_x & k_y & k_z \end{bmatrix}^T$$
$$\mathbf{g} = \begin{bmatrix} g_x & g_y & g_z \end{bmatrix}^T$$
$$\mathbf{r} = \begin{bmatrix} r_x & r_y & r_z \end{bmatrix}^T \qquad (10)$$

And express (9) as

$$S(t) = \int_{-\infty}^{\infty} \int_{-\infty}^{\infty} \int_{-\infty}^{\infty} I(r_x, r_y, r_z) e^{-j2\pi\left(k_x(t) r_x + k_y(t) r_y + k_z(t) r_z\right)} dr_x dr_y dr_z \quad t \geq t_0 \qquad (11)$$

[PARA 198] In general **k**(t) represents a curvilinear path within K-space as a function of time.

[PARA 199] Initially, to facilitate explaining the initial concept, evaluation is confined along a single dimension by assuming $\mathbf{k(t)} = [k_x(t)\ 0\ 0]^T$. Equation (11) then simplifies to

$$S(t) = \int_{-\infty}^{\infty} \rho(r_x) e^{-j2\pi k_x(t) r_x} dr_x \quad t \geq t_0 \tag{12}$$

Where

$$\rho(r_x) = \int_{-\infty}^{\infty} \int_{-\infty}^{\infty} I(r_x, r_y, r_z) dr_y dr_z \tag{13}$$

And equation (8) reduces to

$$k_x(t) = \gamma \int_{t_0}^{t} g_x(\tau) d\tau + k_x(t_0) \tag{14}$$

Define

$$R(k) := \mathcal{F}\{\rho(x)\}(k) = \int_{-\infty}^{\infty} \rho(x) e^{-j2\pi kx} dx \tag{15}$$

Which is occasionally expressed as

$$R(k) \Leftrightarrow \rho(x) \tag{16}$$

To concisely indicate that $R(k)$ and $\rho(x)$ are Fourier Transform pairs. By comparing (12) to (15), it can be seen that $S(t)$ is just a time dependent progression across various Fourier coefficients represented by

$$S(t) = R(k(t)) \tag{17}$$

Where the mapping between the time-value *t* and the corresponding K-space coordinate is given by equation (14).

[PARA 200] To generally model the receive signal In an actual MRI machine, a combination of the desired signal and noise received by the antenna. That signal is then filtered, amplified, down-converted, sampled, and quantized.

[PARA 201] The specific details are machine-dependent, but a simple model can be developed to represent the output of the machine as follows:

[PARA 202] Let $Y(t)$ represent a combination of the signal of interest, and a noise signal as

$$Y(t) = S(t) + W(t) \tag{18}$$

Where

$S(t)$ is given in equation (17) and

$W(t)$ is a complex-valued zero-mean, Additive White Gaussian Noise Process with variance σ_w^2, i.e. $E\{W(t)\} = 0$ and $E\{W(t)W^*(t+\tau)\} = \sigma_w^2 \delta(\tau)$

[PARA 203] The received signal $Y(t)$ is then uniformly sampled

$$Y_n = Y(t)\big|_{t=n\cdot\Delta t} = R(k(t))\big|_{t=n\cdot\Delta t} + W(t)\big|_{t=n\cdot\Delta t} \tag{19}$$

Which can be expressed more simply as

$$Y_n = R(k_n) + W_n \tag{20}$$

Where the sequence k_n is given by

$$k_0 = k(t)\big|_{t=0}$$
$$k_{n+1} = k_n + \gamma \int_{n\Delta t}^{(n+1)\Delta t} g(\tau)\, d\tau \tag{21}$$

[PARA 204] Define

$$\Delta k_{n+1} = \gamma \int_{n\Delta t}^{(n+1)\Delta t} g(\tau)\, d\tau \tag{22}$$

Then (21) can be simply expressed as

$$k_0 = k(t)\big|_{t=0}$$
$$k_{n+1} = k_n + \Delta k_{n+1} \tag{23}$$

[PARA 205] In words, then, the sequence k_n is defined by a sequence of increments which is determined by the integral between samples of the gradient function.

[PARA 206] Equations (20), (22) and (23) may be employed to describe the signals under different gradient conditions disclosed herein.

[PARA 207] Collecting samples of an echo which has been "pre-phased" through some gradient activity before-hand, but now the gradient is no longer held to zero as described above with respect to FIGs. 12, 14 and 15 can be analyzed as follows.

[PARA 208] The signal is then given by equation (20) as

$$Y_n = R(k_n) + W_n \tag{24}$$

And k_n is given by equation (21) as

$$k_0 = k(t)\Big|_{t=0}$$
$$k_{n+1} = k_n + \gamma \int_{n\Delta t}^{(n+1)\Delta t} g(\tau)\, d\tau \tag{25}$$

[PARA 209] Since, measurement is occurring in a non-zero gradient regime, the integral term is no longer zero, which implies that the sequence k_n is no longer constant, and in turn the sequence $R(k_n)$ is no longer constant.

[PARA 210] Since no assumptions have been made on the underlying structure of $I(\mathbf{r})$, it cannot be implied that there is any particular structure or relationship amongst the values of $R(k_n)$. This puts us at a distinct disadvantage when wanting to estimate useful signals in a very low SNR environment.

[PARA 211] A structure may be imposed on the values of $R(k_n)$ by applying a multiplicative window function in the image domain. This is accomplished by leveraging two Fourier Transform identities:

Multiplication in one domain corresponds to convolution in the reciprocal domain.

Define the following Fourier Pairs:

$$\nu(x) \Leftrightarrow N(k)$$
$$\rho(x) \Leftrightarrow R(k)$$
$$\zeta(x) \Leftrightarrow Z(k) \tag{26}$$

Then, the product in one domain corresponds to convolution in the reciprocal domain:

$$\nu(x) = \rho(x)\zeta(x) \Leftrightarrow N(k) = R(k) * Z(k) \tag{27}$$

[PARA 212] Scaling in one domain corresponds to an inverse scaling in the reciprocal domain.

If $\zeta(x) \Leftrightarrow Z(k)$ then

$$\zeta\left(\frac{x}{a}\right) \Leftrightarrow |a| Z(a \cdot k) \tag{28}$$

[PARA 213] Windowing functions are typically used to limit the image space to a finite, compact region of interest, while at the same time, minimizing the adverse consequences on the corresponding image spectrum due to the window itself. Those skilled in the art will appreciate there are a wide variety of window functions which have been developed, each of which have their own particular set of characteristics.

[PARA 214] For sake of illustration, consider the most basic window function:

$$rect(t) = \Pi(t) = \begin{cases} 0 & |t| > \frac{1}{2} \\ \frac{1}{2} & |t| = \frac{1}{2} \\ 1 & |t| < \frac{1}{2} \end{cases} \tag{29}$$

The corresponding Fourier transform is given by

$$F\{\Pi(t)\} = \int_{-\infty}^{\infty} \Pi(t) e^{-j2\pi ft} dt = \frac{\sin(\pi f)}{\pi f} = \mathrm{sinc}(f) \tag{30}$$

which is frequently expressed as the Fourier pair

$$\Pi(t) \Leftrightarrow \mathrm{sinc}(f) \tag{31}$$

Using equation (28) a slightly generalized version and its Fourier pair is

$$\Pi\left(\frac{t}{T}\right) \Leftrightarrow |T| \mathrm{sinc}(Tf) \tag{32}$$

Using equation (27), the windowed profile and Fourier pair is

$$v(x) = \Pi\left(\frac{x}{X}\right) \rho(x) \Leftrightarrow N(k) = |X| \mathrm{sinc}(Xk) * R(k) \tag{33}$$

Using equation (24) as a reference, the sampled MRI signal can be expressed as

$$Y_n = N(k_n) + W_n \tag{34}$$

Which, using (33), can be expanded as

$$Y_n = \int_{-\infty}^{\infty} |X| \operatorname{sinc}(Xq) R(k_n - q) dq + W_n \tag{35}$$

Where the convolution integral has been specifically expanded.

[PARA 215] The value of the convolution integral taken at k_n is no longer a function of just one point of $R(k_n)$. For each point k_n the convolution integral computes a weighted sum of the values of $R(k)$ centered around k_n The extent of the neighborhood in k-space is inversely proportional to the parameter X : Smaller values of X increase the width of the neighborhood in k-space.

[PARA 216] For the embodiments herein the extent of the domain of values of interest correspond to the collection of k-space values $k_0, k_1, k_2, \cdots k_{N-1}$. Define

$$\begin{aligned} k_{\min} &= \min_n k_n \\ k_{\max} &= \max_n k_n \end{aligned} \tag{36}$$

Which in turn are functions of the time interval Δt and the function $g(\tau)$.

[PARA 217] For example, making a simplifying assumption that $g(\tau) = G$ where G is a positive constant, then k_n is just a uniform sampling across a portion of k-space, and is given by

$$k_n = k_0 + nG\Delta t \tag{37}$$

Then $k_{\min}$ and $k_{\max}$ is given by

$$\begin{aligned} k_{\min} &= k_0 \\ k_{\max} &= k_0 + (N-1)G\Delta t \end{aligned} \tag{38}$$

[PARA 218] While a simple sampling of k-space may be chosen, it is not specifically required. Indeed there could be applications where non-uniform and/or even non-monotonic sampling strategies could be useful.

[PARA 219] Ideally, the parameter X (and the window function) are chosen so that the resulting weighted sum across the neighborhood of k_n is "wide enough" so that $N(k_n) \approx C$

where C is a complex-valued constant, but not so wide so as to lose significant spectral resolution

[PARA 220] For purposes of the disclosed embodiments herein a "small" non-zero gradient may be determined based on selection of desired windowing. From equation (10)

$$R(k) := \mathcal{F}\{\rho(x)\}(k) = \int_{-\infty}^{\infty} \rho(x) e^{-j2\pi kx} dx \tag{41}$$

[PARA 221] Assume that the nominal center point of the profile has shifted to be centered around a point x_0. This results in

$$R_{x_0}(k) := \int_{-\infty}^{\infty} \rho(x - x_0) e^{-j2\pi kx} dx = e^{-j2\pi kx_0} R(k) \tag{42}$$

Which indicates that each point in k-space is rotated in complex space proportional to the offset x_0.

[PARA 222] It can be assumed that the gradient is a positive constant, then, by equation (39)

$$k_n = k_0 + nG\Delta t \tag{43}$$

Substituting in (42) produces

$$R_{x_0}(k_n) = e^{-j\theta_0} e^{-jn\Delta\theta} R(k_n) \tag{44}$$

Where the initial phase offset θ_0 and the phase increment $\Delta\theta$ is given by

$$\theta_0 := -2\pi k_0 x_0$$
$$\Delta\theta := -2\pi G \Delta t x_0 \tag{45}$$

[PARA 223] In the event that, due to the application of a properly specified windowing function, $R(k_n) \approx C$ a complex constant within the neighborhood, the post-acquisition estimator would first multiply an offsetting phase increment $e^{jn\Delta\theta}$ to each acquired sample of $R_{x_0}(k_n)$ before combining and generating the final estimate.

[PARA 224] An estimate of $\Delta\theta$ can be obtained from a sequence of k-space samples taken of the windowed profile over lower k-values (where the SNR is higher).

[PARA 225] Correlation may be induced by windowing as one parameter as discussed previously. Multiplication of the profile $\rho(x)$ by a real-valued window function $\zeta(x)$ corresponds to convolution in k-space by the Fourier relation

$$\nu(x)=\rho(x)\zeta(x)\Leftrightarrow N(k)=R(k)*Z(k) \tag{46}$$

[PARA 226] $Z(k)$ is treated as an impulse response of a linear filter which is applied to the complex-valued signal $R(k)$ in k-space to produce a complex-valued output signal $N(k)$.

[PARA 227] The autocorrelation function of the output signal $R_{NN}(\kappa_1,\kappa_2)$ can be expressed as a function the autocorrelation of the input signal $R_{RR}(\kappa_1,\kappa_2)$, and the impulse response $Z(k)$ as

$$R_{NN}(\kappa_1,\kappa_2)=\int_{-\infty}^{\infty}\int_{-\infty}^{\infty}R_{RR}(\kappa_1-\alpha,\kappa_2-\beta)Z(\alpha)Z(\beta)d\alpha d\beta \tag{47}$$

[PARA 228] Equation (47) is inconvenient because the autocorrelation function of the underlying signal $R_{RR}(\kappa_1,\kappa_2)$ is not usually known. A simplifying assumption is made that $R(k)$ is a white-noise, wide-sense stationary process, and express the autocorrelation as

$$R_{RR}(\kappa_1,\kappa_2)=\sigma_R{}^2\delta(\kappa_1-\kappa_2) \tag{48}$$

With this assumption, (47) reduces to

$$R_{NN}(\kappa_1,\kappa_2)=\sigma_R{}^2R_{ZZ}(\kappa_2-\kappa_1) \tag{49}$$

Where $R_{ZZ}(\kappa)$ is the autocorrelation function of the impulse response $Z(k)$ and is given by

$$R_{ZZ}(\kappa):=\int_{-\infty}^{\infty}Z(k)Z(k+\kappa)dk \tag{50}$$

[PARA 229] The mapping of k vs time is mapped as follows.

$$k_n = k_0 + nG\Delta t \tag{51}$$

The normalized correlation

$$\eta(NG\Delta t) := \frac{R_{NN}(k_0, k_0 + NG\Delta t)}{R_{NN}(k_0, k_0)} = \frac{R_{ZZ}(NG\Delta t)}{R_{ZZ}(0)} \tag{52}$$

measures the degree to which the underlying sample points are correlated. In low SNR regimes, a high correlation is desired across all of the samples and therefore establish a lower bound:

$$\eta_{\min} \le \frac{R_{ZZ}(NG\Delta t)}{R_{ZZ}(0)} \tag{53}$$

[PARA 230] Equations (50) and (53) provide the defining relationship between the window function impulse response $Z(k)$, the gradient strength G, the sample interval Δt, the number of samples N, and the correlation lower bound $\eta_{\min}$.

[PARA 231] For example, assume that the window function is defined to be

$$\zeta(x) = \Pi\left(\frac{x}{X}\right) \tag{54}$$

Where $\Pi(x)$ is a standard so-called rectangular function defined below, and X is a constant.

$$\Pi(x) = \begin{cases} 0 & |x| > \frac{1}{2} \\ \frac{1}{2} & |x| = \frac{1}{2} \\ 1 & |x| < \frac{1}{2} \end{cases} \tag{55}$$

[PARA 232] The impulse function $Z(k)$ is given by the Fourier transform

$$Z(k) = |X| \frac{\sin(\pi X k)}{\pi X k} = |X| \operatorname{sinc}(Xk) \tag{56}$$

[PARA 233] The corresponding normalized correlation function $\eta(\kappa)$ is given by

$$\eta(\kappa) = \operatorname{sinc}(X\kappa) \tag{57}$$

[PARA 234] Restricting the correlation to be lower bounded by $\eta_{\min} = 0.95$ then, by (53) the condition arises that

$$\eta_{\min} \le \operatorname{sinc}\left(X \cdot N \cdot G \cdot \Delta t\right) \tag{58}$$

This can be approximated using the first two terms of a Taylor series as

$$\frac{\sin(\theta)}{\theta} \approx 1 - \frac{\theta^2}{3!} \tag{59}$$

Which can be inverted and applied to (58) to produce

$$N \cdot G \cdot \Delta t \le \frac{\sqrt{3!(1-\eta_{\min})}}{\pi X} \tag{60}$$

Which now explicitly expresses an upper bound on the product of the gradient strength G, the sample interval Δt, and the number of samples N.

[PARA 235] Typically the sample interval Δt, and the number of samples N are determined by other considerations. Taking these as given, the maximum gradient level is then given by

$$G \le \frac{\sqrt{3!(1-\eta_{\min})}}{\pi X \cdot N \cdot \Delta t} \tag{61}$$

[PARA 236] For a non-zero gradient data acquisition in this case, as long as the gradient G is below the calculated upper bound, the samples acquired will have the defined correlation level. This condition as defined for purposes herein as a “small gradient” level.

[PARA 237] Sampling past this limitation will result in lower sample correlation and therefore have less of a potential post acquisition SNR gain. A ”higher” gradient may be defined as operating in this condition. Gradient determination is affected by a number of parameters including (1) choice of the window function (e.g. rectangular, Tukey, Hamming, etc.) which influences the shape (and to a certain extent, the width) of the “main lobe” in the impulse response, (2) choice of window extent (the larger the extent in the profile domain, the narrower the “main lobe” in the impulse response), (3) the impulse response which may create an autocorrelation function, (4) the desired level of correlation which determines the effective width in k-space, within which the samples must be contained, and (5) sampling rate*Number of samples*gradient size which determines the

actual sampling neighborhood size (note, as long as this number is bounded by the number contained in element (4)) the gradient remains in the "lower gradient level" regime.

[PARA 238] An exemplary embodiment maintains a constant ratio of textural wavelength to length of VOI acquisition axis. As the targeted k-value varies, the length of the VOI acquisition axis is varied such that the ratio of the corresponding textural wavelength to the acquisition length remains constant. The aim here is to keep the number of textural "cells" sampled constant. In this way the differential broadening observed at specific points in k-space, Δk, is expected to arise from sources other than sampled length in real space, such as the finite width of the RF pulse or the edges of the gradient pulse.

[PARA 239] MR-based diagnostic Techniques may be combined. Certain MR-based techniques designed to look at very fine tissue structure provide data that may be difficult to interpret in certain pathologies, as they provide only an indirect measure of the underlying structures. Diffusion weighted imaging and Magnetic Resonance Elastography (MRE) are two such techniques. The method of this provisional filing is a direct measure and hence would provide, in many cases, a better measure of fine texture, and in some cases provides complementary data to increase diagnostic capability. Combining acquisition techniques can provide more robust measure of texture, and hence of pathology.

[PARA 240] The embodiments disclosed may be used in combination with Magnetic Resonance Elastography (MRE). Currently, the main application of MRE is as a diagnostic for liver disease to determine therapy response, progression, need for biopsy, etc. Though the targeted pathology is fibrotic development, the technique measures this indirectly, through measurement of tissue stiffness. In many cases, it is difficult to distinguish fibrotic development from other stiffness-inducing conditions such as portal hypertension and inflammation. Further, hepatic iron overload, which often results from a compromised liver, will lead to low signal, hence inadequate visualization of the induced mechanical waves.

[PARA 241] The method disclosed herein can provide direct measure of fibrotic development in the liver and, as such, would provide additional data on disease progression or response to therapy in the case of the various triggers of fibrotic liver disease. It provides a local measure within the targeted anatomy for calibration of other, indirect measures, such as MRE, DTI, DWI, etc.

[PARA 242] The embodiments disclosed may be used in combination with, or replacement for, diffusion weighted imaging in tumors. The ability to detect the edge of tumors with high accuracy would facilitate accurate surgical removal. Can acquire data using the method disclosed herein in VOIs along a direction through a tumor region looking for the edge of the region of angiogenic vasculature.

[PARA 243] The ability to measure inside of tumors to gauge therapy response would help in targeting intervention. As an example of the latter, immunotherapy treatment of melanoma tumors induces swelling of the tumor due to T-cell infiltration which, on a structural MR scan, looks similar to malignant tumor growth. Hence, it is difficult to decide whether to continue the therapy. The ability to look at the state of the vasculature within the tumor would enable discernment of whether the growth was cancerous or due to immune system response. The method disclosed herein would also provide local calibration of the currently used DTI measures, which are often difficult to interpret.

[PARA 244] The embodiments disclosed may be used as a bone degradation measure in oncology. It is well known that radiation and/or chemotherapy often compromise bone health. A measure of changes to bone resulting from cancer therapy would help in tailoring therapy and determine if there is need for intervention to protect bone health.

[PARA 245] Currently, as a follow on to surgery and treatment for breast cancer, patients are routinely put in the MR scanner to image the breast tissue. The sternum is within the field of view for such exams, enabling easy application of a short add-on sequence of this method to measure changes to trabecular bone and thus obtain a measure of bone health.

[PARA 246] As further examples of potential use of the method disclosed herein in oncology, the embodiments disclosed may be used to measure and quantify hyperplasiac development of mammary duct growth in response to tumor formation and development or to measure and quantify angiogenic growth of vasculature surrounding tumors to stage development, type, and response to therapy. Ongoing treatment after breast surgery often involves reducing estrogen levels, further compromising bone health and, as such, referral for MR scans for bone monitoring is common; use of the method of disclosed herein would enable robust and detailed evaluation of bone health by direct measurement of the trabecular bone structure.

[PARA 247] The disclosed embodiments are also complementary with Big Data and machine learning schemes. The method disclosed also complements the trend towards use of comparison among large aggregates of medical data to learn more about disease, increase predictive power for individual patients and for specific diseases, and note trends across various populations. Benefits of using the method of this filing in conjunction with Big data/ machine learning include:

instead of 20 instances of the output of the method disclosed herein compared over a population of unknown pathology, for example, k-value distribution vs. fracture in femur may be evaluated, or changing k-values in cortical neuron bundles can be measured and correlated with performance on Alzheimer's mini-mental state exams or other assessment of AD, or the local k-values in liver compared with other inferences of liver disease over a huge population;

use of machine learning over large populations enables determination of specific biomarkers in pathology;

the ability to make useful correlations in big data gets much better with high SNR measure input such as that provided by the method of the embodiments disclosed;

such machine learning can indicate, for example, if a disease is defined by appearance of a specific k-value appearing in the diseased tissue.

[PARA 248] In advance of the macroscopic pathology attendant with disease development, pathological changes occur near the cellular level in affected tissue. For instance, in bone diseases, fracture is often the downstream effect of ongoing progressive thinning of the trabecular elements. In soft tissue diseases, such as liver disease, fibrotic structures develop over a long time in the affected organ, leading eventually to cirrhosis. And in neurology, tissue textures in the brain, in both white and grey matter, change in response to disease onset and progression. The ability to measure the early-stage changes in disease, those affecting fine tissue textures, will enable early stage diagnosis, thus enabling earlier treatment, subject targeting for trial inclusion, and sensitive monitoring of therapy response.

[PARA 249] The methods introduced herein enable this direct and sensitive measure of tissue texture, through its ability to provide clinically robust measure of the pathologic

changes in tissue textures attendant with disease onset and with early-stage progression, providing the needed diagnostic capability.

[PARA 250] One of the most valuable features of the disclosed method is that it can be used in conjunction with most contrast methods applied in MRI. As the method results in a texture measurement, as opposed to an image, it needs only to have contrast between the tissue textural elements. This contrast can be generated in many ways, selected to optimize tissue contrast in specific pathologies. The tissue texture measurement yields high spatial resolution due to its relative immunity to subject motion. As the acquisition time for the methods previously disclosed herein is short, the data can be acquired interspersed with image acquisition in various sequences.

[PARA 251] For instance, in bone, for which there is effectively no signal from the trabecular bone elements themselves, a standard T1 pulse sequence, which yields high signal from fat, provides the requisite high contrast between bone and marrow. Thus, the texture measurement employing the methods herein can yield high sensitivity in bone when applied with T1 contrast. T2 contrast can be used to highlight fluid towards determining if a bone lesion is lytic or sclerotic, as there may be little fat remaining around the calcified bone to provide signal. T2 weighted imaging has a host of applications, including abdominal lesion imaging, imaging of iron deposition in the brain, and cardiac imaging, hence use in conjunction with the methods previously disclosed herein enables highlighting of tissue texture in these organs/pathologies.

[PARA 252] MRI contrast generation has become increasingly sophisticated over time. In addition to exogenous contrast agents, such as gadolinium, and the standard T1, T2, T2*, proton density contrast, fat suppression, Inversion Recovery sequences as examples. Many new contrast techniques, often dependent on functional contrast, have been developed to highlight different tissues involved in pathology. MR angiography, a method of visualizing vasculature and blood flow, makes use of MR signal saturation, or induced phase contrast in flowing blood, to assess vascular density and permeability. BOLD (Blood Oxygenation Level Dependent) contrast uses metabolic changes in blood to image active brain regions. Diffusion weighting, both DWI (Diffusion Weighted Imaging) and DTI (Diffusion Tensor Imaging), is used to assess pathology in an increasing range of diseases, providing a signal reflective of the microscopic state of the targeted tissue. ASL (Arterial Spin Labelling),

traces the diffusion of magnetically-labelled blood (endogenous contrast) through the brain to assess pathology. Perfusion imaging is used to assess blood microcirculation in capillaries, another measure of functional response. In both these contrast schemes, the time-course of blood flow, is followed to assess the state of the vasculature near a tumor, as this is a key feature in the diagnosis of gliomas. Blood vessels are present in higher numbers within tumors than in normal brain tissue, and they tend to have a larger volume. Higher-grade tumors also tend to have higher blood volume, and the degradation and remodeling of extracellular matrix macromolecules results in loss of blood-brain barrier integrity, which is seen as contrast leakage. These measures can capture the degree of tumor angiogenesis, an important biologic marker of tumor grade and prognosis, particularly in gliomas. Application of the methods disclosed herein near the peak of the signal contrast would provide a direct measure of the density and size of blood vessels providing direct measure of the fine-scale vasculature texture as correlational data robustly measuring the degree of angiogenesis within or in the vicinity of the tumor. Combined in this way, a robust measure of pathologic vasculature development for staging neuropathology such as stroke and tumor can be made.

[PARA 253] As an example, diffusion weighting in its simplest form, DWI, uses the random Brownian motion of water molecules to generate contrast in an MR image. The correlation between pathology (histology) and diffusion is complex but, generally, densely cellular tissues exhibit lower diffusion coefficients. Obstacles such as macromolecules, fibers, and membranes also affect water diffusion in tissue. Water molecule diffusion patterns can therefore reveal microscopic details about tissue state. By measuring the differential rate of water diffusion across a region of tissue, a map of diffusion rates, reflecting local pathology, can be produced. Diffusion weighting is particularly useful in tumor characterization, vasculature typing, and diagnosing/monitoring cerebral ischemia, among other pathologies. Ischemic infarcts within the brain, abscesses, and certain tumors result in highly restricted diffusion; cysts and edema offer little restriction to diffusion.

[PARA 254] Diffusion imaging presents several problems with data interpretation, the most salient of which are: 1) the long diffusion gradients increase the echo time, TE, reducing SNR, 2) the high diffusion gradients required result in eddy currents in metal surfaces in the scanner, which cause signal distortion, 3) the low signal amplitude

necessitates use of a relatively large voxel, on the order of 2.5mm on a side, hence low resolution, 4) the sequence, by design, is highly sensitive to motion, so data recording must be very fast; hence, the ability to increase SNR by averaging signal from multiple acquisitions is limited. Additionally, as at least six different directions are needed to determine fractional anisotropy (FA) the motion sensitivity can lead to difficulty in data interpretation across the course of the acquisition. 5) Interpretation of diffusion weighted signals is not straightforward. The measured diffusion coefficients can arise from many sources, as the exact mechanisms governing water diffusion processes in tissues, especially in the brain, are not clearly understood. What is inferred from the measurement regarding the barriers and restrictions to free diffusion is based on certain assumptions about the underlying tissue pathology. This can take many forms, involving cell membranes, organelles, cell spacing, axon density, glial density, myelin state, etc. 6) Each DWI voxel represents an average, the standard voxel size being on the order of 2 to 2.5mm on a side. In order to interpret changes in the Average Diffusion Coefficient (ADC) within the voxel, certain assumptions are made, such as tissue homogeneity and type of structure causing the diffusion variation.

[PARA 255] The methods disclosed herein entail acquisition within either a single VOI or within multiple, interleaved VOIs, within one TR. Data is acquired without use of a spatial encoding gradient to form an image. This significantly shortens the acquisition time and, combined with the narrowly targeted acquisition in k-space, enables acquisition of the requisite data fast enough to provide immunity to subject motion. Though multiple measures of single volume acquisition can be mapped across the anatomy under study, each measure is acquired rapidly within a single volume. High SNR is assured by this single volume technique as, before motion effects set in, there is time for repeat measure of each targeted k-value. The number of repeats and number of/range of k-values for which data is acquired is limited by the requirement to keep the acquisition fast enough to provide the requisite motion immunity.

[PARA 256] The high motion sensitivity of standard DWI, the fact that it is an indirect, or inferred, measure, and its low SNR combine to make it not as robust a measure as would be desired in a clinical setting. Use of the methods disclosed herein for data acquisition when using diffusion contrast can mitigate the motion problem as, though the echo time is still

long, data acquisition is fast enough that the motion blurring of the signal is minimized. Further, additional data can be acquired by the disclosed methods during the scan, relying on contrast such as T1 or T2 weighting. The standard DWI images, diffusion weighted acquisition by the methods disclosed herein, and data acquired by those methods using contrast, can all be input into a machine learning algorithm, to determine correlation between the measures, and to correlate all three measures against pathology data and outcomes. Though correlation with outcome data takes time, it will provide the best assessment of the capabilities of the method disclosed herein.

[PARA 257] Due to the long echo time and sensitivity to patient motion, most diffusion weighting is done using fast Echo-Planar Imaging pulse sequences to provide relatively fast data acquisition. However, chemical shift artifact is highlighted by single shot EPI (around 10 pixels of shift).

[PARA 258] Further, as there is not much motion of water through fat, resulting in a bright signal that can obscure lesions, fat suppression is often used as part of the DWI data acquisition.

[PARA 259] In one embodiment of the methods disclosed herein described in greater detail subsequently, crusher gradients are used on either side of the 180° gradients to eliminate focusing of noise signal generated during the 180° pulse. Replacing these crusher gradients with diffusion weighting gradients, allows acquisition of both the diffusion weighted signal as well as the subsequent restricted k-value signals. As such, the diffusion weighting would be a measure in the VOI.

[PARA 260] DTI (Diffusion Tensor Imaging)—in highly oriented tissues, such as nerves and white matter tracts, diffusion occurs preferentially along one direction, diffusion along the nerve/axon tracts being much preferred to that of the across-track orientation. The degree of directionality, or anisotropy, in tissue is an indicator of pathology, as many neurologic conditions degrade the order of neurologic structures, such as the minicolumns ordering of cortical neurons, or lead to order degradation through demyelination of the axons that form the white matter tracts in the brain. In anisotropic diffusion, the value of the diffusion constant varies with direction. As this anisotropy is a measure of pathology advancement, measurement of the diffusion constant in multiple directions can be used to yield the "fractional anisotropy" arising from the tissue structures and hence provide a

measure of pathology advancement. In practice, at least six non-collinear gradients are used to measure fractional anisotropy, leading to a symmetric 9 x 9 matrix, the "diffusion tensor", the eigenvalues of which yield the major diffusion axes in the 3 orthogonal directions.

[PARA 261] Along with using the anisotropy of diffusion to diagnose and monitor pathology in the brain, the diffusion tensor mapped across the brain can be used to delineate the path of white matter tracts. This is called tractography. A possible application of the methods disclosed herein is to measure texture in the white matter tracts affected in multiple sclerosis (MS) using standard T1 or T2 contrast or using the method disclosed herein in conjunction with diffusion weighting to determine anisotropy of the measure for correlational input for machine learning with standard DTI acquisitions.

[PARA 262] The methods disclosed herein provide the ability to obtain tissue texture using contrast that may be applicable to the particular tissue form being examined. A contrast is applied using any one of the previously described mechanisms enhancing the contrast between the component tissue types in a multiphase biologic sample being measured. As described subsequently in greater detail, the contrast mechanism and its application may occur at various locations within the NMR inducing pulse sequence. Using pulse sequencing such as that described with respect to FIGs. 3 and 8 a volume of interest (VOI) is selectively excited employing a plurality of time varying radio frequency signals and applied gradients. An encoding gradient pulse, as also previously described with respect to FIGs. 3 and 8, is applied to induce phase wrap to create a spatial encode for a specific k-value and orientation, the specific k-value determined based on anticipated texture of the tissue within the VOI. A time varying series of acquisition gradients is initiated to produce a time varying trajectory through 3D k-space of k-value encodes as previously described with respect to, for example, FIGs. 8, 11, 16 or 18, with the k-value set being a subset of that required to produce an image of the VOI. Multiple sequential samples of the NMR RF signal encoded with the specific k-values are simultaneously recorded. The recorded NMR signal samples are then post-processed to produce a data set of signal vs k-values for the k-values in the set determined by the trajectory.

[PARA 263] A first tissue for application of the methods herein is bone. Though the effect on quality of life is huge, no accurate and non-invasive method for sensitive assessment of

bone fracture likelihood exists. The current gold standard measure, DEXA, which relies on x-ray absorption, measures areal density of bone. The main determinant of bone strength which predicts fracture, is trabecular microarchitecture, a measure of which is not currently available in vivo. The method disclosed herein enables this measure.

[PARA 264] Bone degradation occurs due to several factors, including disease, cancer therapy, eating disorders, and aging/life style. As trabecular structure erodes in bone, three main morphometric figures vary—the trabecular element thickness, TbTh, the repeat spacing of trabecular cells, TbSp, and TbN, the trabecular number, which is a redundant figure that can be determined from TbSp and TbTh. TbTh decreases continuously with bone degradation. Eventually, as the trabecular elements, or struts, break, there is a discontinuity in the local value of TbSp. Bone degrades anisotropically over time, the anisotropy driven in large part by the effect of load bearing stresses. With progression of bone disease, the TbSp increases faster along the primary load bearing direction than it does normal to this direction, the variation between the two measures being a marker for bone degradation. In addition to the developing anisotropy of bone morphometry, variability in the measure of the trabecular spacing, TbSp, increases, due to the thinning of the trabecular struts to the point where they break, causing discontinuities in the measure of TbSp.

[PARA 265] The most definitive measure of bone health is the thickness of the trabecular elements, which is currently impossible to measure directly in vivo, due to the spatial resolution required of the measure.

[PARA 266] The method disclosed herein enables this measure, as it provides the needed resolution for measuring TbTh in thinning trabeculae, down to tens of microns, near the range where the sudden discontinuities in TbSp can then be measured to assess further degradation. As the trabeculae thin to the point of breaking, a sudden shift to increasing TbSp should be visible in the signal distribution vs. k-value, due to the breaking trabecular elements. Additionally, the degree of anisotropy of TbSp can be used as a correlative measure for fracture likelihood Data can be acquired using the method disclosed herein by positioning the VOI within the targeted bone region, acquiring data within a single TR or across multiple TRs to enable acquisition across the pertinent range of k-values spanned by TbTh and TbSp. Data acquired quickly within one TR can be averaged to improve SNR, the only requirement being that the data is acquired from similar bone tissue.

[PARA 267] The requisite contrast is between bone and marrow. T1 weighting provides high signal in marrow, bone offering negligible MR signal. Alternatively, an IR sequence, which results in heightened T1 contrast, can be used. Some work has been done using diffusion weighting to image bone—this is a possible contrast mechanism when using the method disclosed herein.

[PARA 268] In healthy bone, TbSp and TbTh are closer in magnitude than they are in diseased bone. This can be seen in FIGs. 22A and 22B, by comparing the image of healthy bone, FIG. 22A, with the image of highly osteoporotic bone, FIG. 22B. The exact form of this relationship varies somewhat, the difference in these two morphometric parameters being higher in spine, for instance, than in the hip across pathology. The increasing difference in measure of these two morphometric parameters provides a marker of disease development.

[PARA 269] Because of this increasing separation of the two measures, to measure both TbSp and TbTh in osteoporotic bone involves acquiring signal data in two spatially separate regions of k-space. In healthy bone, if gradients are used to select a region in k-space, it may be possible to define a region that encompasses both TbTh and TbSp in the distribution of signal vs. k- value in some skeletal regions. With progressing bone disease the variation in the measured values of TbSp becomes wider, as does the percentage variation of TbTh; additionally, TbSp becomes larger (wider spacing) with disease progression, and TbTh comes narrower. Hence, the center of each of these distributions separates progressively with increasing pathology. Using either gradient on or gradient off acquisition, broadened by gradient height or VOI windowing, or a combination of the two, the general shape of these distributions can be determined. These broadened distributions can be used in real time to determine the regions of k-space to sample more finely in successive TRs.

[PARA 270] As desired, data can be acquired using multiple interleaved VOIs within each TR. This method allows determination of the variability in signal at specific k-values within a region of bone. The data acquired from the different VOIs can be mapped, a value/color/icon assigned to signal or peak k-value in the distribution, or to the difference between the k-values associated with, respectively, the peak position of TbTh and that of TbSp. The specific k-value and k-value set established by the time varying gradients may encompass a range of TbSp and TbTh from 0.01 mm to 5mm in exemplary applications.

[PARA 271] The methods disclosed herein can be applied within and around the location of a bone lesion identified with, for example, conventional T1, T2 or proton density contrast, or flow or diffusion contrast MR imaging, to assess the state of the trabecular bone in the region. What is of interest here is a determination of the lesion type; is the lesion indicative of an erosive tumor, or is the lesion in a region of inflammation/ degraded bone surrounding a fracture. Some lesions are dangerous and erosive tumors, some lesions are benign. Acquiring data by the method disclosed herein in multiple VOIs in the area of the lesion would enable a determination of whether the trabecular structure is degraded in the vicinity, and how progressed the degradation is, both spatially and temporally. Further biomarkers can be derived by inputting the MR images of lesions to machine learning algorithms and correlating them with the trabecular data of TbTh, TbSp, TbN, anisotropy and measure variability. By this novel method, the diagnostic content of MR images can be improved, as the appearance of the lesion on the image can be tied to a specific degree of bone pathology.

[PARA 272] T2 contrast can be used in conjunction with the method disclosed herein to highlight fluid in an oncological bone lesion to type it as either lytic or sclerotic. In such pathology there may be little fat/marrow remaining around the calcified bone to provide signal. In an oncologic bone lesion there is usually a mix of fluid, and of marrow in various states of inflammation. To yield a signal from outside the hard bone, proton density can be used. Alternatively, diffusion weighting would return signal based on diffusion of water molecules in the fluid imbued marrow phase.

[PARA 273] Use of the method disclosed herein to acquire signal vs. k-value data in bone, applying the various methods disclosed above, yields several biomarkers for assessing bone health. Measurement of TbSp, TbTh, and TbN in multiple VOIs at different locations in the bone, and with different orientations of the textural encode gradient, yields information on the magnitude and variation of the morphometric parameters, their variation with direction relative to the load bearing axis of the bone, and the variability in the measures locally and across larger bone regions. While, for instance, a measure of TbTh in one orientation locally in advanced disease will clearly reflect pathology, a more sensitive marker for bone health can be derived by combining the sum of the data acquired.

[PARA 274] However, correlational data is required for feature/biomarker development or extraction. The highest content predictor of fracture likelihood is fracture history. Bone biopsy is also very sensitive but, as it is a highly invasive biomarker, this procedure is rare. Though DEXA is the current gold standard for bone health, it measures areal bone density, and is not sensitive to trabecular architecture; hence, it is at best a mediocre predictor of fracture likelihood. However, with a large enough sample, this metric can provide increased correlation for diagnostic definition. Taken together, DEXA data and patient fracture history provide a high level learning framework for correlation with the entirety of the output data derived by the method disclosed herein, enabling definition of a sensitive diagnostic tool from the method disclosed herein.

[PARA 275] Rather than try to derive biomarkers from the acquired data by individual comparison to look for feature extraction, machine learning algorithms will provide the best correlational data between multiple measurements.

[PARA 276] Further, besides correlation between TbTh, anisotropy data, and measure of TbSp and its variance, fracture data from subjects will be correlated with these measures, also using machine learning algorithms, to develop markers for fracture likelihood. Biomarkers can be derived directly from the signal vs. k-value data by inputting it into machine learning algorithms and correlating it with, for instance, fracture occurrence data from the same patient, DEXA measurements, or bone biopsy report data.

[PARA 277] Liver tissue or other tissues subject to fibrotic invasion provide a second example of the use the methods disclosed herein. Although the underlying causes of liver disease are complex and varied, the salient feature of the disease is the development of fibrotic depositions within the liver. Disease onset and progression are marked by increasing accumulation of proteinaceous deposits, mainly collagen fibers, on the hepatic structures. Though fibrotic development can, in the short term, promote healing, if the disease is left untreated, the healing response itself becomes a problem, the excess of proteinaceous substance impeding the normal functioning of the organ. In the case of liver disease, this process, left unchecked, advances to cirrhosis—with attendant carcinoma and/or liver failure. For this reason, diagnosing liver disease early on, when a range of management

options are available, is optimal. Use of the method disclosed herein to assess disease-induced pathologic changes to liver tissue would provide a low- cost, non-invasive, fast add-on to a routine MR exam that would be ordered to check liver health. While the focus here is on liver fibrosis, the pathology, and the application of the method disclosed herein, is similar to that of a range of diseases characterized by fibrotic invasion. A partial list of these diseases—cardiac fibrosis, cystic fibrosis, idiopathic pulmonary fibrosis, pancreatitis, kidney disease. Additionally, pathologies such as prostate disease, lose proteinaceous deposits in response to disease progression. Though the mechanism is reversed, the tissue texture assessment needed for diagnosis and monitoring is the same.

[PARA 278] Though biopsy is the current gold standard for liver disease diagnosis, sampling errors within an organ, significant read errors, and non-negligible morbidity, and even mortality, make this other than an optimal diagnostic. For sufficient statistics, many samples would be required, given the high spatial variability of fibrotic development within the liver; however, only a small number of samples can be taken due to the highly invasive nature of the biopsy technique.

[PARA 279] Though what is needed is an accurate assessment of the advancement of fibrosis, currently nothing exists that can measure this directly, aside from pathology. By the time liver disease is diagnosable with liver function tests, ultrasound, or MR imaging, it is well advanced. What is needed is a diagnostic that can track the development of the disease in the early stages, when it is still reversible. Application of the method disclosed herein to measurement of fibrotic structure offers a direct and non-invasive measure, enabling multi-sample, longitudinal monitoring of disease onset, progression, and response to therapy.

[PARA 280] In liver, as in other fibrotic diseases, collagen accumulates in specific patterns within the organ, “decorating" the underlying structural elements. Liver tissue is composed of a multiplicity of adjoining units, or “lobules”, the structure of which is delineated by a central vein, and portal veins that form in a hexagonal pattern around it (see diagram below). As such, in the healthy liver (absence of fibrotic development = F0 stage) the salient dimensions that would appear in a signal distribution of tissue texture feature sizes arise from the spacing between these elements—a range of approximately 0.5 mm to 0.7 mm. With disease onset, fibrotic development starts on the portal triads, then progresses,

eventually forming bridges linking the portal triads to the central veins (Stages F1 through F3). These bridges enlarge and coalesce, forming islands of regenerative tissue surrounded by fibrotic deposition. In this process, vessel to vessel structural spacing in tissue texture becomes gradually replaced by lobule to lobule spacing (Stages F3 to F4). Thus, a clear marker of disease progression is the shift in distribution of textural wavelengths from shorter to longer wavelength (decreasing k-value), this shift being from about 0.5mm to about 2mm, and often longer. As collagen accumulates on the surfaces of the lobules in response to ongoing disease, and even the intra-lobule hepatocytes become decorated, the lobule itself becomes the main textural feature, and the inter-lobule repeat spacing the salient repeat width in a power distribution in k-space. This change happens gradually over the course of disease progression, shifting the power density in textural wavelengths (inverse k-values) from the healthy range out to approximately 2-3mm feature sizes. The salient textural features involved in this textural wavelength shift are well known from histology studies.

[PARA 281] In order to diagnose liver disease in its early stages, the shift of the signal as a function of k-value from that expected for healthy liver to longer wavelengths (lower k-values) indicative of disease onset and progression, can be tracked using the method disclosed herein. This measurement at a particular point in time along the arc of disease progression and response to therapy, can be made either by acquiring successive samples at individual k-values over the desired range of textural wavelength or, alternatively, a gradient can be applied during data acquisition to span the desired range in k-space. A hybrid of these two acquisition methods can also be used.

[PARA 282] Contrast between the collagen decorating the various hepatic structures and the underlying tissue can be achieved using either endogenous or exogenous contrast: signal from fibrosis is dark in standard T1 imaging, and can be bright in T2 imaging, due to the large water content in the fibrotic structure. Use of Gd contrast agent shortens T1 such that on T1 weighting the fibrosis shows up bright against the background tissue. Higher contrast makes for a more robust measure. However, although these contrast mechanisms provide contrast between fibrosis and underlying tissue, standard MR imaging is not capable of sufficient resolution to discern the pattern of fibrotic development on the various hepatic structures, which characterizes early stage disease. Patient motion blurs the image, even

when using breath-hold imaging or respiratory triggering. Using standard MR imaging, liver disease can only be assessed at the more advanced stages, when the liver may be irreversibly damaged. Though advanced disease is diagnosable, what is needed for therapy justification and response monitoring is early stage diagnosis.

[PARA 283] Diverse MR imaging based techniques have been used in assessment of liver fibrosis, besides conventional T1 and T2 contrast with or without contrast agents. MRE (Magnetic Resonance Elastography), diffusion-weighted imaging (DWI), and MR perfusion imaging, can yield some information on liver disease, though none are capable of robust diagnosis in the earlier stages of the disease. A major difficulty with them is that they rely on surrogate markers for fibrotic development. MRE relies on stiffness measurement, perfusion imaging measures blood perfusion parameters, DWI (Diffusion Weighted Imaging) measures the ADC (Apparent Diffusion Coefficient) of water in the liver tissue. These parameters all vary in response to many factors besides fibrotic development, such as inflammation, portal hypertension, steatosis, edema, iron overload, and hepatic perfusion changes. Currently, there is no direct way to measure fibrotic development in early stage disease. By providing the ability to achieve robust resolution at the k-values pertinent for measuring fibrotic development, using standard MR contrast methods, the method disclosed herein enables assessment of disease state in early stage liver disease.

[PARA 284] One of the features of the method disclosed herein that makes it novel, is that it can be used in conjunction with most contrast mechanisms. One application of this method is its use in conjunction with diffusion weighting, using diffusion-weighted contrast (see FIG. 23 below), but acquiring signal only in the k-value ranges of the fibrotic deposits in early stage disease rather than the entire image acquired in standard DWI. By using the method disclosed herein for signal acquisition, the data is acquired with a much finer spatial resolution than is possible with diffusion-weighted MR imaging. The texture being measured is on the scale of the fiber-decorated structures, between actual fiber clumps, rather than an averaged measure affected by partial volume imaging. Fibrotic deposition lowers the diffusion coefficient for water, the lower ADC (apparent diffusion coefficient) in areas of fibrosis making for a brighter signal than the surrounding tissue. By using diffusion weighting in conjunction with the method disclosed herein the structural signal obtained will measure highly localized water diffusion. Hence, as the lobular unit transforms from

one with no delineated boundaries to collagen decoration of the hexagonal boundary and then to filling in the entire lobule, water diffusion at the boundaries will be impeded, increasing diffusion weighted signal intensity. As pathology increases, then a textural signature can be obtained by using diffusion contrast. Two approaches to positioning of the diffusion weighting gradients are as shown in FIGs. 24 and 25. The shown pulse sequence for selecting the desired VOI and initial phase wrap for k is as described in FIG. 3 and is numbered consistently in FIGs. 24 and 25. FIG. 24 shows positioning of the diffusion weighting gradients 2402, 2404 on either side of the second 180° slice selection pulse, while in FIG. 25, the diffusion weighting gradients 2502, 2504 are positioned before the first, and after the second, 180° slice select pulses to provide more diffusion time for the same TE than would be available when placing the pair either side of the last 180° slice-selection pulse.

[PARA 285] Fibrotic texture development can also be assessed using the methods disclosed herein in conjunction with contrast, such as T1 or T2 weighting, with or without exogenous agents such as Gd. By use of localized sampling in both real and k-space, the methods disclosed herein enables fast acquisition of signal at the requisite k-values, enabling robust assessment of pathologic tissue texture at a specific location in the liver—providing a measure of the textural frequencies present at that location, immune from the subject motion-induced blurring that limits current MR imaging methods. Using the methods disclosed herein, the problem of respiratory motion is circumvented by the speed of acquisition of the requisite data. To sample pathology variability within the liver, VOIs 2602a-2602d can be positioned at various locations in the liver as represented in FIG. 26, using either interleaved acquisition within one TR, or measurements in separate multiple TRs. By use of the methods disclosed herein, texture coherence is maintained within each defined VOI throughout the data acquisition at specific k-values or k-value ranges, so as to enable SNR maximization through signal averaging. If desired, repeat sampling can be made in subsequent TRs at the same location, to obtain an average measure of the degree of fibrotic invasion at that location, for assessment of stage of disease progression.

[PARA 286] While the application to liver disease has been called out in some detail here, assessment of other fibrotic diseases is enabled by the method disclosed herein. Fibrotic development is the hallmark of lung disease (e.g. cystic fibrosis, idiopathic pulmonary

fibrosis), myocardial fibrosis, muscle fibrosis, pancreatic fibrosis and kidney disease. Additionally, as mentioned previously, some diseases, such as prostate disease, induce reduction in proteinaceous deposits.

[PARA 287] Many neurologic diseases and conditions have a vascular component that may serve as a marker for disease onset and progression, allowing diagnosis and therapy tracking which provides a third exemplary implementation of the methods disclosed herein. The ability to sensitively assess changes in micro-vessels would enable monitoring of pathology progression in a number of diseases which are often not diagnosed until pathology is well advanced.

[PARA 288] Angiogenesis, formation of new blood vessels from pre-existing micro vessels, is necessary for tumor growth and metastasis. Rather than the ordered formation of vessels that exist in healthy tissue, pathogenic angiogenesis tends to form chaotic, tortuous vessels, replete with blocked, dead end structures—see FIG. 23. Vessel diameter and wall thickness are highly variable in angiogenic micro-vessels, with marked vessel permeability in places.

[PARA 289] For example, tumor aggressiveness is closely correlated with neovascular density, as angiogenesis is needed to supply the tumor with oxygen and nutrients. The ability to assess the amount of angiogenic development at a tumor site, and to characterize the vascular morphology, would enable assessment of tumor aggressiveness. By determining the extent of the angiogenic vasculature within and surrounding the tumor, it is possible to determine the necessary boundaries for surgical removal. Likewise, therapy response may be trackable in part by measurement of vasculature as it reverts to a more normative state. Degree of angiogenic vasculature development can be assessed to some extent using serum markers, or by biopsy. But biopsy is highly invasive, and prone to sampling errors and read variability.

[PARA 290] As a second example, several forms of dementia, most notably Alzheimer's disease (AD), are now recognized as having a large vascular component with pathogenic vessel development. Additional forms of dementia, such as Huntington's disease (HD), Parkinson's disease (PD), and Frontotemporal dementia are also found to have compromised vasculature. In some cases, the salient cause of the dementia appears to be pathogenic vasculature in the brain, such as CVD.

[PARA 291] Chronic inflammation is another important factor that can lead to abnormal neurovascular structure, exhibiting permeability and hemorrhage. Some microvasculature pathogenesis is linked to permeability of the blood brain barrier. Multiple Sclerosis, a brain disorder with pathology associated with inflammation and axonal demyelination, exhibits microvessel disruption. Stroke and the resultant ischemia result in development of angiogenesis modifying the capillary network, as the body attempts to heal the damage. As angiogenesis features increased vascularity, involving both structural and functional alterations within the neurovascular system, this increased density, and the high variability in vessel spacing, is a promising biomarker that can be used for the characterization of ischemic conditions in the brain following stroke. For all of these conditions—tumor development, ischemic stroke, and brain pathology in dementia, a means of assessing the micro-vasculature in brain tissue, is needed—both for determination of pathology advancement, and for assessment of therapy response.

[PARA 292] Currently, MRI assessment of the health of microvasculature is most commonly made by perfusion imaging. Perfusion is the irrigation of tissues via blood delivery through the microvessels. Because the state of the vessels changes the dynamics of blood flow, such measure can be used to assess vascular health. For perfusion MR imaging, either endogenous or exogenous contrast is used. Exogenous contrast is most commonly provided by use of Gd-based contrast agent. Endogenous contrast is obtained through a technique known as ASL (Arterial Spin Labelling) in which the blood flowing into a region of the brain is magnetically labelled. In both cases, sequential images are made via fast imaging techniques, as the contrast moves into, and exits, the imaging plane. One of the key features of dynamic imaging, such as perfusion imaging, is that differential contrast can be obtained via subtraction of the image obtained with no contrast agent/blood tagging in the imaging plane from that obtained when contrast is at a maximum in the imaging plane.

[PARA 293] When using a contrast agent for this measure, a bolus of the agent is injected intravenously and successive images are acquired as the contrast agent passes through the microcirculation. (Opposite to what is observed when no contrast agent is used, use of T2 weighting results in dark blood when a contrast agent is used, and T1 weighting results in bright blood.) In order to enable fast data acquisition to allow multi-image tracking of the flow before the contrast agent leaves the imaged tissue region, images are usually acquired

using a variant of the fast MRI acquisition sequence known as EPI (Echo Planar Imaging). To characterize the state of the vessels, various flow related quantities are measured: (MTT) mean transit time through the voxels, time to peak signal, CBF (Cerebral Blood Flow), and CBV (Cerebral Blood Volume). These quantities, which vary with vascular condition, are all measurable via perfusion imaging. In addition to the sequential acquisition of images obtained while the bolus of contrast agent is present in the blood, or the magnetically labelled blood is flowing in the imaging plane when using ASL, at least one image is taken following passage of the bolus, or of the labelled spins, through the microvasculature, when contrast between the blood and surrounding tissue is minimal. This image is then subtracted from the early images to allow calibration of the absolute signal level from the microvasculature. Temporal tracking by acquisition of multiple images enables flow characterization and determination of regions of compromised vessels.

[PARA 294] Angiogenic vasculature is denser, and more varied in vessel diameter and spacing, than are healthy vessels. The high spatial variation in vessel thickness and spacing is one of the hallmarks of angiogenic vasculature and hence, along with increased vessel density, serves as a marker for angiogenesis-related pathology. However, image resolution in perfusion imaging is not high enough to determine detailed vascular morphology. Flow contrast highlights locally averaged signal variation due to the pathogenic flow parameters, offering indirect assessment of vessel morphometry. However, the methods disclosed herein can be used to directly measure vessel density, and vessel spacing variability, to provide direct, robust assessment of angiogenic vessel development. Using the methods disclosed herein to acquire signal vs. k-value data disclosing tissue texture enables robust resolution of the morphometric features of the vessels. This acquisition can be done in one TR, fast enough that the sequence can be injected into the multi-image-acquisition perfusion series. To provide best resolution, this morphometry acquisition would be done near peak contrast, either acquiring data for one TR or for multiple TRs acquired either sequentially or interspersed at various time points with the perfusion image acquisitions.

[PARA 295] Obtaining a differential measure of the vasculature by the methods disclosed herein, obtaining signal vs. k-value data both with and without contrast, provides validation of the origin of the textural signal as arising from the vasculature. Making these two measures as close in time as possible allows best spatial and phase correlative value

between the two data acquisitions, to accurately highlight the signal arising from the vessels.

[PARA 296] The best way to keep the time between the two acquisitions short when using ASL contrast is by 1) acquiring data, by the methods disclosed herein, in a specified imaging plane with proton density contrast; 2) immediately following the first acquisition, spin labelling in a second plane, upstream in the blood flow, in close proximity to the imaging plane; 3) acquiring spin-labelled data in the imaging plane, by the methods disclosed herein, the labelling and 2nd acquisition as close in time as possible following the first acquisition. Signal vs. k-value data can be acquired using either gradient on or gradient off acquisition, or a combination of the two, to provide measure of signal across the desired span in k-space

[PARA 297] Because the morphometric parameters being measured are expected to vary significantly, acquisition of signal across a range of k-values is required, to determine the underlying structural signature of the vessels. The broadness of the distribution of signal vs. k-value, and where its peak lies in k-space are the critical features of interest. The peak assesses the average vessel density and the broadness assesses the variability of vessel spacing; both markers for angiogenesis characterization. The acquisition can be done either with a gradient on or with the gradient off during acquisition. Appropriate windowing in the direction of the acquisition axis of the VOI will allow sampling at a targeted spread of k-values, the exact window function determining the degree of correlation across the k-value range. Additionally, hybrid acquisition is possible wherein a gradient is on for some part of the data acquisition within one TR and off for part of the acquisition. The aim here is to, while acquiring a range of k-values, ensure sufficient repeats of, say, a set of highly correlated k-values, to allow SNR maximization by averaging, while ensuring fast enough acquisition to provide immunity to subject motion.

[PARA 298] Alternatively, rather than temporally intersperse data acquisition by the methods disclosed herein into standard perfusion imaging, the methods disclosed herein can be used in conjunction with any blood contrast method to measure vessel morphology directly, in regions exhibiting pathogenic flow parameters. Both vessel spacing and the variability in this measure are known markers of angiogenesis, the vasculature spacing becoming more random with degree of pathology. For contrast, either structural contrast

such as T2 or T1 weighting, which yield, respectively, bright or dark blood, can be used. Additionally, both black blood and bright blood flow contrast can be achieved by various standard methods, including arterial spin labelling. This structural measure of the vessels can be carried out in as many tissue regions, using as many acquisition directions, as desired. Angiogenic vasculature would be expected to exhibit a high degree of anisotropy, so varying the orientation of the acquisition axis between acquisitions provides another marker of pathology. Correlation of the flow data from the perfusion imaging with the structural vessel data from application of the methods disclosed herein, can be made through machine learning.

[PARA 299] For tracking angiogenesis relating to ischemic stroke, or in the vicinity of a tumor, acquisition by the methods disclosed herein to assess the vessel structure, can be carried out in the vicinity of lesions. To achieve this, a real time response to an imaging scan that defines the location of these lesions would be used to target the location for the subsequent vessel structure measurements by the methods disclosed herein. Acquisition using multiple VOIs/locations and multiple acquisition orientations can be done for correlation with the various lesions appearing on the imaging sequence.

[PARA 300] To study vascular pathology associated with brain disease such as dementia, the VOI can be positioned in the vasculature near the cortical region(s) implicated in the dementia. Data can be acquired in one or more VOIs in one TR. Additionally, in scanners capable of parallel imaging, multiple VOIs can be defined with simultaneous record of data to sample extended areas of the brain vasculature. For example, in dementia in which multiple cortical regions seem to be damaged, VOIs can be placed in the vasculature feeding these different regions and data recorded simultaneously.

[PARA 301] The usual path for diagnostic development is feature extraction from the output data towards biomarker identification. Though feature extraction may define a specific biomarker, often in diagnostic development extended clinical work (years, dollars) is needed to strongly correlate biomarkers with pathology. This reliance on statistical correlation of individual inspection- derived biomarkers with outcomes is further stymied by the small size of initial test populations.

[PARA 302] Medical data analysis is changing rapidly. Recently developed analysis techniques enable efficient determination of the total information content of data acquired

using new diagnostic methods. In contrast to the previous "hunt and peck" method, current pattern recognition and machine learning techniques enable rapid correlation with other diagnostic content. In this way, feature extraction and biomarker development can be done by machine learning rather than by human observation of data. In effect, rather than isolating one characteristic (biomarker) from the entire signal vs. k-value dataset is correlated with other patient data to yield strong pathology correlations. As such, focusing on the acquisition end of the method disclosed herein enables highest possible SNR as input to the machine learning algorithms used in this effort.

[PARA 303] Computer programs are now adept at determining patterns within single images as well as performing highly efficient correlation of data with other medical history/diagnostic information. Data output from application of the method disclosed herein, when taken in its entirety, provides the highest information content. Rather than reducing the information content through front-end feature extraction, the entire distribution of signal vs. k-value acquired from each VOI will be fed into a machine learning algorithm with pertinent diagnostic data taken by the current standard measures. For example, correlational data could be liver disease staging (F0-F5) derived from a doctor's report derived from histology images, the current gold standard measure for liver disease, liver function tests (liver serum), and physical exam.

[PARA 304] Alternatively, the correlational data could be the output from any of those tests individually. With sufficient number of cases, this would enable finer gradations to be defined in disease staging, for instance, steps in between each stage— F0 and F1, between F0 and F2, and between F0 and F3, would be possible to define using this method. Additionally, outcomes—progression to more advanced pathology, or therapy-induced healing—can provide correlational data for machine learning algorithms for correlation with textural assessment from application of the methods disclosed herein. .

[PARA 305] The assessment stage obtained by the methods disclosed herein can be mapped on top of a standard MRI morphology image of the diseased liver. (For easier viewing, an icon can replace the staging number.) This will facilitate visualization of the disease variability through the organ. Additionally, these staging values can be correlated by machine learning with the imaging output obtained on the same patient by MRE, standard DWI, or perfusion, for instance to track possible correlations.

[PARA 306] A final example of pathology assessment employing the methods herein is brain tissue. Brain pathology is often problematic to diagnose and treat because of the sensitivity of the organ to intervention. Further, changes in cognition and behavior can occur over a long time span such that the underlying pathology can go unchecked for years. In AD there is a long pre-symptomatic period, with underlying, ongoing development of pathology at the molecular and tissue level, leading eventually to neuronal damage. Though several have been tested in large clinical trials, there has been a stunning lack of approval for new therapies for AD or other forms of dementia. As the population ages, swelling the ranks of those afflicted with the disease, the situation is dire. The negative results of several of these clinical drug trials highlight the need for targeting subjects earlier in pathology development. However, this requires a diagnostic capable of targeting subjects in the pre-symptomatic phase. A test to identify such subjects has remained elusive.

[PARA 307] Studies indicate that gray matter is affected earlier than white matter with dementia onset and progression. The cortical structures found to be earliest to suffer degradation are the hippocampus and entorhinal cortex, pathology which leads to memory loss and disorientation. Recent research applying image processing to 3 T1-weighted MR images of the brain has indicated a statistically significant correspondence between textural features on images of the hippocampus and MMSE (Mini Mental State Exam) scores. The texture is not directly measurable with MR imaging, due to insufficient resolution, but image analysis metrics correlate specific textural gradations with glucose uptake reduction in the hippocampus and subsequent hippocampal shrinkage, a marker for AD, in addition to the correlations with reduced MMSE scores. These texture features are not discernible except as a result of image processing, and their source is not known. Research indicates that these textural changes precede cognitive decline, and track with symptom onset. Thus, the hippocampus is a good target for application of the method disclosed herein of texture measurement for pathology assessment.

[PARA 308] As the exact etiology of dementia within the hippocampus and entorhinal cortex is unknown, the method disclosed herein will be used to gather a sufficiently complete data set to provide detailed assessment of tissue texture within the organ—either the hippocampus or the entorhinal cortex. Both textural wavelength content and variability, as well as orientation and location dependence will be measured. Signal acquisition across a

range of k-values, in at least 3 (orthogonal) directions, using a plurality of contrast methods (as the origin of the texture is unknown), is requisite to well-characterize the texture. Acquisition of data across the organ, by defining VOI dimensions to enable fitting the VOI fit into the organ entirely at different locations will enable determination of the spatial variability of the texture. By acquiring signal data across a range in k-space corresponding to wavelengths of tens of microns out to about 1 - 2mmensures that a large variety of textural signals contribute to the information content of the measurement. The method disclosed herein can be used in conjunction with any contrast mechanism, such as inversion recovery, a heightened form of T1 weighting, or diffusion weighting.

[PARA 309] The predictive value of the novel biomarker provided by the textural data acquired by the method disclosed herein, towards assessment of the degree of AD pathology, can be defined by correlation with a range of diagnostic information from the same patient. The main correlation marker will be drawn from patient outcomes—i.e. definitive diagnosis of AD or other dementia—as this has the highest diagnostic information content, though definitive diagnosis is well-downstream from the pathology we are assessing. Additional correlation will be drawn from patient MRI imaging data on hippocampal shrinkage, a proven, and continuous, marker of advancing AD (as well as other forms of dementia). This correlation will be made longitudinally with disease progression, if possible. Again, changes in tissue texture in the hippocampus are expected to predate noticeable cognitive decline, and measurable change in volume via MRI. A third correlative marker is FDG-PET, as decline in glucose metabolism is expected to occur early relatively in disease progression. As a fourth correlative biomarker, the MMSE (Mini Mental State Exam) provides longitudinal data on cognitive functioning and decline. Genetic predilection for AD provides an additional marker for correlation with the textural measure acquired by the method disclosed herein. While the previous markers provide downstream correlative value (on the outcome side), genetic markers exist in advance of any pathology development. Correlation of this varied set of biomarkers with the data acquired by the method disclosed herein in the hippocampus and entorhinal cortex, across a broad range of patients, will enable a clear definition of diagnostic content of the use of the method disclosed herein for early stage prediction of AD pathology.

[PARA 310] Current machine learning algorithms are capable of pathology level classification of non-specific features, as will be obtained from MR data acquisition by the method disclosed herein. As such, the disclosed sources of correlational data above will be input into machine learning algorithms to highlight the correlation with textural features and disease.

[PARA 311] Though research has indicated that the hippocampus may be the earliest affected cortical structure with AD progression, its depth within the brain results in lower SNR due to distance from the MR sensing coil. Texture within the neocortex provides a target for assessment of dementia and other brain pathology that, due to its proximity to the skull, offers higher SNR. In the healthy brain, very ordered neuronal architecture is found in the neocortex. The neurons form in bundles of approximately 50microns in width and 80 micron spacing, with about 80 to 100 myelinated neurons grouped together in each bundle. This is the minicolumn organization visible in histology of neocortical tissue. In specific regions of the brain that are seen by histology studies to be affected early in AD progression, this columnar order loses coherence over the prodromal stages. These changes happen in advance of general brain atrophy, an often-used marker for AD progression, making them a better target for early stage diagnosis. Further, the temporal progression of minicolumn thinning and loss of coherence across specific brain regions reflects the regionally selective progression of tangle pathology in Alzheimer's Disease (AD). Hence, tracking the changes in cortical minicolumns spatially in the brain using the method disclosed herein enables typing of dementia, as each form of dementia follows a specific spatial progression through the brain.

[PARA 312] The structure of these minicolumns in healthy brain can be seen in FIG. 27, a histology image stained to reveal myelin 2702—the coating sheathing the neurons. FIGs. 29A – 29C are a series of three histology images stained to reveal the pyramidal neuron cells in the bundles. FIG. 29A is of neuronal order in healthy brain and FIGs. 29B and 29C show progressive pathology with AD advancement—the columnar spacing shrinks and the ordered structure becomes increasingly random.

[PARA 313] Changes in the spacing and order of the minicolumns in these cortical regions are early harbingers of disease. Though research in this area is in early stages, as with other pathology, the underlying tissue changes must predate symptoms. The problem is

that currently there is no technique able to reach the resolution needed to assess these early-stage changes in the columnar texture. The method disclosed herein enables this measurement.

[PARA 314] There are several methods by which the method disclosed herein can be implemented to measure the change in spacing and order of neocortical minicolumns. For this measurement to reflect early stage changes, it would be applied to the regions of the neocortex that appear to affect behavior earliest in the onset of AD, such as the temporal cortex. As these regions are in the neocortex on the outside of the brain, they will yield a strong SNR in a brain coil. FIG. 28 is a representation showing possible positioning of the VOI 2802a, 2802b, 2802c and 2802d in the neocortex 2804.

[PARA 315] As the axonal component of the neurons forming the minicolumn bundles are sheathed in myelin, a fatty substance, T1 contrast can be used to highlight the axon bundles against the background tissue and hence is a good choice for contrast when assessing these structures.

[PARA 316] A difficulty in measuring the columnar spacing results from the semi-crystallinity of these structures. In healthy neocortex, they are highly ordered in the vertical (parallel to columns) direction. As a result, because the acquisition axis of the VOI must intercept several of these columns to make a measurement, the differential signal that contrasts the neuronal bundle from the background tissue is extremely sensitive to orientation of the acquisition axis. To measure the columnar spacing, the acquisition axis of the VOI is aligned normal to the length of the columns. Slight misalignment diminishes contrast— precise orientation is required for the measurement. To achieve proper alignment, rocking the acquisition gradient angle over incremental angles of approximately a degree or two will show a signal resonance at the proper alignment i.e. consecutively repeating the time varying series of gradients to produce trajectories through 3D k-space with resulting k-value sets oriented around the specific k-value to locate resonance. (The slight curvature of the cortex would be expected to provide a finite width to this resonance of signal amplitude vs. angle.) A trajectory through 3D k-space and a resulting k-value set oriented within 10 degrees of the initially encoded specific k-value is employed in exemplary embodiments. As the columnar structure loses coherence with pathology advancement, the width of this resonance would be expected to broaden, and eventually

disappear when the structure becomes highly random, as shown in the histology image in FIG. 29C.

[PARA 317] Using the method disclosed herein, acquisition of signal can be at a (nominally) single k-value, or over a band of k-values defining in advance of t the measure a finite extent in k-space over which to acquire the signal.

[PARA 318] As the spacing of minicolumns in healthy human brain is approximately 80 microns, sampling from about 70 microns to 110 microns would encompass the resonance. In exemplary embodiments this is accomplished by placing the VOI within the cortex and providing the spatial encode in the range of k-values corresponding to spatial wavelengths of 40 micrometers to 200 micrometers.

[PARA 319] Making measurements in the cortex with the method disclosed herein involves these basic steps:1) A contrast mechanism is selected to highlight the structure. 2) individual k-values or the span of k-values for which signal is to be acquired is determined. 3) the timing of the k-value acquisitions— how many repeats at each k-value or spread of k-values is determined. 4) the size of the VOI and orientation(s) of the acquisition axis in the neocortical tissue are selected.

5) A VOI is positioned in the center of the cortex height, aligning the acquisition axis parallel to the top and bottom surfaces at the VOI midpoint, as closely as possible. 6) Signal vs. k-value data is then acquired with the gradient on or off to measure the minicolumn spacing; measurement across a broad range of k-values encompassing on the average spacing of the minicolumns as indicated in the literature (approximately 80μm) will ensure coverage of the width distribution. Signal intensity maximum should occur when the acquisition gradient is oriented normal to the columns. 6) The acquisition gradient is then rocked in small angular increments to look for the signal resonance—the sharpness of the signal resonance vs. angular deviation reflects the order of the minicolumns. A sharp resonance indicates ordered structure. A broad resonance as a function of angular deviation indicates columnar degradation has introduced randomness into the minicolumn order.

7) Aligning the gradient to maximum signal return to sweep through the range of k-values look for textural wavelength resonances—i.e. the peak of the signal vs. k-value distribution from the texture distribution. This resonance also can be used to determine minicolumn order. A sharp peak (high q-value) in the signal vs. k-value curve indicates ordered

structure, the broadness of the curve is indicative of the degree of loss of order. Locating the resonance in the signal vs. acquisition angle and in the signal vs. k-value distribution can be accomplished as an interactive process.

[PARA 320] Data can be acquired at other positions in the cortex or nearby the original VOI, either within one TR or multiple TRs. Optimal VOI dimensions for characterization of the cortical minicolumns are determined by 1) the need to fit the VOI entirely within the cortex, which is 2-3 mm in height, 2) the requirement to sample sufficient textural repeats along the encode axis for accurate assessment of the textural wavelength, and 3) by signal requirements. Additionally, the
smaller the height of the VOI along the direction of the columns determines the sensitivity to alignment.

[PARA 321] The fewer repeats sampled along the encode axis, the greater the broadening in k-space of the signal acquired by the method disclosed herein. Data can be acquired with the gradient off , relying on selection of the window width to determine the range of k-values contributing to the signal. Keeping the spread in k-space small enough ensures correlation in the signal output..

[PARA 322] A change in spacing of neuronal columns indicates pathology advancement /aging; this can be determined by longitudinal monitoring of the peak of the signal-magnitude vs. K- value distribution.

[PARA 323] As the structure degrades, the orientation resonance becomes broader and more diffuse, spread over a larger span of acquisition angles. Also as the structure degrades, the peak in the signal vs. k-value distribution becomes broader and more diffuse, spread over a larger span of k-values (wavelengths). Eventually, no peak will be visible in either case with progressing degradation of the minicolumn order, a marker of increasing degree of dementia. Further, changes in the minicolumns widths with advancing disease will be reflected in the column spacing, another marker of pathology.

[PARA 324] A variation on this disease marker is the degree of anisotropy of the columnar order. As the columnar order degrades with progressing pathology, the degree of anisotropy of the columnar texture also lessens and the overall cortical tissue texture becomes more isotropic. The degree of anisotropy can be measured by use of T1, or other, contrast using the method disclosed herein, with the VOI 3002 positioned as above, midway

between the two cortical surfaces 3004 as seen in FIG. 30 and comparing the signal vs k-value distribution with the acquisition axis normal to the cortical surfaces (parallel to the minicolumns), with the signal vs. k-value distribution obtained with the acquisition axis aligned tangential to the cortical surfaces 3004 therefore (normal to the minicolumns) as shown in FIG. 30.

[PARA 325] The use of diffusion weighting in brain pathology, including stroke and brain tumors, is increasing. Diffusion weighted imaging (DWI) provides an indirect measure of structure at the cellular level, by applying gradients that first dephase and then rephase signal in a targeted location.

[PARA 326] Stationary water molecules are rephased by the second gradient, but those that have moved between the two gradients are not, hence yielding no signal. The difficulty with the technique is that, by design, it is extremely sensitive to motion. It is also low SNR, due to the late echo time resulting from the need for the long diffusion gradients. Use of the method disclosed herein for data acquisition when using diffusion contrast can remedy the motion problem as, though the echo time is still long, data acquisition is fast enough that the signal loss and blurring due to motion is minimized. The method disclosed herein can be used with diffusion weighting contrast to assess the spacing and order/randomness of the minicolumns. This measure can be made with the diffusion gradients applied parallel to the surfaces of the cortex (normal to the minicolumns), and then normal to the cortical surfaces (parallel to the minicolumn direction). These two measures enable assessment of the anisotropy, which will be highest in healthy brain, pathology then inducing increasing isotropy as the columns degrade.

[PARA 327] Using diffusion weighting, with reference to FIG. 30: applying the gradient as indicated by Gradient 1 3006 will yield low signal if minicolumns still intact. Similarly applying gradient as indidcat4d by Gradient 2 3008 will yield high diffusion signal if minicolumns still intact.

[PARA 328] As minicolumns degrade, signal with the two different gradients approach each other expect diffusion weighted signal to increase overall as minicolumns become highly degraded.

[PARA 329] A refinement on this measure is through application of the diffusion gradient in multiple directions for data acquisition and development of the diffusion tensor similarly

to diffusion tensor imaging (DTI), but with data acquisition being by the method disclosed herein. Development of a diffusion tensor requires using at least 6 non-collinear directions of diffusion gradient orientation to yield sufficient data to generate the tensor, the eigenvalues of which determine the level of Fractional Anisotropy (FA) in the cortex, reflective of the order of the minicolumns. The FA should change, moving toward more isotropic organization as columnar organization degrades—an FA value of 1 indicates highest anisotropy, and a value of 0 indicates maximum isotropy of the underlying diffusion, hence revealing the order of the columnar texture.

[PARA 330] As with the other types of contrast mechanisms used in conjunction with the method disclosed herein, the targeted k-values are selected by a combination of knowledge of the approximate location in k-space of the minicolumns from the literature and from measure when they are still sufficiently ordered to define a clear textural wavelength signature, and pre-measure to determine the distribution of signal vs. k-value. One method to achieve this is with a gradient on to provide sufficient spread in k-space during data acquisition to enable finer sampling on the subsequent acquisition(s), though this measure can also be made using gradient off acquisition.

[PARA 331] In the cortex, the mean diffusivity (MD) of water is found to decrease with increasing dementia. Using the method disclosed herein it can be determine if this is due to minicolumn disorder by measuring the spacing, order, and anisotropy of the minicolumns as described above. The signal vs. k-value data obtained using the method disclosed herein, can be input into a machine learning algorithm, with correlational data from cognitive evaluation tests such as the MMSE exam, downstream neuropathology outcomes, and serum and imaging data.

[PARA 332] In addition to Alzheimer's dementia, changes in, or abnormal morphology in, minicolumn structures occur with Parkinson's disease, Dementia with Lewy bodies, Amyotrophic Lateral Sclerosis, autism (autism spectrum disorder is reflected in wider, hence more tightly packed, minicolumns), and schizophrenia (for which the normal thinning of the columns with age does not appear to take place, leading to more widely spaced minicolumns), dyslexia and ADHD. Hence, the method disclosed herein can be used to assess degree of pathology in any of these conditions. Correlation for machine learning to determine the association between measured data and pathology can be obtained from

cortical atrophy segmentation, MMSE, doctor's evaluation of degree of pathology from observational data, etc.

[PARA 333] Additionally, the method disclosed herein can be used with stationary contrast mechanism to highlight tissue texture changes and flow contrast to highlight vasculature changes in the vicinity of a lesion showing up on an MR image, that may indicate stroke or tumor related pathology.

[PARA 334] Studies indicate that gray matter is affected earlier than white matter with dementia onset and progression. The cortical structures found to be earliest to suffer degradation are the hippocampus and entorhinal cortex, pathology which leads to memory loss and disorientation. Recent research applying image processing to T1-weighted MR images of the brain has indicated a statistically significant correspondence between textural features on images of the hippocampus and MMSE (Mini Mental State Exam) scores. The texture is not directly measurable with MR imaging, due to insufficient resolution, but image analysis metrics correlate specific textural gradations with glucose uptake reduction in the hippocampus and subsequent hippocampal shrinkage, a marker for AD, in addition to the correlations with reduced MMSE scores. These texture features are not discernible except as a result of image processing, and their source is not known. Research indicates that these textural changes precede cognitive decline, and track with symptom onset. Thus, the hippocampus is a good target for application of the method disclosed herein of texture measurement for pathology assessment.

[PARA 335] As the exact etiology of dementia within the hippocampus and entorhinal cortex is unknown, the method disclosed herein will be used to gather a sufficiently complete data set to provide detailed assessment of tissue texture within the organ—either the hippocampus or the entorhinal cortex. Both textural wavelength content and variability, as well as orientation and location dependence will be measured. Signal acquisition across a range of k-values, in at least 3 (orthogonal) directions, using a plurality of contrast methods (as the origin of the texture is unknown), is requisite to well-characterize the texture. Acquisition of data across the organ, by defining VOI dimensions to enable fitting the VOI fit into the organ entirely at different locations will enable determination of the spatial variability of the texture. By acquiring signal data across a range in k-space corresponding to wavelengths of ten microns out to about 1-2 mm ensures that a large variety of textural

signals contribute to the information content of the measurement. The method disclosed herein can be used in conjunction with any contrast mechanism, such as inversion recovery, a heightened form of T1 weighting, or diffusion weighting.

[PARA 336] The predictive value of the novel biomarker provided by the textural data acquired by the method disclosed herein, towards assessment of the degree of AD pathology, can be defined by correlation with a range of diagnostic information from the same patient. The main correlation marker will be drawn from patient outcomes—i.e. definitive diagnosis of AD or other dementia—as this has the highest diagnostic information content, though definitive diagnosis is well-downstream from the pathology we are assessing. Additional correlation will be drawn from patient MRI imaging data on hippocampal shrinkage, a proven, and continuous, marker of advancing AD (as well as other forms of dementia). This correlation will be made longitudinally with disease progression, if possible. Again, changes in tissue texture in the hippocampus are expected to predate noticeable cognitive decline, and measurable change in volume via MRI. A third correlative marker is FDG-PET, as decline in glucose metabolism is expected to occur early relatively in disease progression. As a fourth correlative biomarker, the MMSE (Mini Mental State Exam) provides longitudinal data on cognitive functioning and decline. Genetic predilection for AD provides an additional marker for correlation with the textural measure acquired by the method disclosed herein. While the previous markers provide downstream correlative value (on the outcome side), genetic markers exist in advance of any pathology development. Correlation of this varied set of biomarkers with the data acquired by the method disclosed herein in the hippocampus and entorhinal cortex, across a broad range of patients, will enable a clear definition of diagnostic content of the use of the method disclosed herein for early stage prediction of AD pathology.

[PARA 337] Current machine learning algorithms are capable of pathology level classification of non-specific features, as will be obtained from MR data acquisition by the method disclosed herein. As such, the disclosed sources of correlational data above will be input into machine learning algorithms to highlight the correlation with textural features and disease.

[PARA 338] Having now described various embodiments of the invention in detail as required by the patent statutes, those skilled in the art will recognize modifications and

substitutions to the specific embodiments disclosed herein. Such modifications are within the scope and intent of the present invention as defined in the following claims.

WHAT IS CLAIMED IS:

1. A method for selective sampling to assess texture using magnetic resonance (MR) comprising:

transmitting a first RF pulse with a first gradient chosen for first slice selection;

transmitting a second RF pulse with application of a second gradient chosen for slice selective refocusing in a region defined by an intersection of the first slice and a second slice;

encoding a specific k-value with a selected gradient pulse;

transmitting a third RF pulse with a third gradient activated, said third gradient adapted for slice selective refocusing, defining a region defined by the intersection of the first and second slices and a third slice selection to define a volume of interest (VOI);

turning off all gradients;

recording multiple samples of an RF signal encoded with the specific k-value;

applying a non-zero magnitude gradient as a time-dependent phase-encode while recording samples of sequential k-values across a neighborhood of k-values defined by height and pulse width of the non-zero magnitude gradient;

post processing a combination of sequential k values, recorded within a time span while the non-zero magnitude gradient is applied in which the k-values remain correlated, , with all recording in a single TR.

2. The method as defined in claim 1 wherein the step of encoding comprises:

applying an encoding gradient pulse to induce phase wrap to create a spatial encode for the specific k-value and orientation, the specific k-value determined based on texture within the VOI.

3. The method as defined in claim 2 further comprising:

following the recording of multiple samples of an RF signal encoded with the specific k-value, issuing a k-value selection pulse on a selected vector combination gradient to determine a second k-value;

turning off the vector combination gradient; and,

recording multiple samples of the RF signal at the second k-value in the TR.

4. The method as defined in claim 3 further comprising:

applying additional k-value selection pulses for a predetermined plurality of pulses on a selected vector combination gradient, each k value selection pulse determining a next k-value;

turning off the vector combination gradient after each pulse; and,

recording multiple samples of the RF signal at the next k-value determined by each k value selection pulse in the TR.

5. The method as defined in claim 1 further comprising:

transmitting a refocusing RF pulse prior to applying the non-zero magnitude gradient.

6. The method as defined in claim 2 further comprising:

applying a higher magnitude gradient as a time-dependent phase-encode while recording samples of a second set of sequential k-values in the neighborhood of the specific k-value relatively widely spaced across K-space outside the inter-sample correlation imposed by the window function, with all recording in a single TR

7. The method as defined in claim 6 further comprising:

transmitting a second refocusing RF pulse prior to applying the greater magnitude gradient.

8. The method as defined in claim 1 wherein the non-zero magnitude gradient comprises a gradient inducing samples in k-space which will be sufficiently closely spaced so that the samples are highly correlated.

9. The method as defined in claim 2 wherein the specific k value is in a range of $0.2mm^{-1}$ to $100\ mm^{-1}$ and the neighborhood of k-values induced by the non-zero magnitude gradient are a subset of the range.

10. The method as defined in claim 6 wherein the higher magnitude gradient comprises a gradient inducing samples in k-space outside a neighborhood where the underlying values are highly correlated.

11. The method as defined in claim 10 wherein the specific k value is in a range of $0.2mm^{-1}$ to $100\ mm^{-1}$ and the neighborhood of k-values induced by the non-zero magnitude gradient are a subset of the range with sample to sample correlation with blocks in the range.

12. The method as defined in claim 1 wherein the non-zero magnitude gradient is determined based on a windowing function and is defined as $G \leq \frac{\sqrt{3!(1-\eta_{\min})}}{\pi X \cdot N \cdot \Delta t}$.

13. The method as defined in claim 1 wherein, while defining the VOI, correlation across a range of k-space created by the non-zero magnitude gradient is induced by selection of a windowing function.

14. The method as defined in claim 1 wherein correction for change in k across a set neighborhood created by the non-zero magnitude gradient is induced by a set of k measurements with proscribed k encodes.

15. A method for selective sampling to assess texture using magnetic resonance (MR) comprising:

transmitting RF pulses and associated gradients to define a volume of interest (VOI);

applying an encoding gradient pulse to induce phase wrap to create a spatial encode for a specific k-value and orientation determined based on texture within the VOI as an initial value in a k-value range with low SNR;

applying a non-zero magnitude gradient as a time-dependent phase-encode while recording samples of sequential k-values across a neighborhood around the specific k-value defined by height and pulse width of the non-zero magnitude gradient; and,

post processing sequential k values, recorded within a time span while the gradient is applied, in which the k-values remain correlated, the number of samples providing high SNR.

16. A method for selective sampling to assess texture using magnetic resonance (MR) comprising:

transmitting RF pulses and associated gradients to define a volume of interest (VOI);

applying an encoding gradient pulse to induce phase wrap to create a spatial encode for a specific k-value and orientation determined based on texture within the VOI as an initial value in a k-value range with high SNR;

applying a non-zero magnitude gradient as a time-dependent phase-encode while recording a range of samples of a set of sequential k-values in a neighborhood of the specific k-value relatively widely spaced outside the inter-sample correlation imposed by the window function.

17. The method as defined in claim 16 wherein recording samples of a set of sequential k-values comprises sampling in overlapping blocks of k-values.

18. The method as defined in claim 17 wherein sequential k-values in the blocks are combined in a manner to be sufficiently correlated to yield an improvement in SNR via the combination and further comprising:

post processing sequential k values in the blocks in which the k-values remain correlated as combined data points, the number of samples providing high SNR; and,

characterizing the power distribution across the a range of recorded samples using the combined data points to measure underlying texture within the VOI.

19. The method as defined in claim 15 wherein the specific k value is in a range of $0.2mm^{-1}$ to 100 mm^{-1} and the neighborhood of k-values are a subset of the range.

20. The method as defined in claim 16 wherein the specific k value is in a range of $0.2mm^{-1}$ to 100 mm^{-1} and the neighborhood of k-values are a subset of the range.

21. A method for selective sampling to assess tissue texture using magnetic resonance (MR) comprising:

applying a contrast mechanism enhancing the contrast between the component tissue types in a multiphase biologic sample being measured;

selectively exciting a volume of interest (VOI) employing a plurality of time varying radio frequency signals and applied gradients;

applying an encoding gradient pulse to induce phase wrap to create a spatial encode for a specific k-value and orientation, the specific k-value determined based on texture within the VOI;

initiating a time varying series of gradients to produce a time varying trajectory through 3D k-space of k-value encodes, a resulting k-value set being a subset of that required to produce an image of the VOI;

simultaneously recording multiple sequential samples of the NMR RF signal encoded with the k-value set;

post processing the recorded NMR signal samples to produce a data set of signal vs k-values for k-values in the k-value set determined by the trajectory, to characterize the textural features of tissue in the VOI.

22. The method for selective sampling to assess tissue texture using MR as defined in claim 21 wherein the step of selectively exciting a VOI comprises:

transmitting a first RF pulse with a first gradient chosen for first slice selection;

transmitting a second RF pulse with application of a second gradient chosen for slice selective refocusing in a region defined by an intersection of the first slice and a second slice;

applying the encoding gradient pulse;

transmitting a third RF pulse with a third gradient activated, said third gradient adapted for slice selective refocusing, defining a region defined by the intersection of the first and second slices and a third slice selection to define the VOI.

23. The method for selective sampling to assess tissue texture using MR as defined in claim 21 wherein component tissue type is fibrotic tissue and wherein the step of applying contrast mechanism further comprises selecting a contrast mechanism from exogenous or endogenous contrast mechanisms to provide contrast between fibrotic structure and surrounding tissue, including T1, T2, or T2*, IR weighting, or functional contrast, such as diffusion or flow contrast, BOLD (Blood Oxygenation Level Dependent), ASL (Arterial Spin Labelling), and diffusion weighting contrast.

24. The method for selective sampling to assess tissue texture using MR as defined in claim 23 wherein applying a contrast mechanism comprises:

applying a first diffusion gradient during the step of selectively exciting a VOI after transmitting a first RF pulse with a first gradient chosen for first slice selection and transmitting a second RF pulse with application of a second gradient chosen for slice

selective refocusing in a region defined by an intersection of the first slice and a second slice, wherein completing exciting of the VOI comprises transmitting a third RF pulse with a third gradient activated, said third gradient adapted for slice selective refocusing, defining a region defined by the intersection of the first and second slices and a third slice selection to define the volume of interest (VOI); and,

applying a second diffusion gradient, said first and second diffusion gradients establishing contrast; and,

said step of applying an encoding gradient pulse further comprises setting the specific k-value based on fibrotic texture.

25. The method for selective sampling to assess tissue texture using MR as defined in claim 23 wherein selectively exciting a VOI comprises:

positioning VOIs at various locations in a liver, using either interleaved acquisition within one TR, or measurements in separate multiple TRs, to sample pathology variability within the liver;

wherein texture spatial coherence is maintained within each defined VOI during the step of recording multiple sequential samples of the NMR RF signal by defining the trajectory through 3D k-space of k-value encodes for specific k-values or k-value ranges, to enable SNR maximization through signal averaging.

26. The method for selective sampling to assess tissue texture using MR as defined in claim 21 wherein the component tissue type is bone and the step of applying contrast mechanism further comprises selecting a contrast mechanism from proton density weighting, T1 contrast, diffusion weighting to highlight diffusion within marrow; using T2 contrast in lesions within the bone to highlight fluid, to type a bone lesion as either lytic or sclerotic, or other contrast mechanism to highlight the trabecular bone microarchitecture.

27. The method for selective sampling to assess tissue texture using MR as defined in claim 26 wherein the specific k-value and k-value set established by the time varying gradients encompasses a range of TbSp and TbTh up to 5mm.

28. The method for selective sampling to assess tissue texture using MR as defined in claim 21 wherein component tissue type is vasculature and wherein the step of applying a contrast mechanism further comprises selecting a contrast mechanism from exogenous or endogenous contrast, with contrast mechanism including ASL (Arterial Spin Labeling), Gd

contrast, T1, T2, T2*, and proton density contrast, BOLD (Blood Oxygenation Level Dependent) contrast.

29. The method for selective sampling to assess tissue texture using MR as defined in claim 28 further comprising:

performing perfusion imaging to provide assessment of vessel health/pathology; and,

defining a VOI for selective excitation in which the perfusion imaging sequence has highlighted possible vessel pathology.

30 The method of claim 21 for selective sampling to assess tissue texture using MR as defined in claim 1 wherein component tissue type is ordered neuronal architecture in brain tissue where applying a contrast mechanism comprises further comprises choosing a contrast mechanism from T1 weighting, T2 IR, T2*, inversion recovery or diffusion weighting.

31 The method of claim 21 for selective sampling to assess tissue texture using MR as defined in claim 1 wherein component tissue type is ordered neuronal architecture in brain tissue wherein the VOI is placed within a cortex and the spatial encode is in the range of k-values corresponding to spatial wavelengths of 40 micrometers to 200 micrometers and the VOI is further aligned tangent to a surface of the cortex.

32 The method for selective sampling to assess tissue texture using MR as defined in claim 30 further comprising consecutively repeating the time varying series of gradients to produce trajectories through 3D k-space with resulting k-value sets oriented around the specific k-value to locate resonance.

33. The method for selective sampling to assess tissue texture using MR as defined in claim 32 wherein the resulting k-value sets are oriented within 10 degrees of the specific k-value.

34. The method for selective sampling to assess tissue texture using MR as defined in claim 30 wherein the VOI is centered in the cortex height, aligning the acquisition axis parallel to top and bottom surfaces at the VOI midpoint; and further comprising:

acquiring signal data with gradient on or off, across a range of k-values centered on the expected spacing of the minicolumns to measure spacing of columns.

35. The method for selective sampling to assess tissue texture using MR as defined in claim 34 further comprising rocking the acquisition gradient in angular increments to determine signal resonance.

36. The method for selective sampling to assess tissue texture using MR as defined in claim 30 wherein selectively exciting the VOI defines VOI dimensions to enable fitting the VOI fit into the brain entirely at different locations to enable determination of the spatial variability of the textural features and the acquisition gradients provide signal data across a range in k-space corresponding to wavelengths of ten microns out to about 1-2 mm with a range of the k-values set, in up to three orthogonal directions, and further comprising:

obtaining biomarkers from as selected set including MRI imaging data on hippocampal shrinkage, FDG-PET, MMSE (Mini Mental State Exam) and genetic predilection for AD;

inputting the data set of signal vs k-values for k-values in the k-value set determined by the trajectory to characterize the textural features of tissue in the VOI and the biomarkers obtained into a machine learning algorithm; and,

receiving an output from the machine learning algorithm correlating with textural features and disease.

37. A method for selective sampling to assess brain tissue texture using magnetic resonance (MR) comprising:

choosing a contrast mechanism from T1 weighting, T2 IR, T2*, inversion recovery or diffusion weighting;

applying the contrast mechanism;

selectively exciting an original volume of interest (VOI) employing a plurality of time varying radio frequency signals and applied gradients such that the VOI is positioned centered in a cortex height of the brain, aligning an axis of the specific k-value parallel to a surface of the cortex at a midtpoint of the VOI;

applying an encoding gradient pulse to induce phase wrap to create a spatial encode for a specific k-value and orientation, the specific k-value centered on the expected spacing of tissue minicolumns to measure spacing of the minicolumns;

initiating a time varying series of acquisition gradients to produce a time varying trajectory through 3D k-space of k-value encodes, a resulting k-value set being a subset of that required to produce an image of the VOI;

simultaneously recording multiple sequential samples of the NMR RF signal encoded with the k-value set to acquire signal across a range of k-values;

rocking the acquisition gradient is in angular increments determining signal resonance wherein sharpness of the signal resonance reflects an order of the minicolumns;

selecting an acquisition angle;

repeating a time varying series of acquisition gradients to produce time varying trajectories through 3D k-space of k-value encodes for a range of k-values swept to determine a peak of the signal vs. k-value distribution; and,

selectively exciting additional VOIs employing a plurality of time varying radio frequency signals and applied gradients, the additional VOIs at other positions in the cortex or nearby the original VOI, either within one TR or multiple TRs.

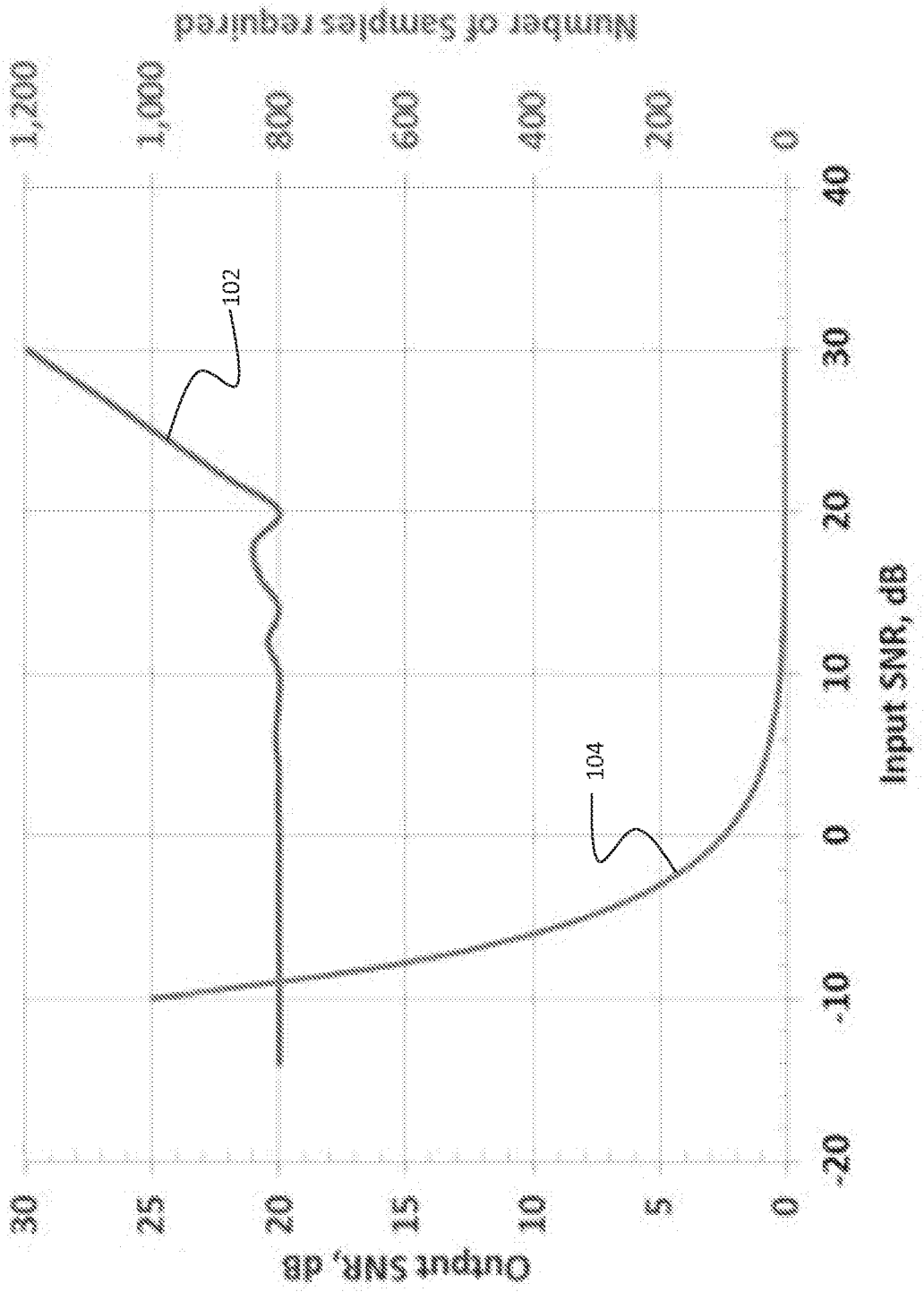
Number of Samples required
1,200
1,000
800
600
400
200
0
102
104
Output SNR, dB
30
25
20
15
10
5
0
Input SNR, dB
40
30
20
10
0
-10
-20

FIG. 1

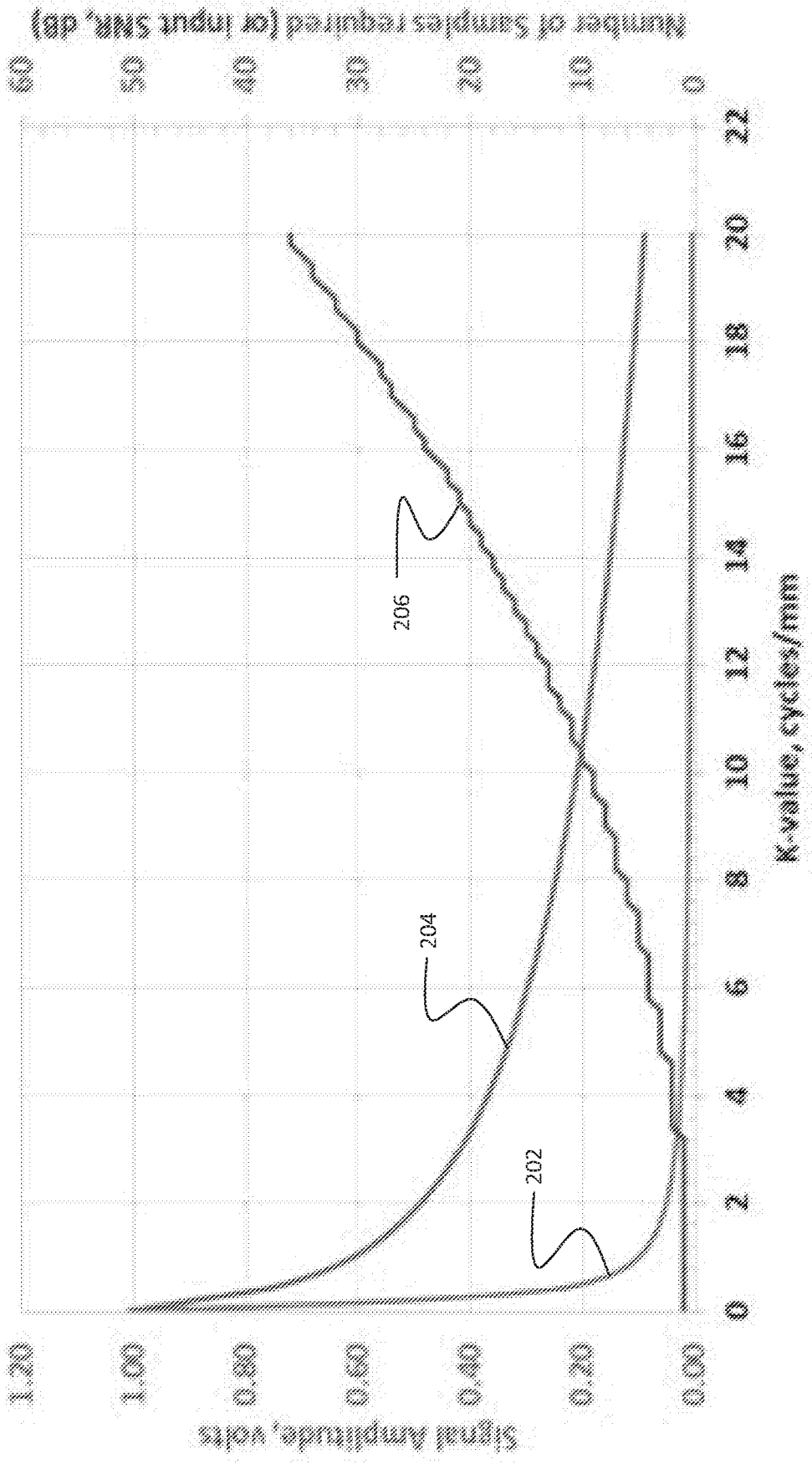
Number of Samples required (or Input SNR, dB)
0
10
20
30
40
50
60
Signal Amplitude, volts
1.20
1.00
0.80
0.60
0.40
0.20
0.00
K-value, cycles/mm
0
2
4
6
8
10
12
14
16
18
20
22
202
204
206

FIG. 2

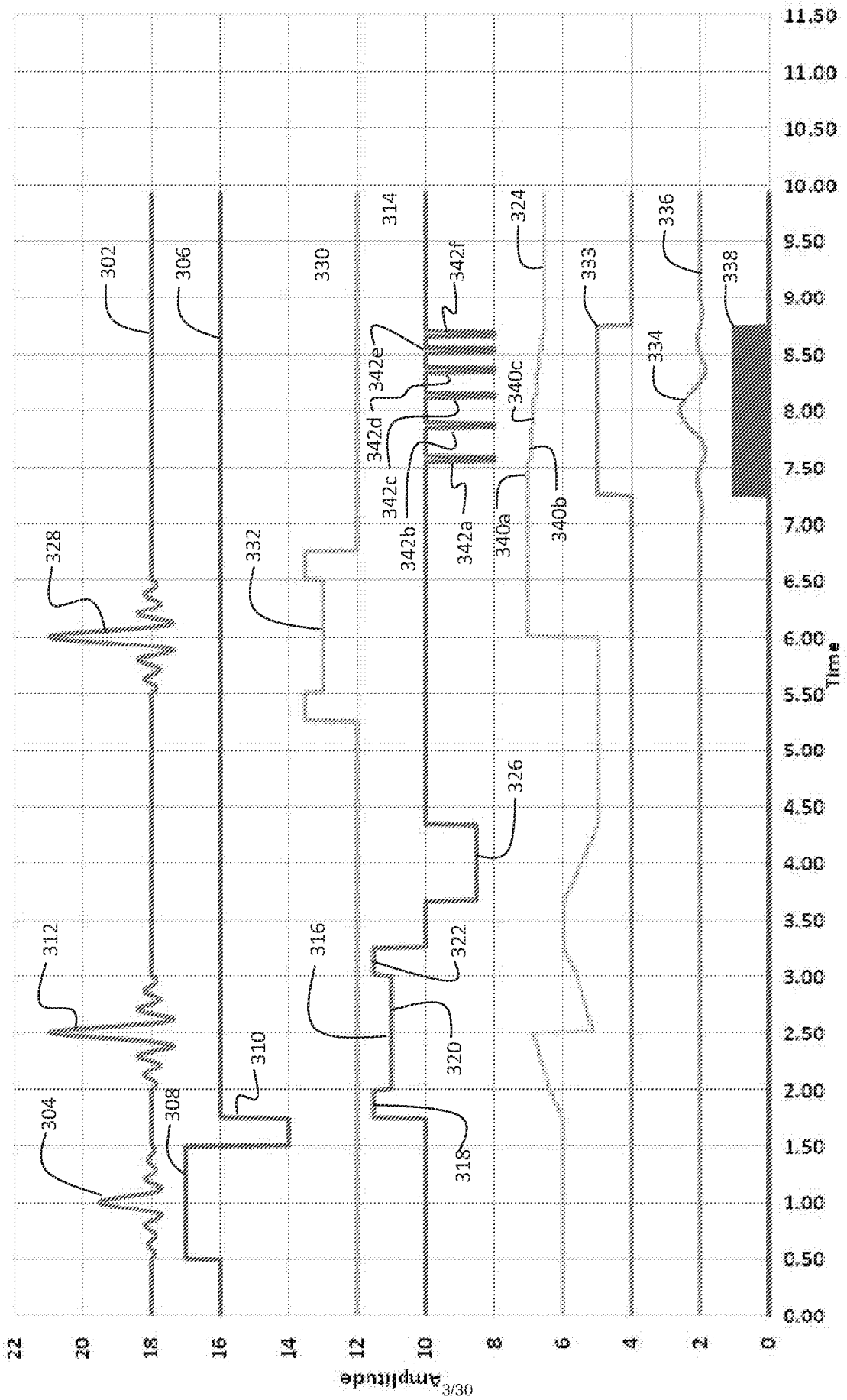
Amplitude
Time
22
20
18
16
14
12
10
8
6
4
2
0
11.50
11.00
10.50
10.00
9.50
9.00
8.50
8.00
7.50
7.00
6.50
6.00
5.50
5.00
4.50
4.00
3.50
3.00
2.50
2.00
1.50
1.00
0.50
0.00
302
304
306
308
310
312
314
316
318
320
322
324
326
328
330
332
333
334
336
338
340a
340b
340c
342a
342b
342c
342d
342e
342f

FIG. 3

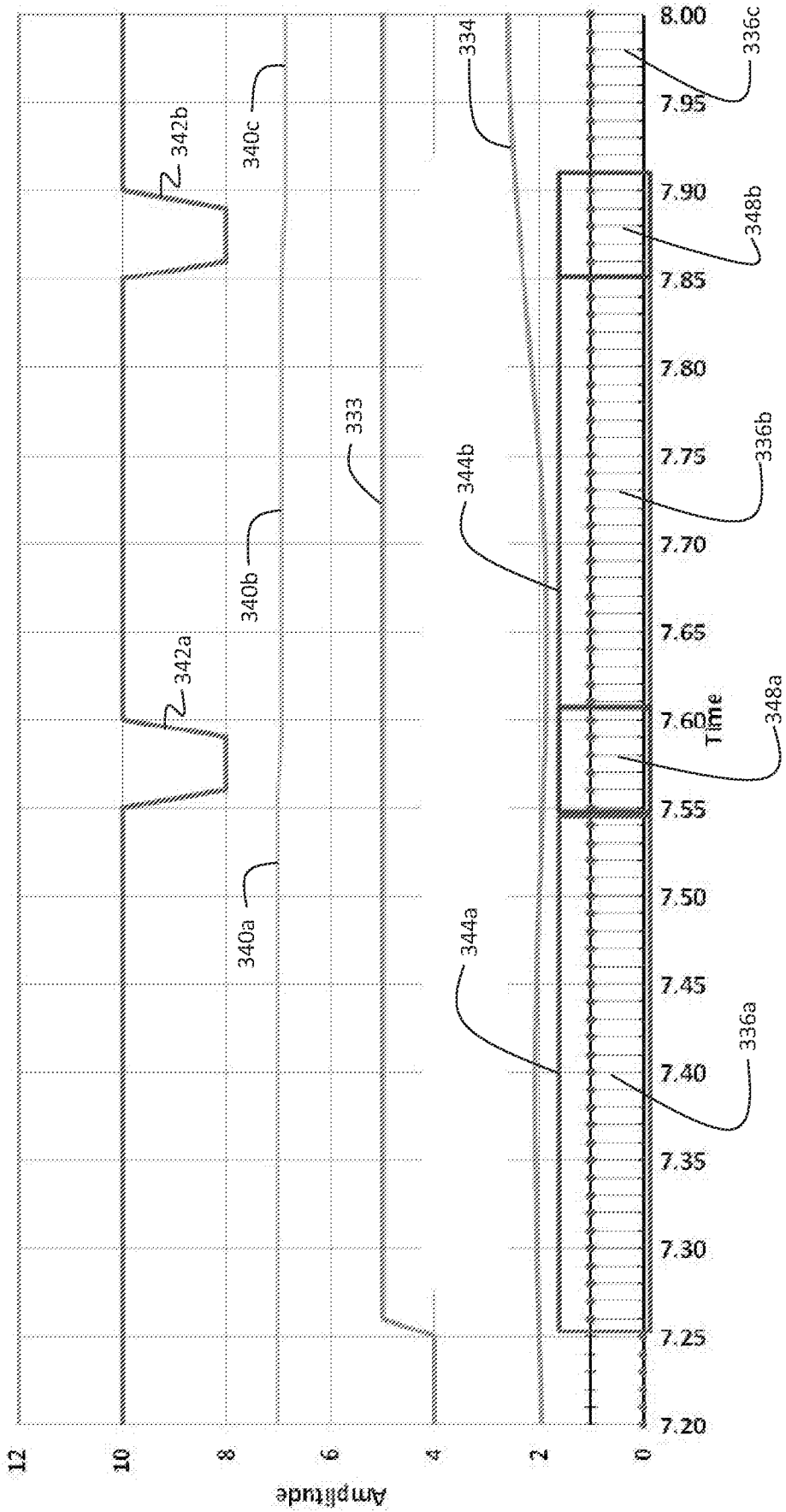
Amplitude
12
10
8
6
4
2
0
Time
8.00
7.95
7.90
7.85
7.80
7.75
7.70
7.65
7.60
7.55
7.50
7.45
7.40
7.35
7.30
7.25
7.20
342b
342a
340c
340b
340a
333
334
344b
344a
348b
348a
336c
336b
336a

FIG. 4

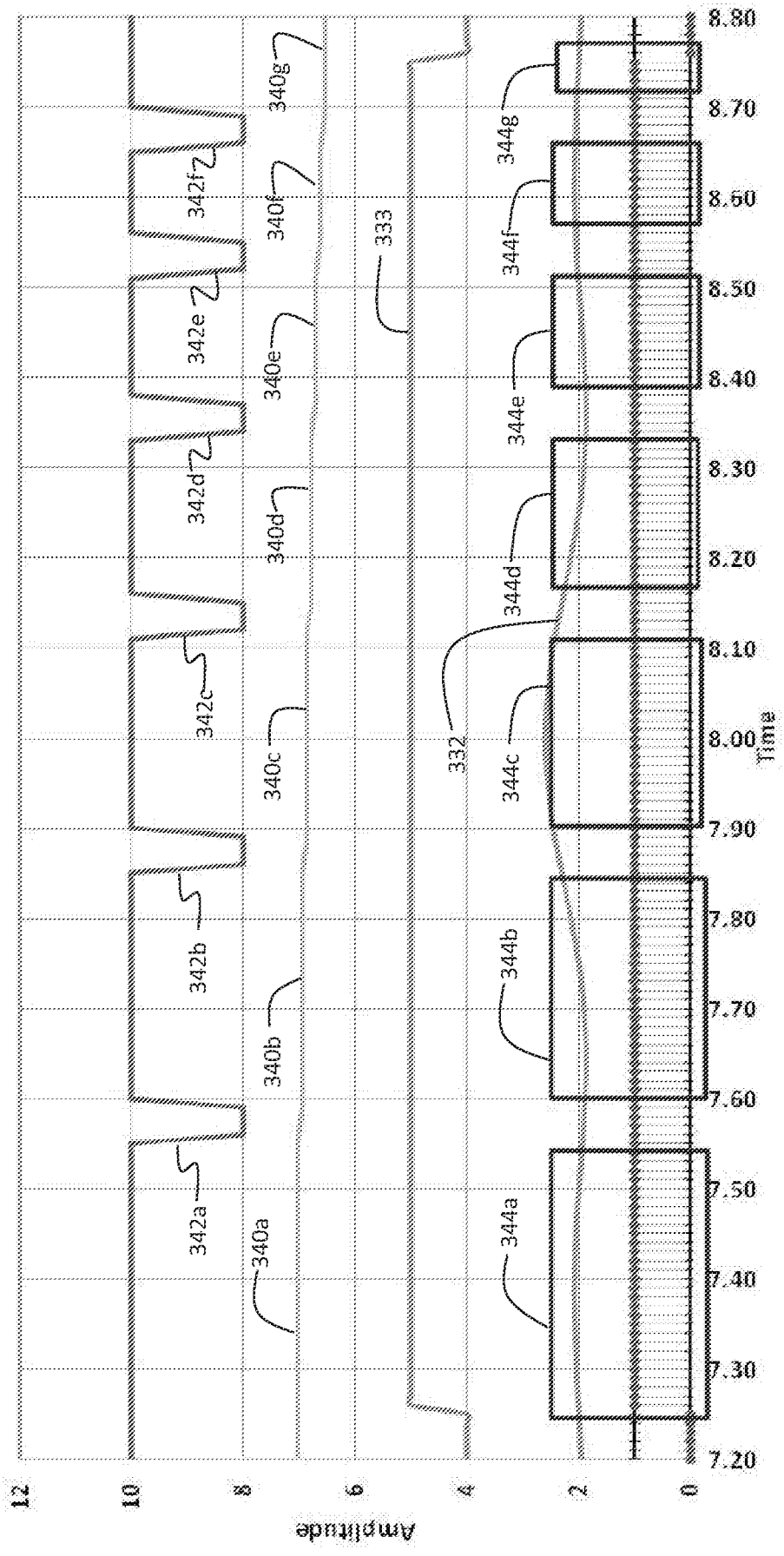
Amplitude
12
10
8
6
4
2
0
Time
8.80
8.70
8.60
8.50
8.40
8.30
8.20
8.10
8.00
7.90
7.80
7.70
7.60
7.50
7.40
7.30
7.20
342a
342b
342c
342d
342e
342f
340a
340b
340c
340d
340e
340f
340g
333
332
344a
344b
344c
344d
344e
344f
344g

FIG. 5

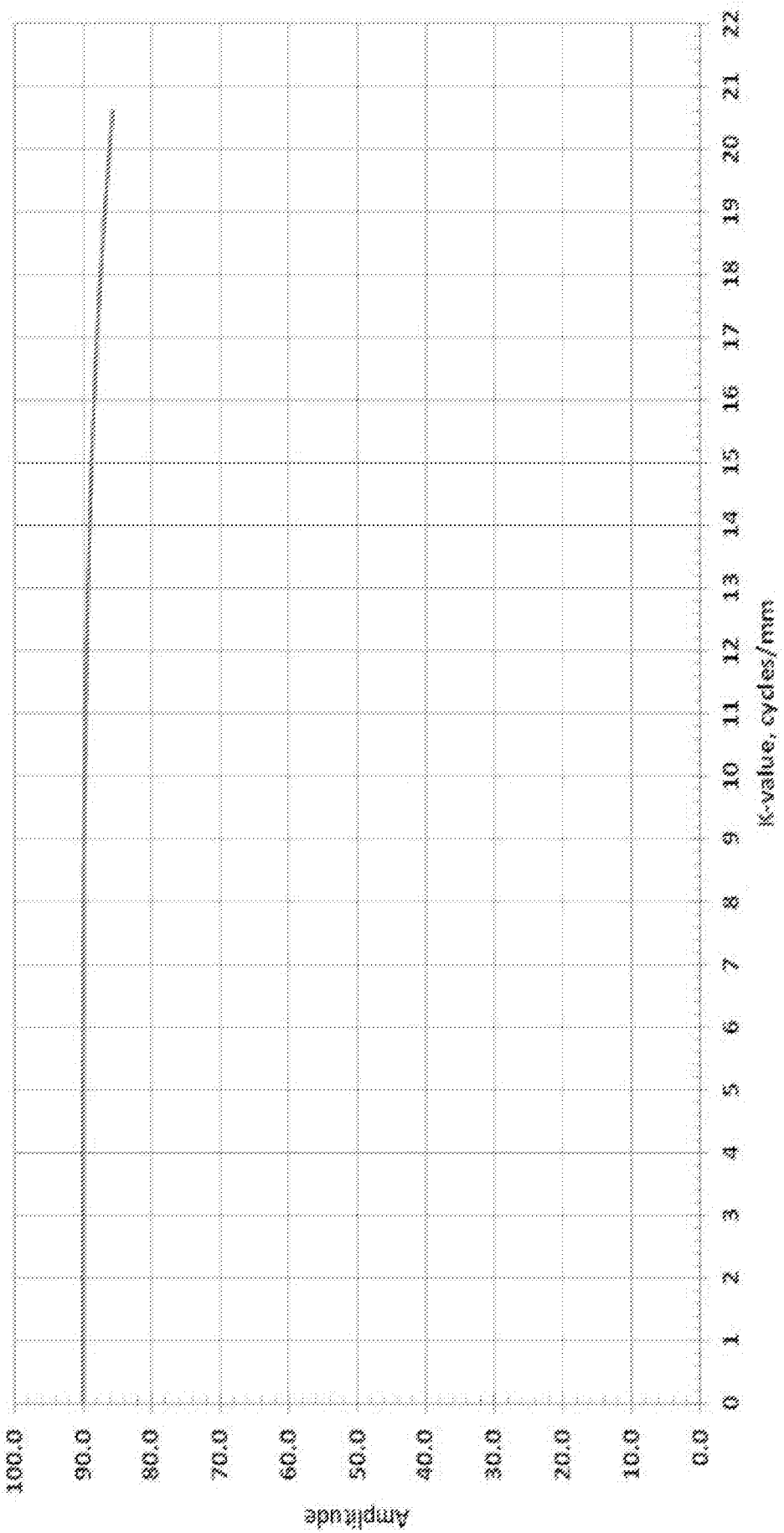
Amplitude
100.0
90.0
80.0
70.0
60.0
50.0
40.0
30.0
20.0
10.0
0.0
0 1 2 3 4 5 6 7 8 9 10 11 12 13 14 15 16 17 18 19 20 21 22
K-value, cycles/mm

FIG. 6

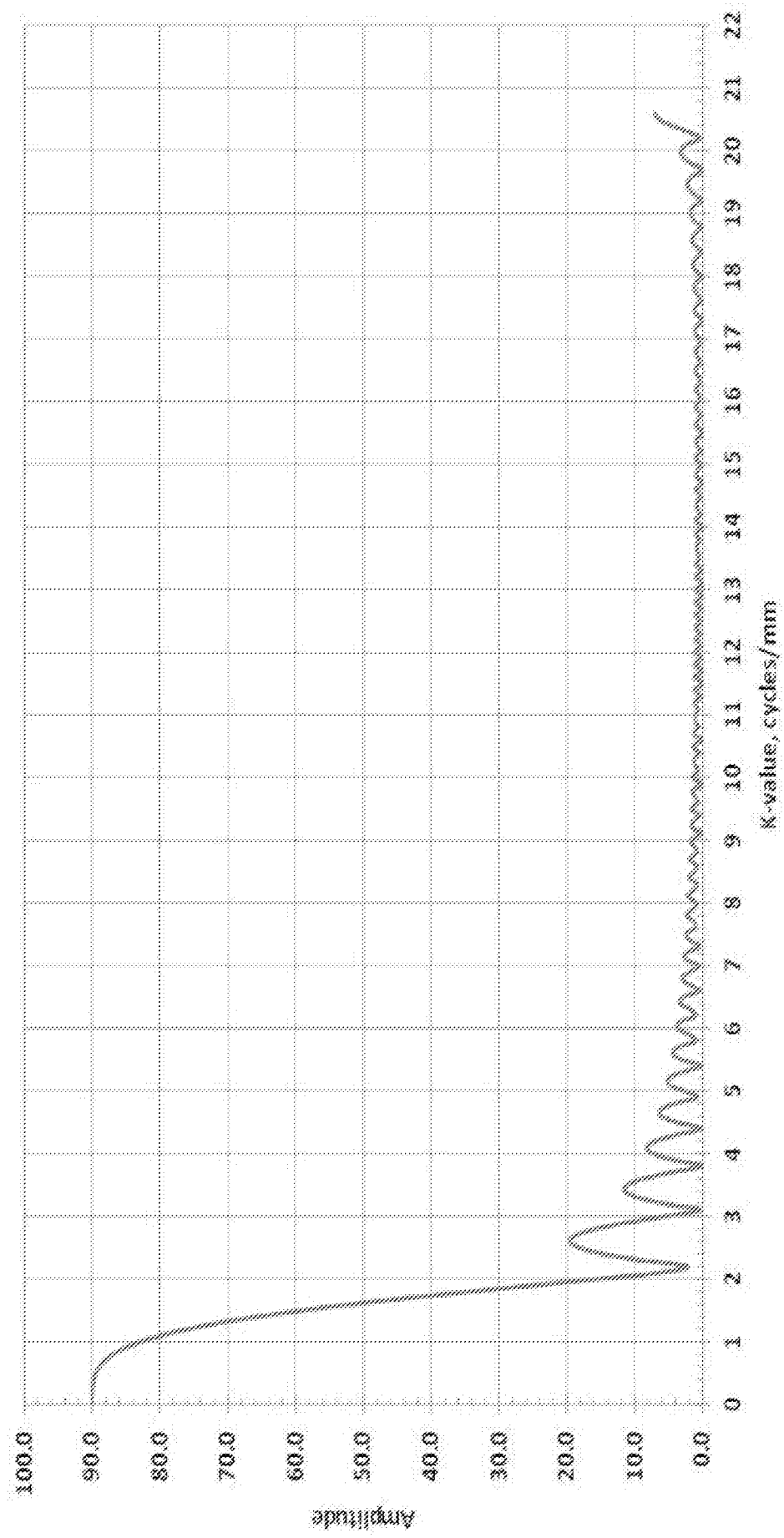
Amplitude
100.0
90.0
80.0
70.0
60.0
50.0
40.0
30.0
20.0
10.0
0.0
0 1 2 3 4 5 6 7 8 9 10 11 12 13 14 15 16 17 18 19 20 21 22
K-value, cycles/mm

FIG. 7

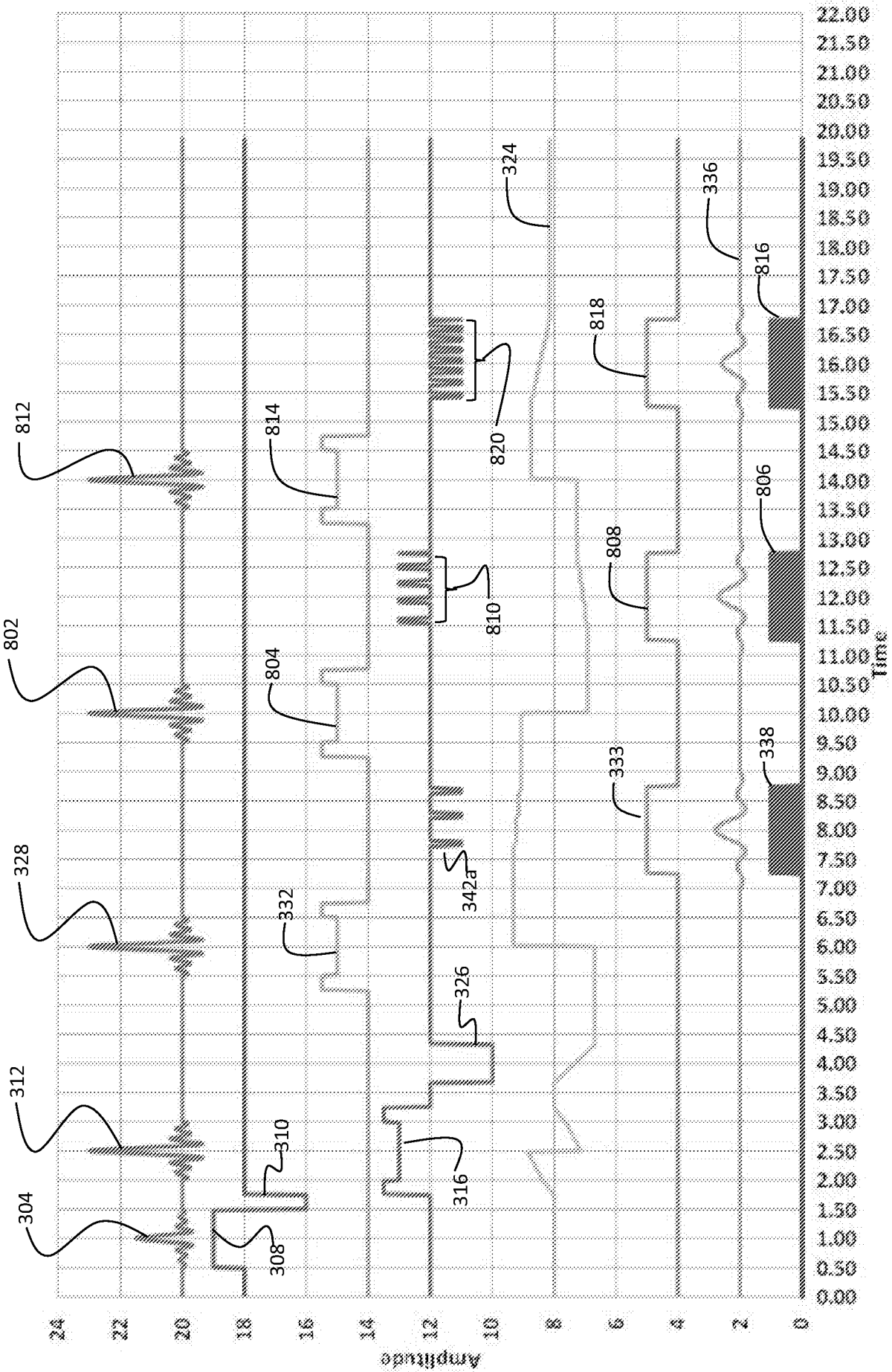
Amplitude
24
22
20
18
16
14
12
10
8
6
4
2
0
Time
22.00
21.50
21.00
20.50
20.00
19.50
19.00
18.50
18.00
17.50
17.00
16.50
16.00
15.50
15.00
14.50
14.00
13.50
13.00
12.50
12.00
11.50
11.00
10.50
10.00
9.50
9.00
8.50
8.00
7.50
7.00
6.50
6.00
5.50
5.00
4.50
4.00
3.50
3.00
2.50
2.00
1.50
1.00
0.50
0.00
304
308
310
312
316
324
326
328
332
333
336
338
342a
802
804
806
808
810
812
814
816
818
820

FIG. 8

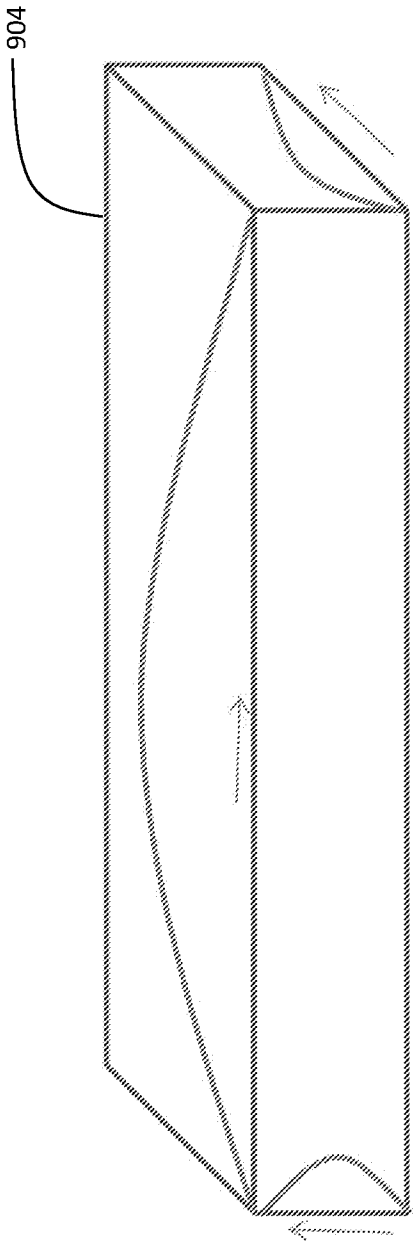

FIG. 9

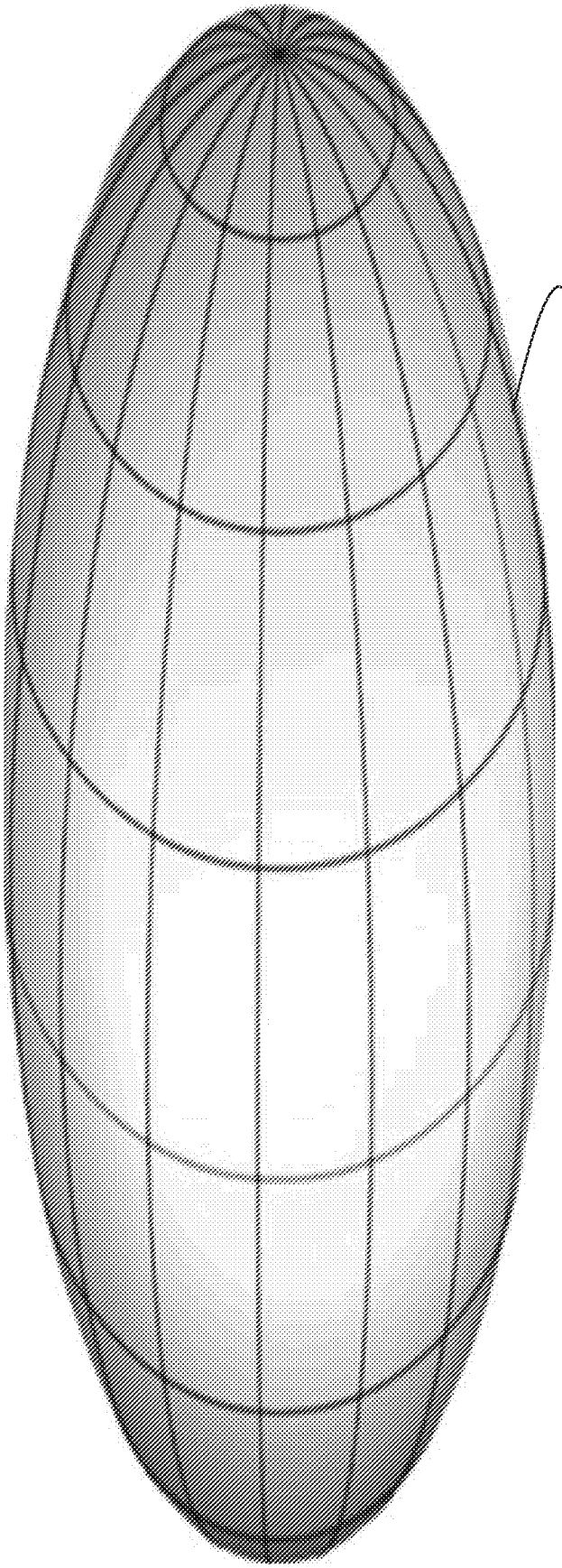

FIG. 10

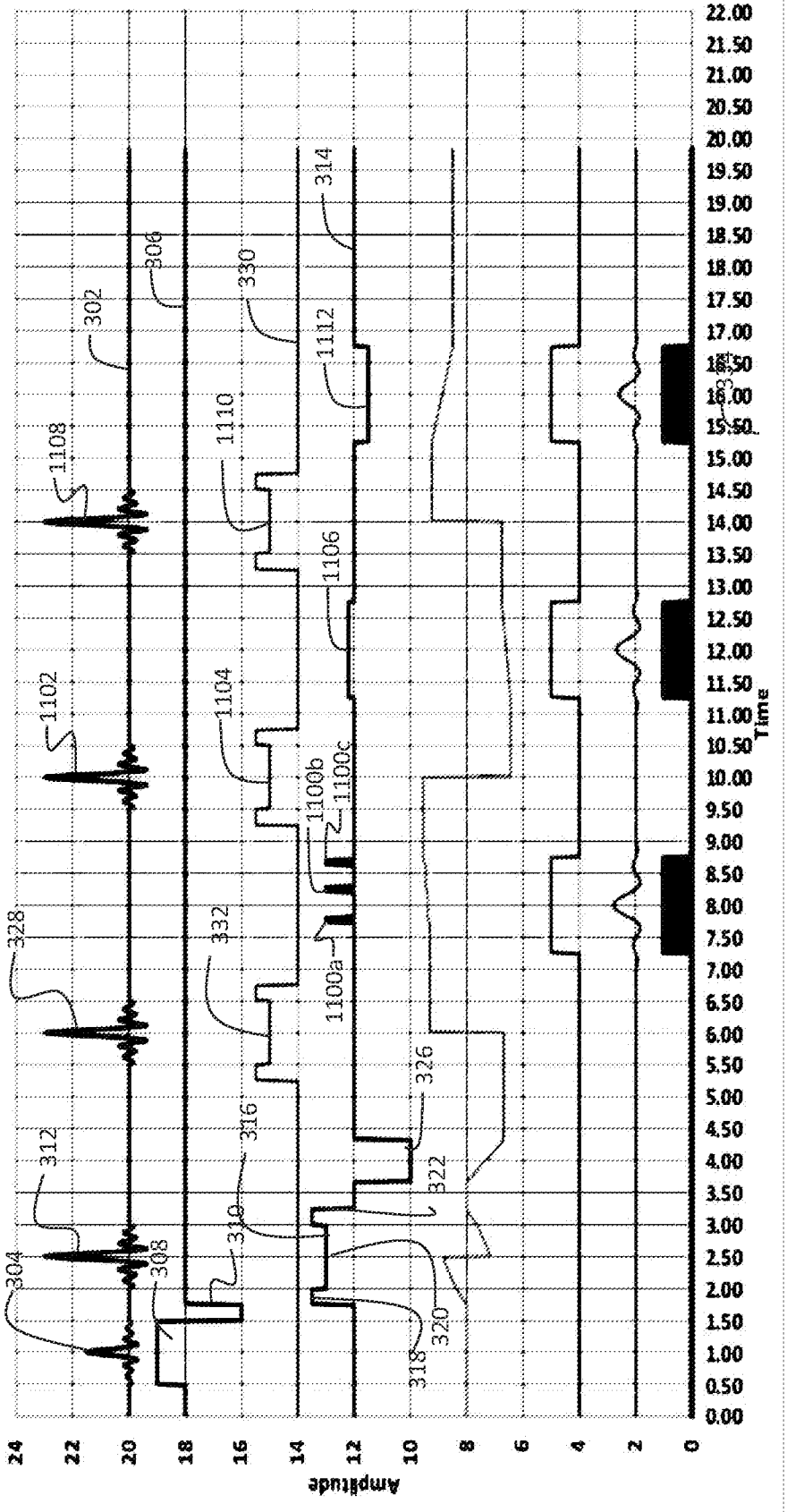
Amplitude
Time
304
308
310
312
316
318
320
322
326
328
332
1100a
1100b
1100c
1102
1104
1106
1108
1110
1112
302
306
330
314

FIG. 11

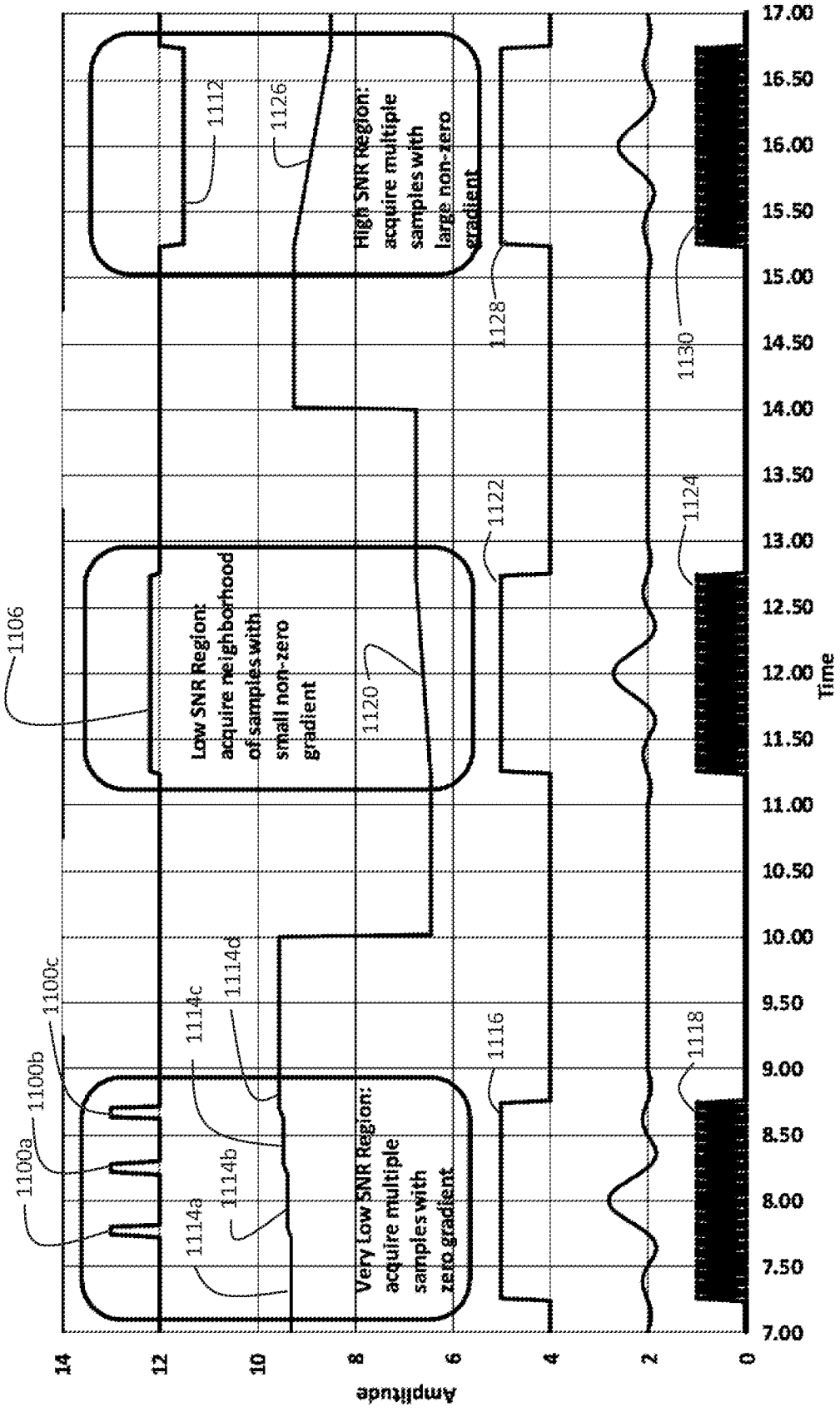
Amplitude
Time
14
12
10
8
6
4
2
0
17.00
16.50
16.00
15.50
15.00
14.50
14.00
13.50
13.00
12.50
12.00
11.50
11.00
10.50
10.00
9.50
9.00
8.50
8.00
7.50
7.00
1100a
1100b
1100c
1106
1112
1114a
1114b
1114c
1114d
1116
1118
1120
1122
1124
1126
1128
1130
High SNR Region: acquire multiple samples with large non-zero gradient
Low SNR Region: acquire neighborhood of samples with small non-zero gradient
Very Low SNR Region: acquire multiple samples with zero gradient

FIG. 12

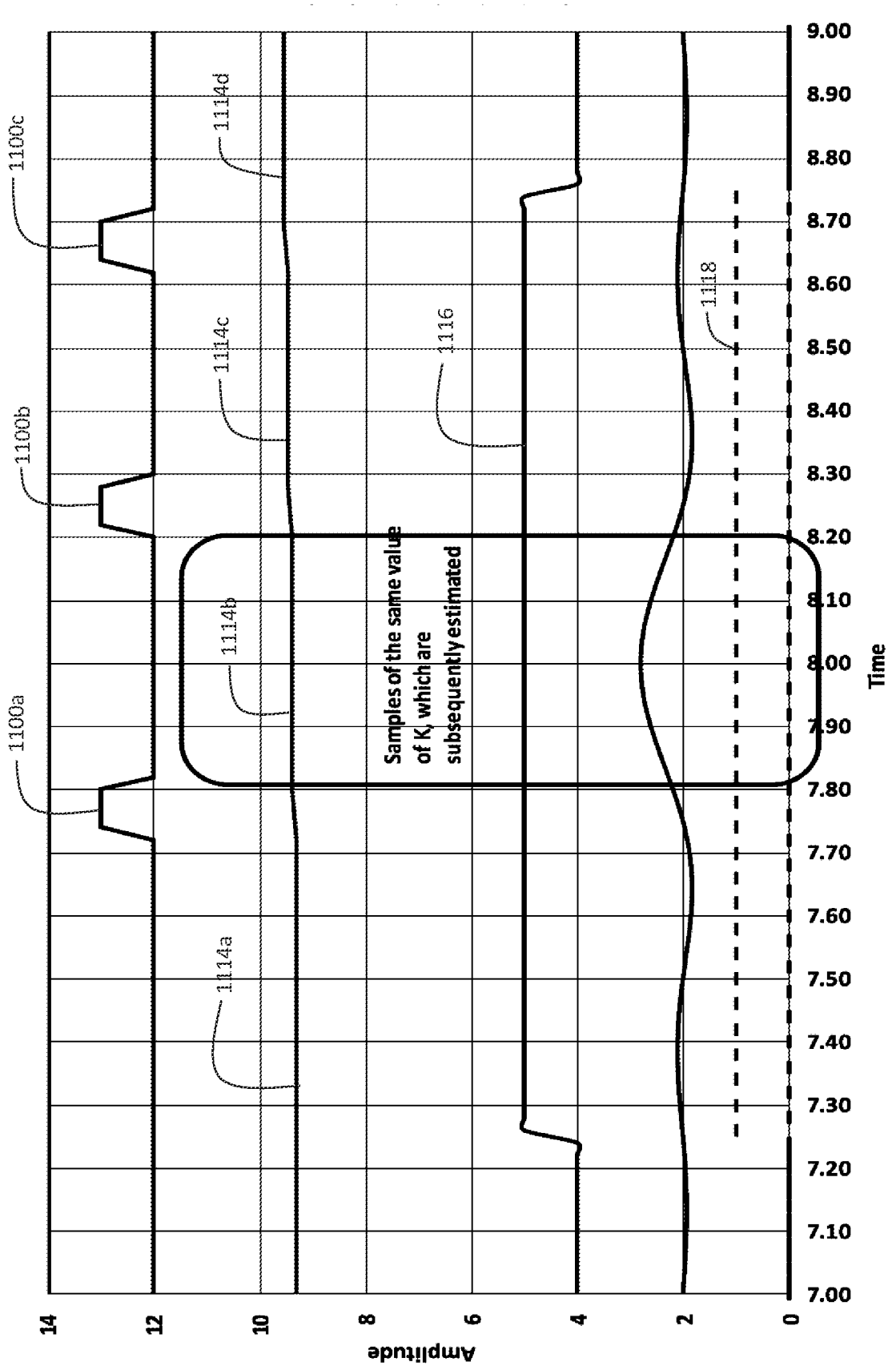
1100a
1100b
1100c
1114a
1114b
1114c
1114d
1116
1118
Samples of the same value of K, which are subsequently estimated
Amplitude
Time
14
12
10
8
6
4
2
0
9.00
8.90
8.80
8.70
8.60
8.50
8.40
8.30
8.20
8.10
8.00
7.90
7.80
7.70
7.60
7.50
7.40
7.30
7.20
7.10
7.00

FIG. 13

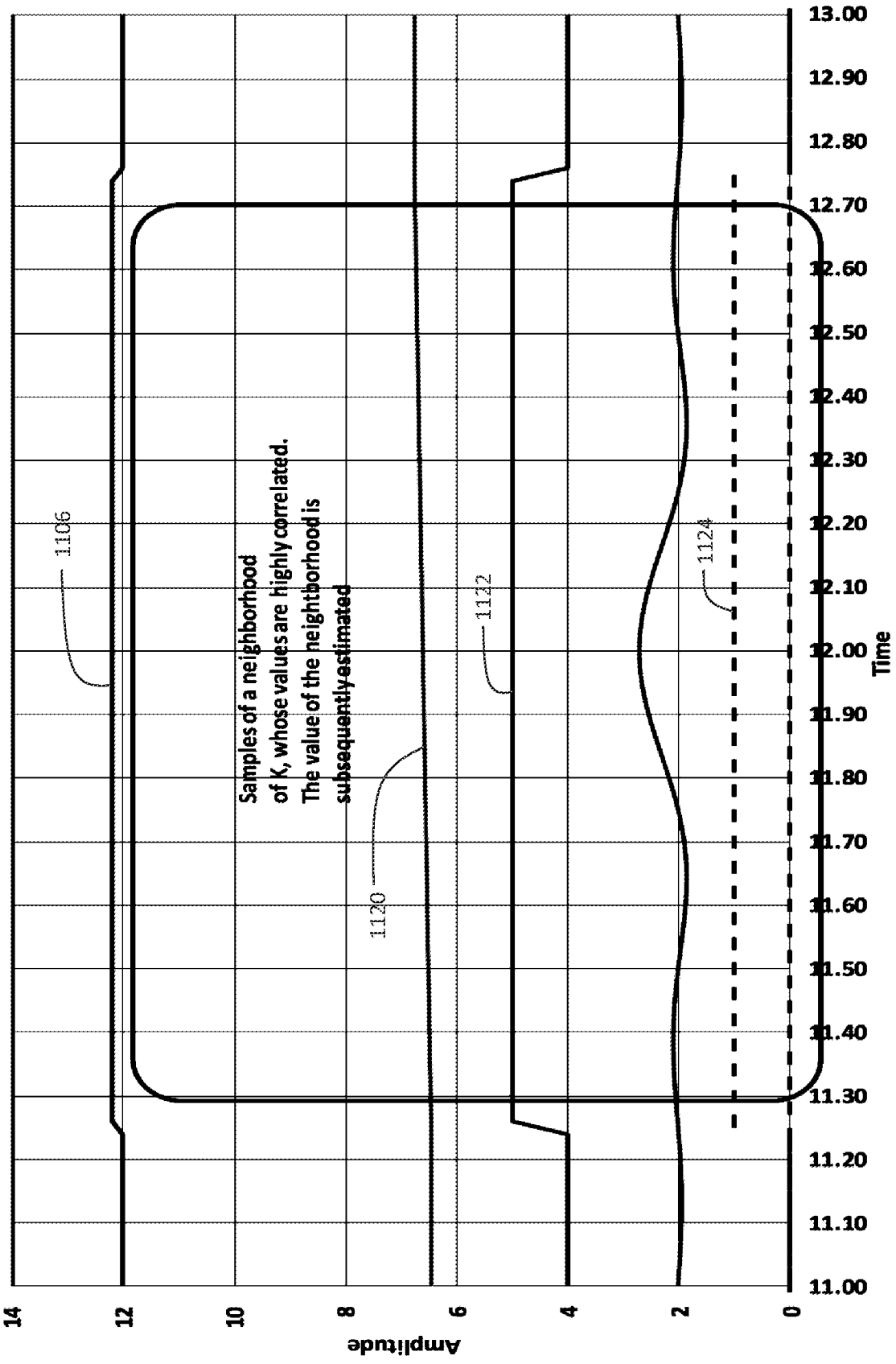
13.00
12.90
12.80
12.70
12.60
12.50
12.40
12.30
12.20
12.10
12.00
11.90
11.80
11.70
11.60
11.50
11.40
11.30
11.20
11.10
11.00
Time
14
12
10
8
6
4
2
0
Amplitude
1106
1120
1122
1124
Samples of a neighborhood
of K, whose values are highly correlated.
The value of the neightborhood is
subsequently estimated

FIG. 14

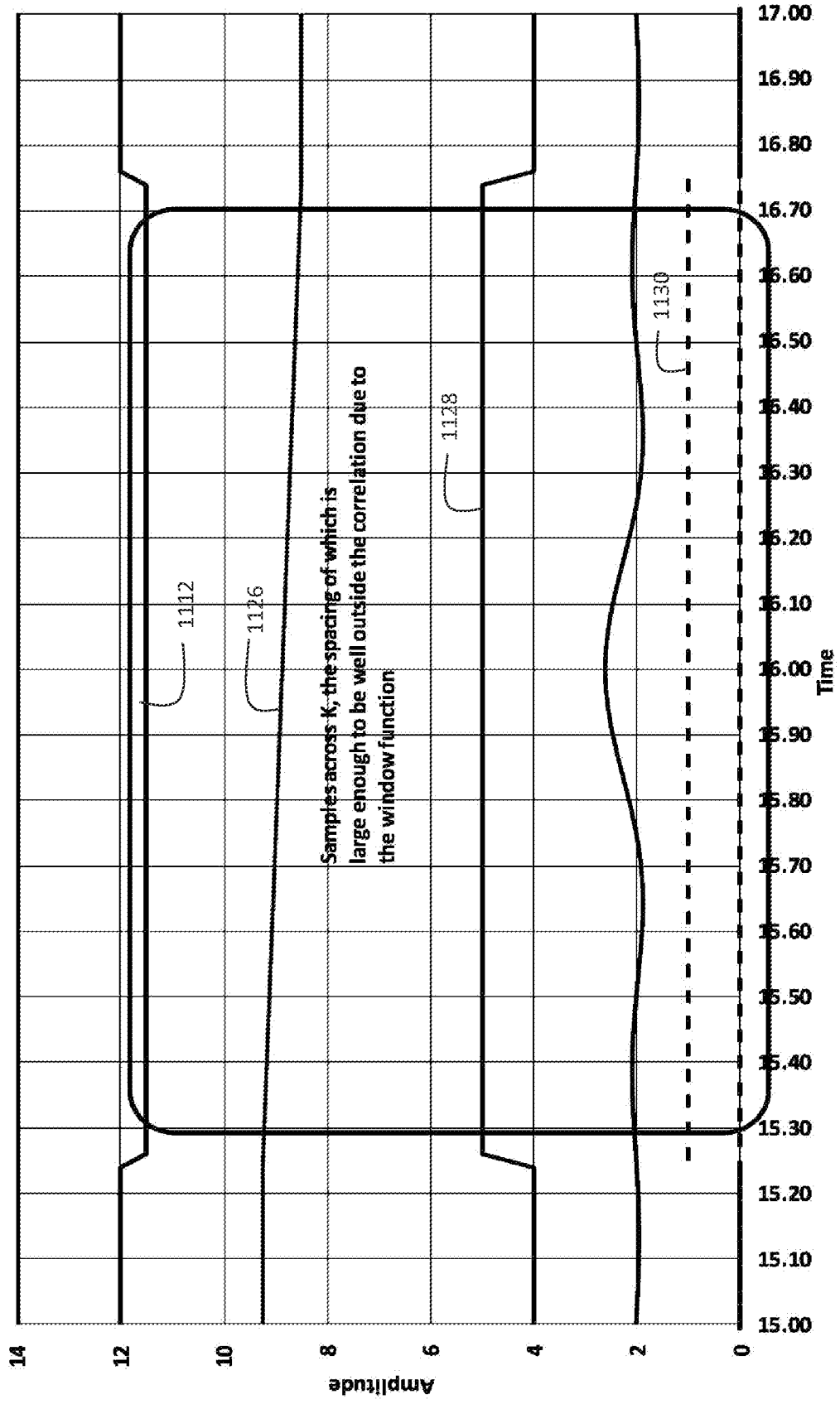
17.00
16.90
16.80
16.70
16.60
16.50
16.40
16.30
16.20
16.10
16.00
15.90
15.80
15.70
15.60
15.50
15.40
15.30
15.20
15.10
15.00
Time
14
12
10
8
6
4
2
0
Amplitude
1112
1126
Samples across K, the spacing of which is large enough to be well outside the correlation due to the window function
1128
1130

FIG. 15

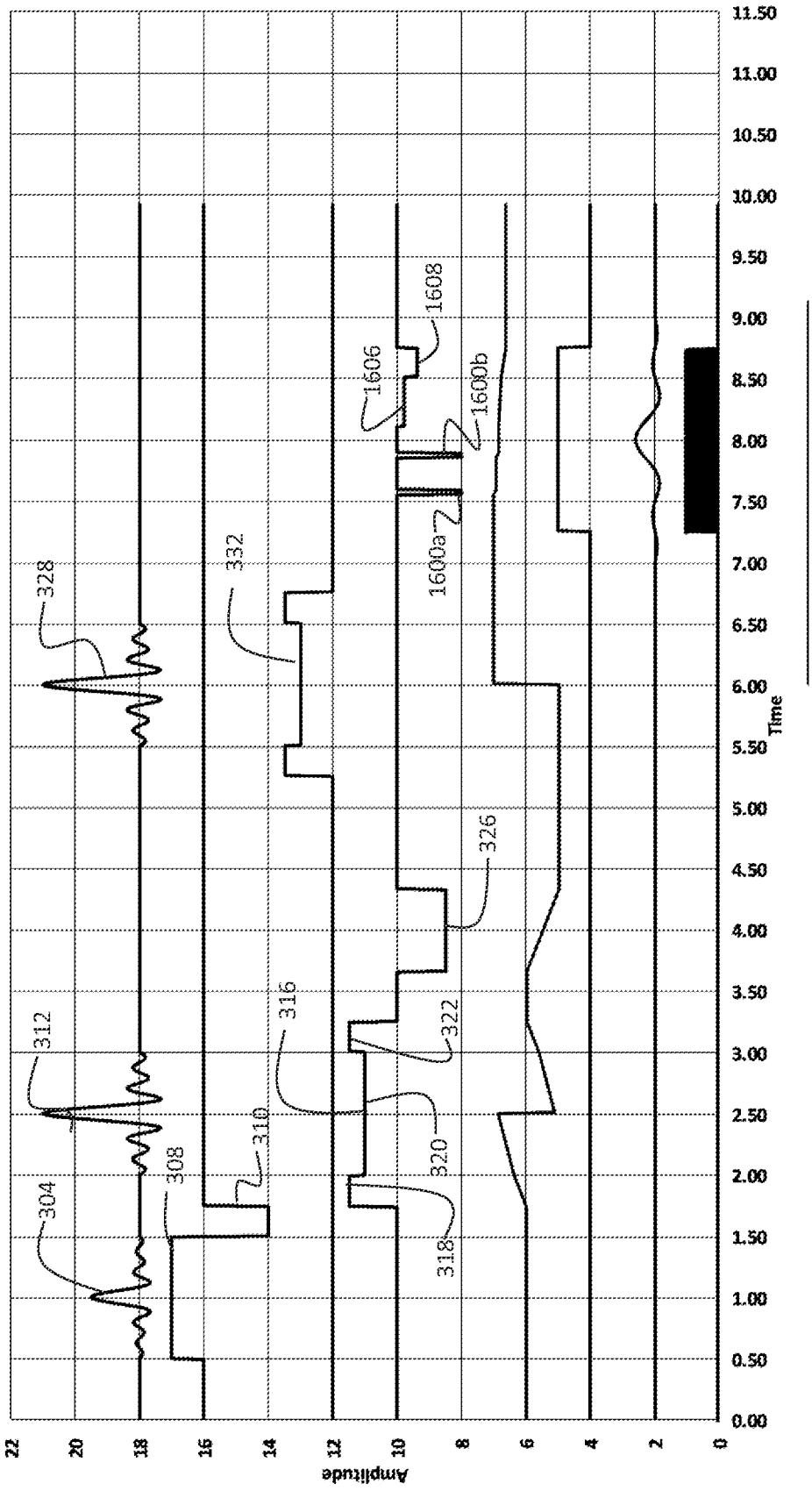
Amplitude
Time
22
20
18
16
14
12
10
8
6
4
2
0
11.50
11.00
10.50
10.00
9.50
9.00
8.50
8.00
7.50
7.00
6.50
6.00
5.50
5.00
4.50
4.00
3.50
3.00
2.50
2.00
1.50
1.00
0.50
0.00
304
308
310
312
316
318
320
322
326
328
332
1600a
1600b
1606
1608

FIG. 16

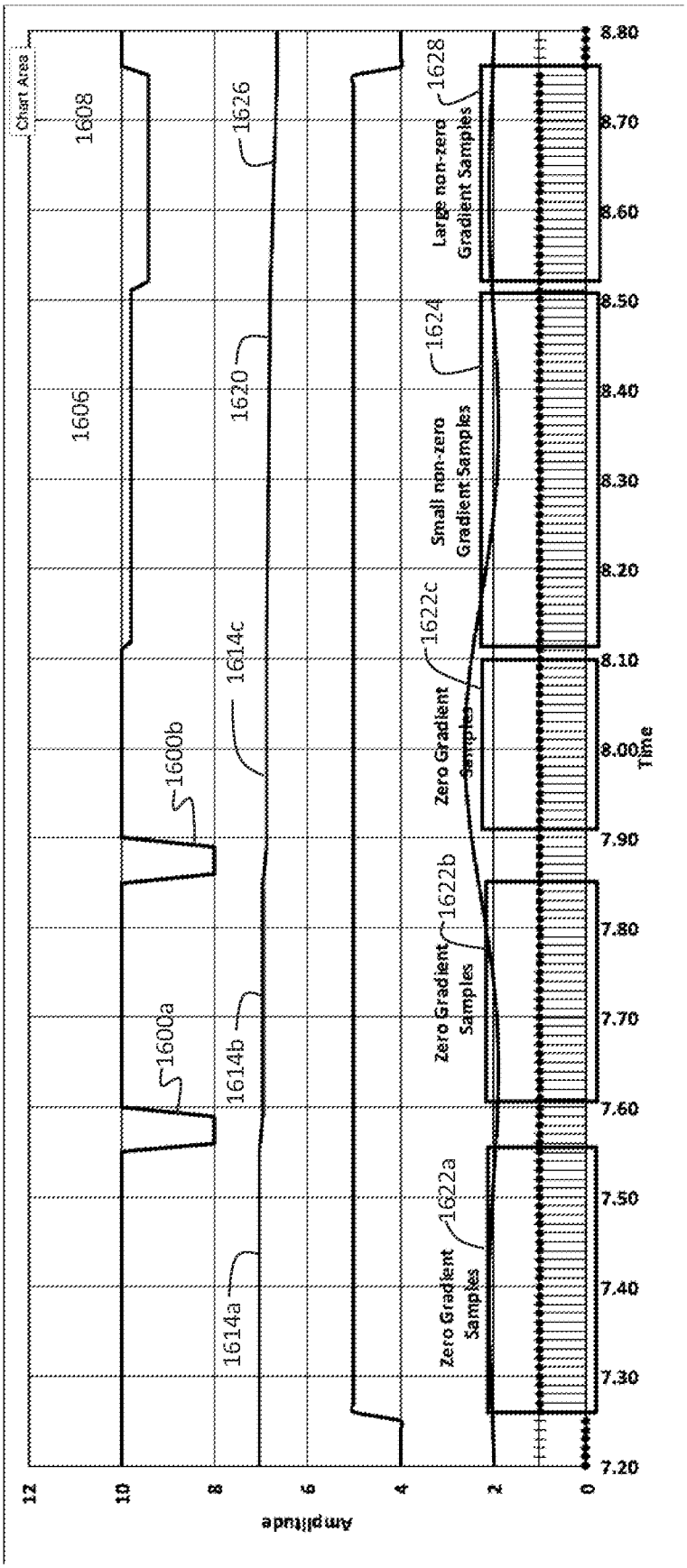
Chart Area
1608
1626
1606
1620
1628
Large non-zero Gradient Samples
1624
Small non-zero Gradient Samples
1622c
Zero Gradient Samples
1622b
Zero Gradient Samples
1622a
Zero Gradient Samples
1600b
1614c
1600a
1614b
1614a
Amplitude
Time
12
10
8
6
4
2
0
8.80
8.70
8.60
8.50
8.40
8.30
8.20
8.10
8.00
7.90
7.80
7.70
7.60
7.50
7.40
7.30
7.20

FIG. 17

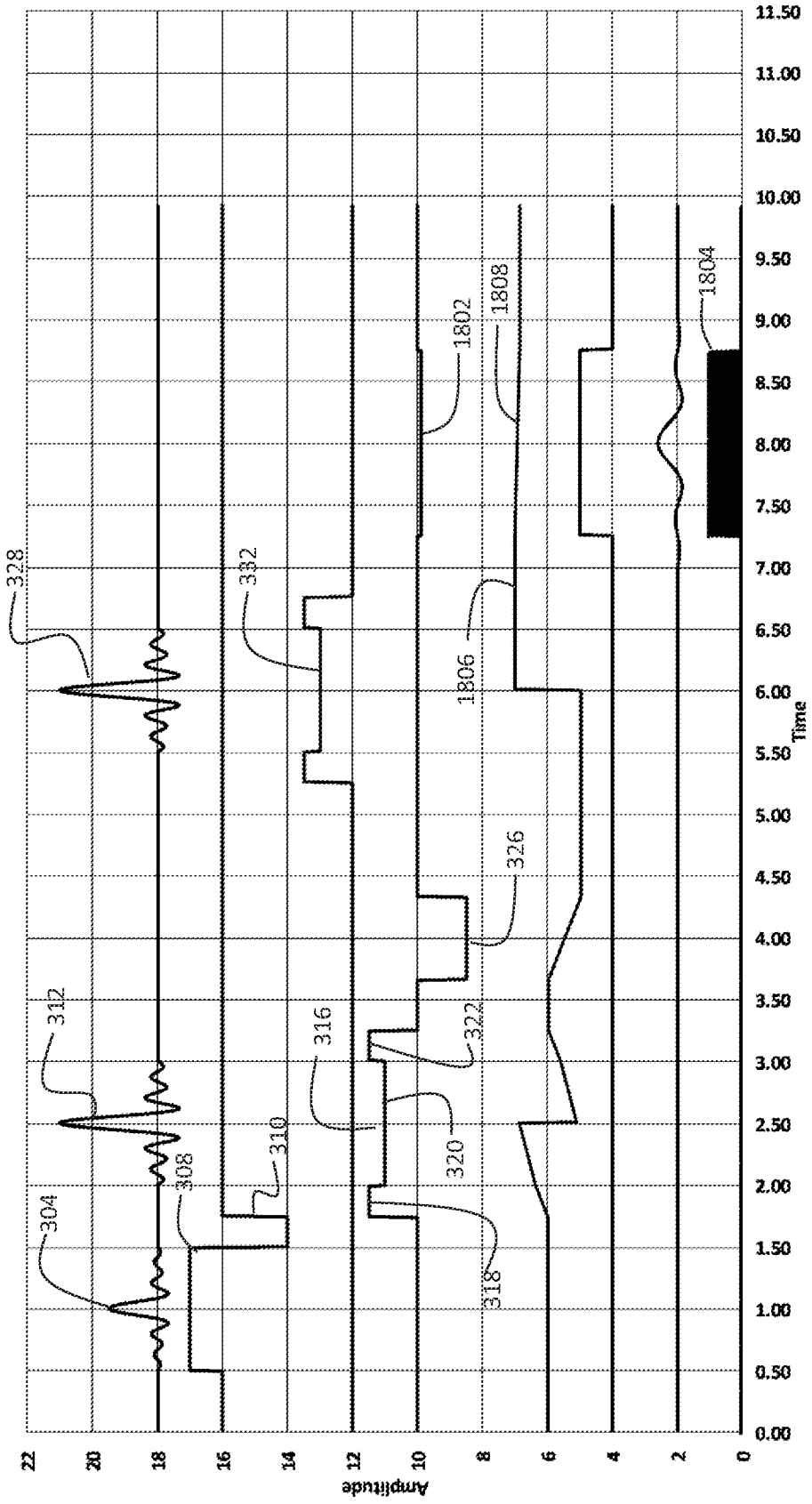
328
312
304
308
310
332
316
322
320
318
326
1806
1802
1808
1804
Amplitude
Time
22
20
18
16
14
12
10
8
6
4
2
0
11.50
11.00
10.50
10.00
9.50
9.00
8.50
8.00
7.50
7.00
6.50
6.00
5.50
5.00
4.50
4.00
3.50
3.00
2.50
2.00
1.50
1.00
0.50
0.00

FIG. 18

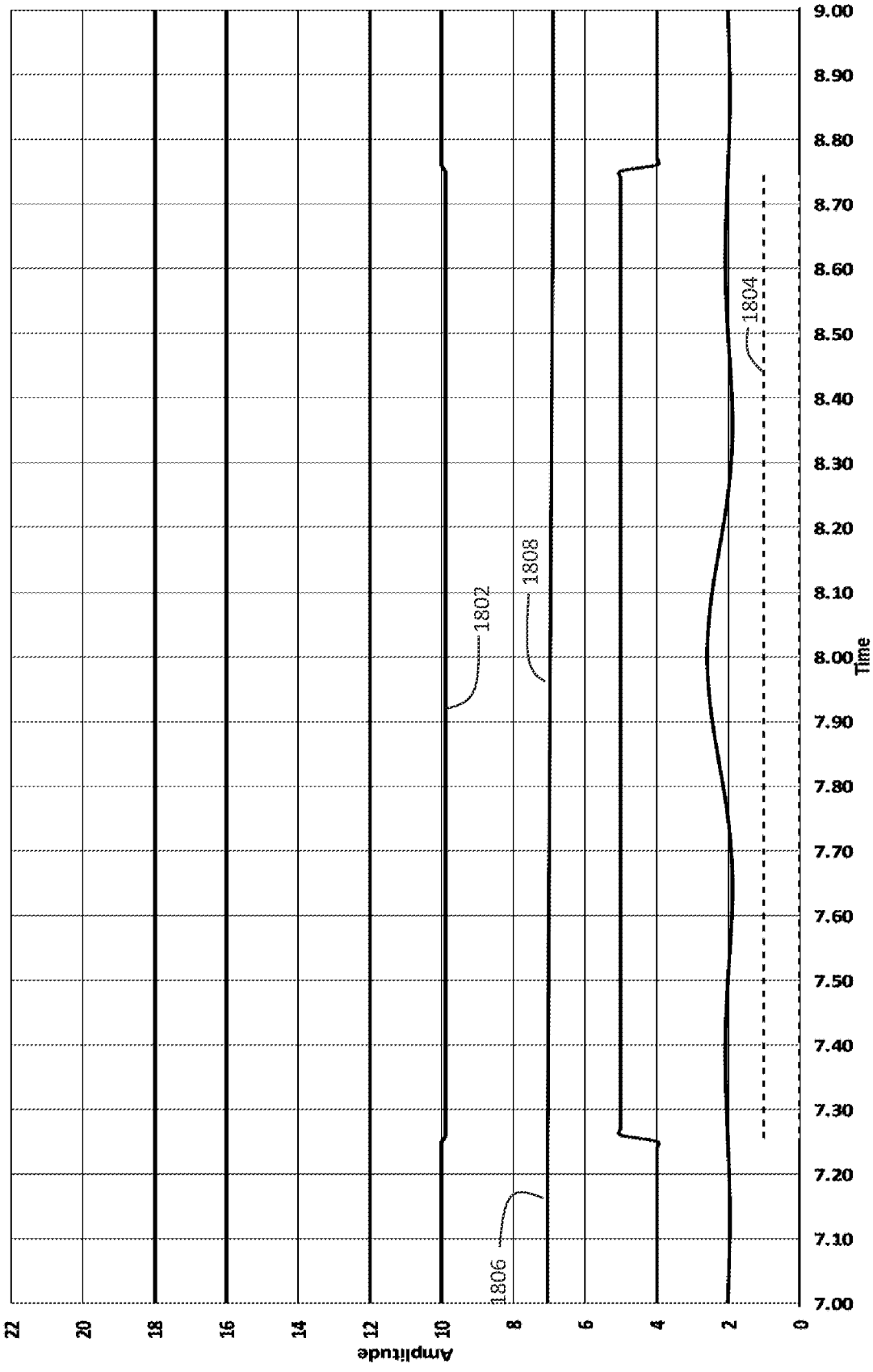
Amplitude
22
20
18
16
14
12
10
8
6
4
2
0
Time
9.00
8.90
8.80
8.70
8.60
8.50
8.40
8.30
8.20
8.10
8.00
7.90
7.80
7.70
7.60
7.50
7.40
7.30
7.20
7.10
7.00
1802
1804
1806
1808

FIG. 19

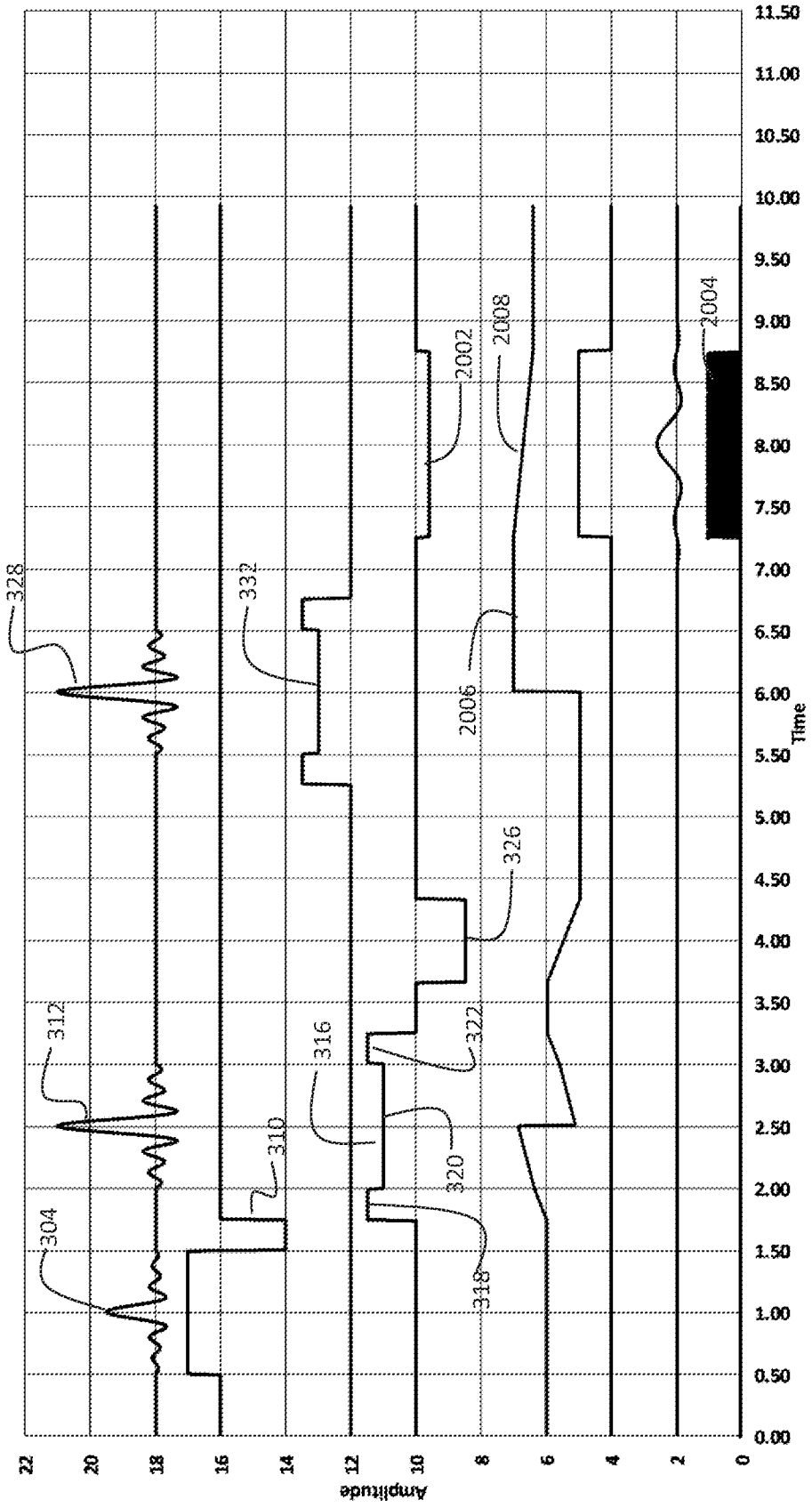
Amplitude
Time
22
20
18
16
14
12
10
8
6
4
2
0
11.50
11.00
10.50
10.00
9.50
9.00
8.50
8.00
7.50
7.00
6.50
6.00
5.50
5.00
4.50
4.00
3.50
3.00
2.50
2.00
1.50
1.00
0.50
0.00
328
332
2002
2008
2004
2006
326
312
316
322
310
320
304
318

FIG. 20

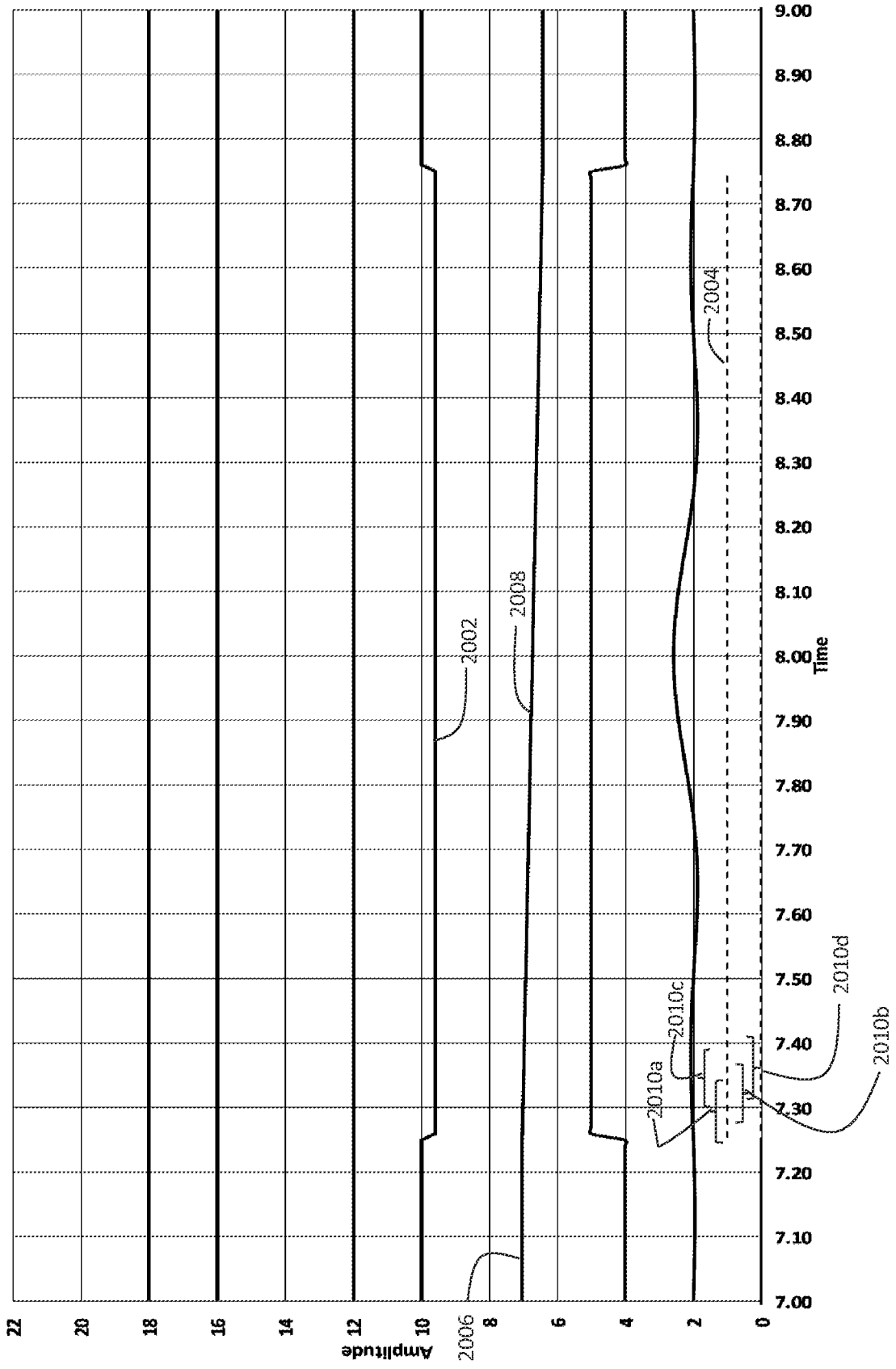
9.00
8.90
8.80
8.70
8.60
8.50
8.40
8.30
8.20
8.10
8.00
7.90
7.80
7.70
7.60
7.50
7.40
7.30
7.20
7.10
7.00
Time
22
20
18
16
14
12
10
8
6
4
2
0
Amplitude
2002
2004
2006
2008
2010a
2010b
2010c
2010d

FIG. 21

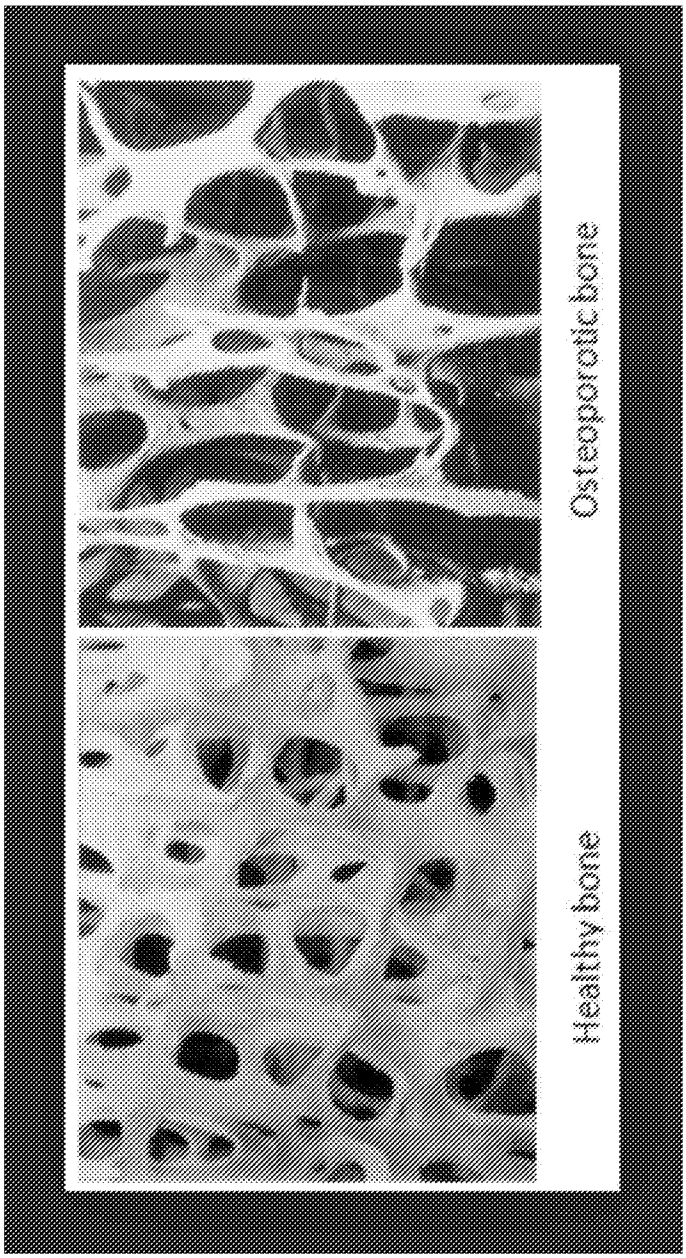

FIG. 22A

FIG. 22B

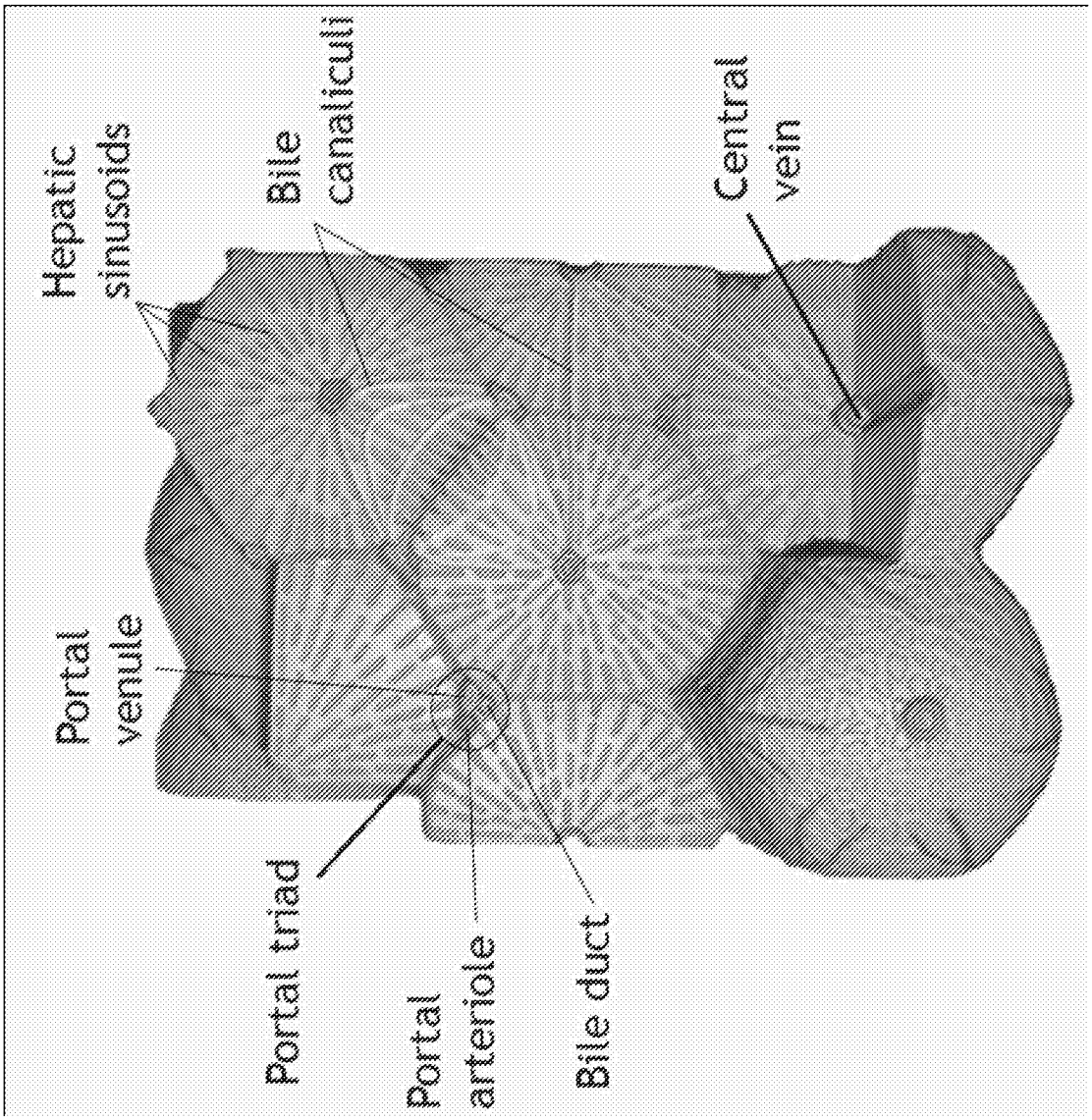
Hepatic sinusoids
Bile canaliculi
Central vein
Portal venule
Portal triad
Portal arteriole
Bile duct

FIG. 23

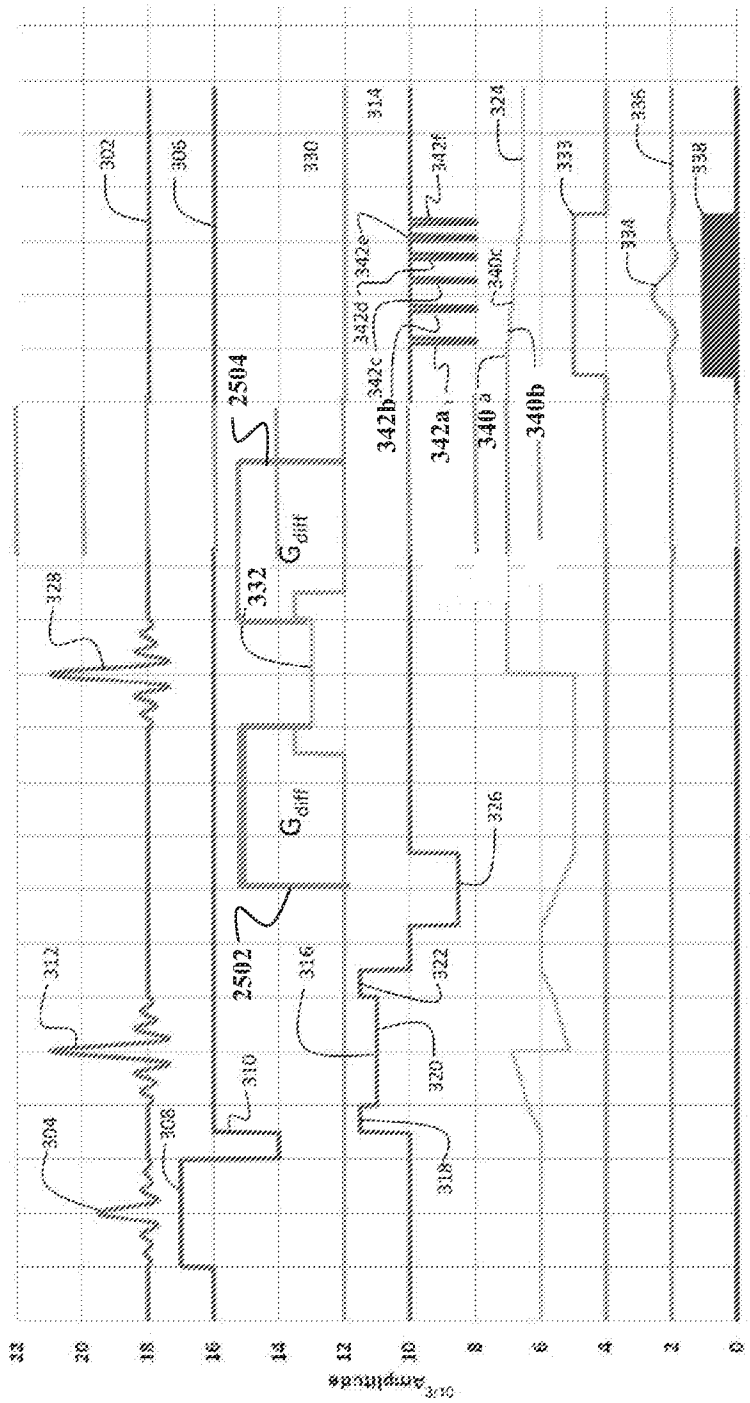
time
2502
2504
G_{diff}
G_{diff}
332
342a
342b
340a
340b
302
304
306
308
310
312
314
316
318
320
322
324
326
328
330
333
334
336
338
342c
342d
342e
342f
340c

FIG. 24

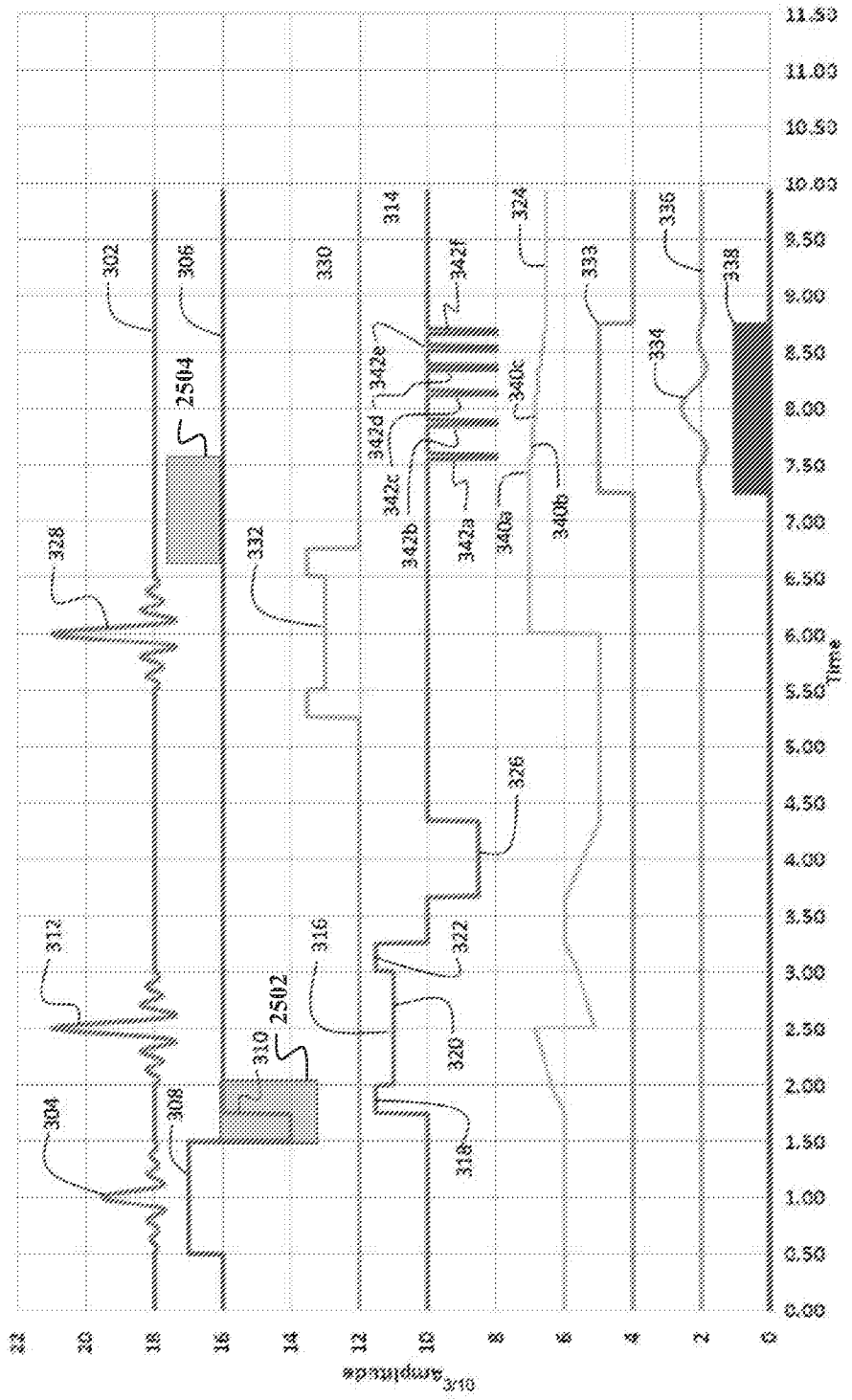
Time
Amplitude
11.50
11.00
10.50
10.00
9.50
9.00
8.50
8.00
7.50
7.00
6.50
6.00
5.50
5.00
4.50
4.00
3.50
3.00
2.50
2.00
1.50
1.00
0.50
0.00
22
20
18
16
14
12
10
8
6
4
2
0
302
304
306
308
310
312
314
316
318
320
322
324
326
328
330
332
333
334
335
336
338
340a
340b
340c
342a
342b
342c
342d
342e
342f
2502
2504

FIG. 25

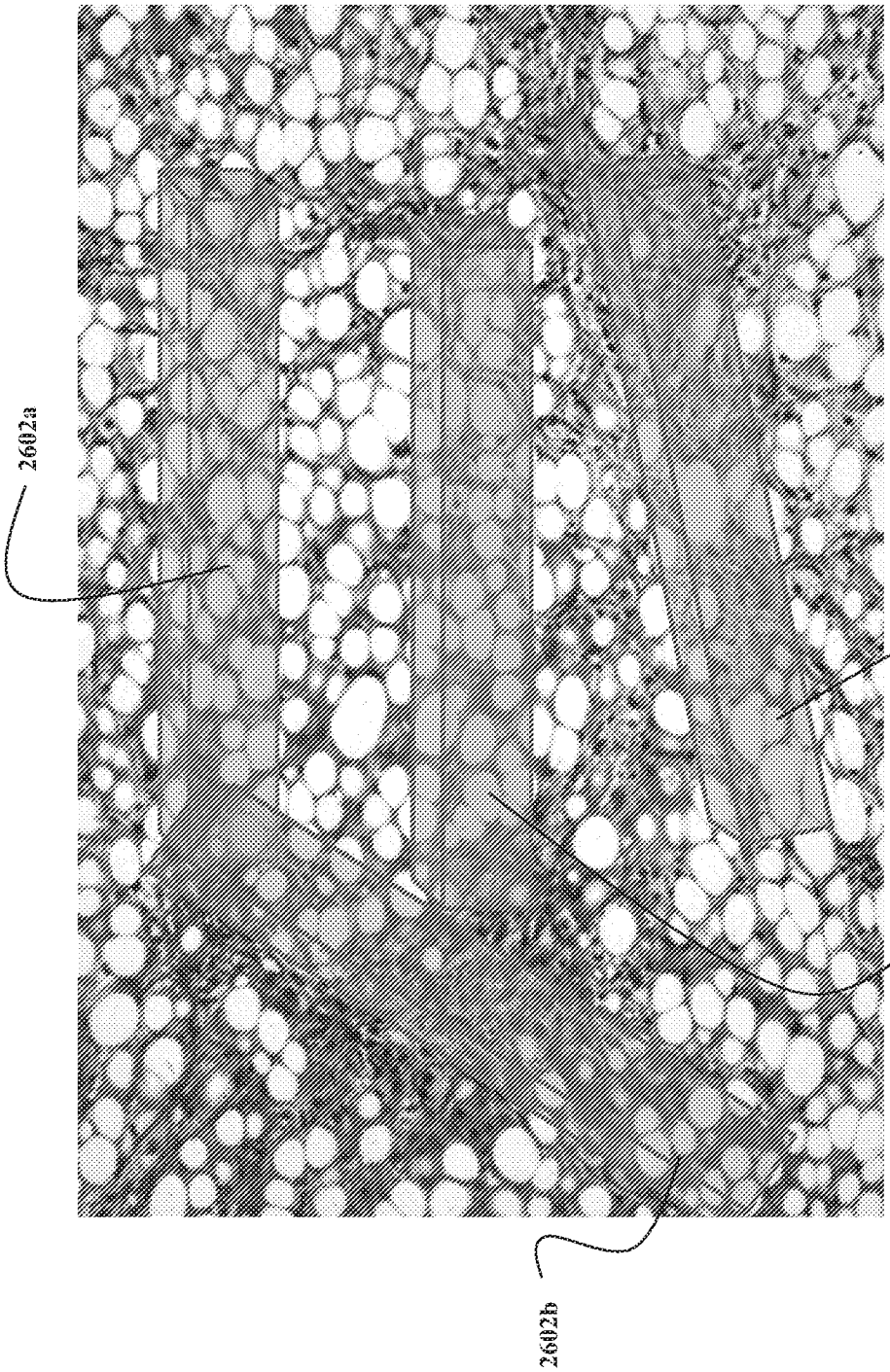

FIG. 26

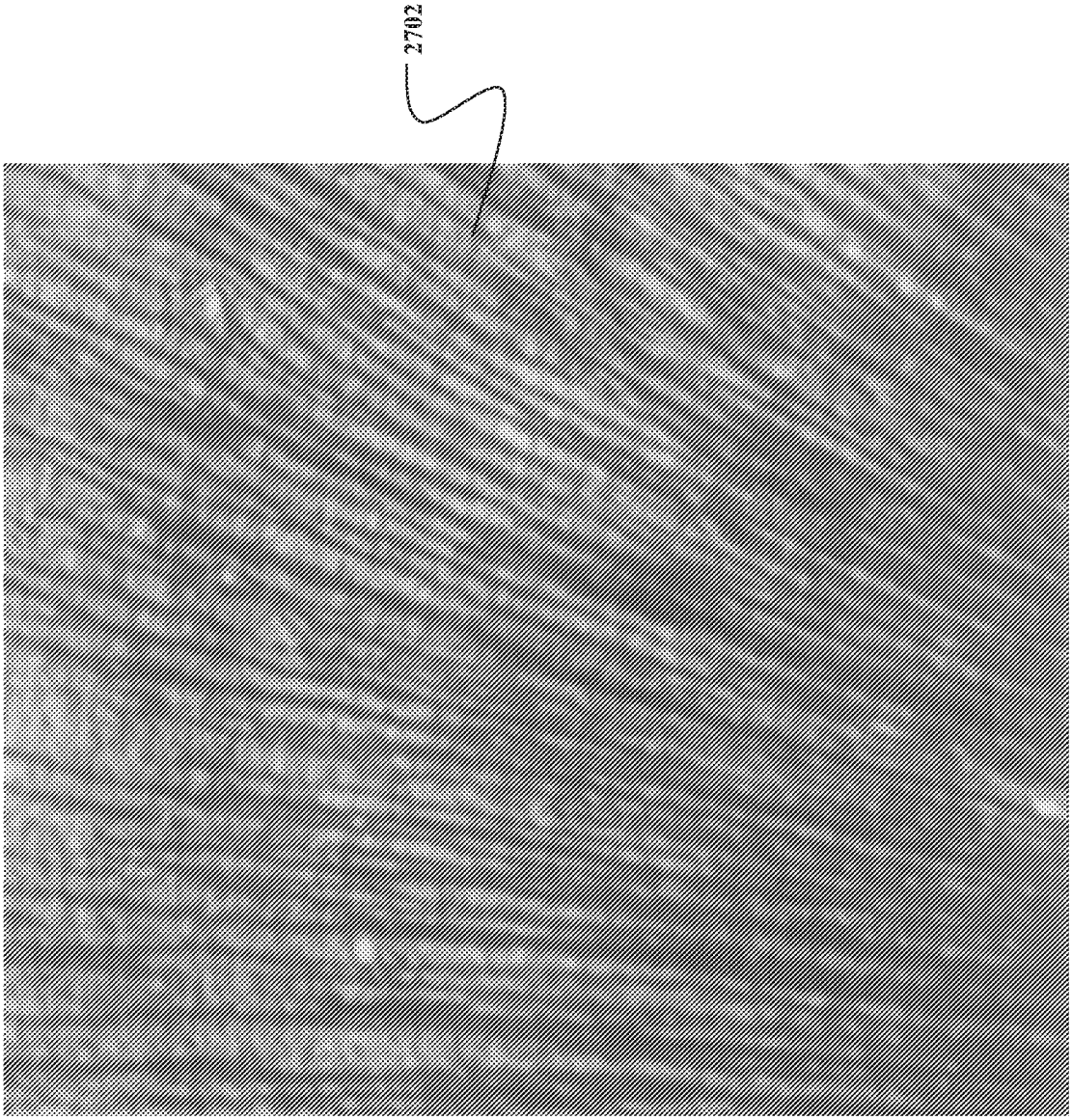

FIG. 27

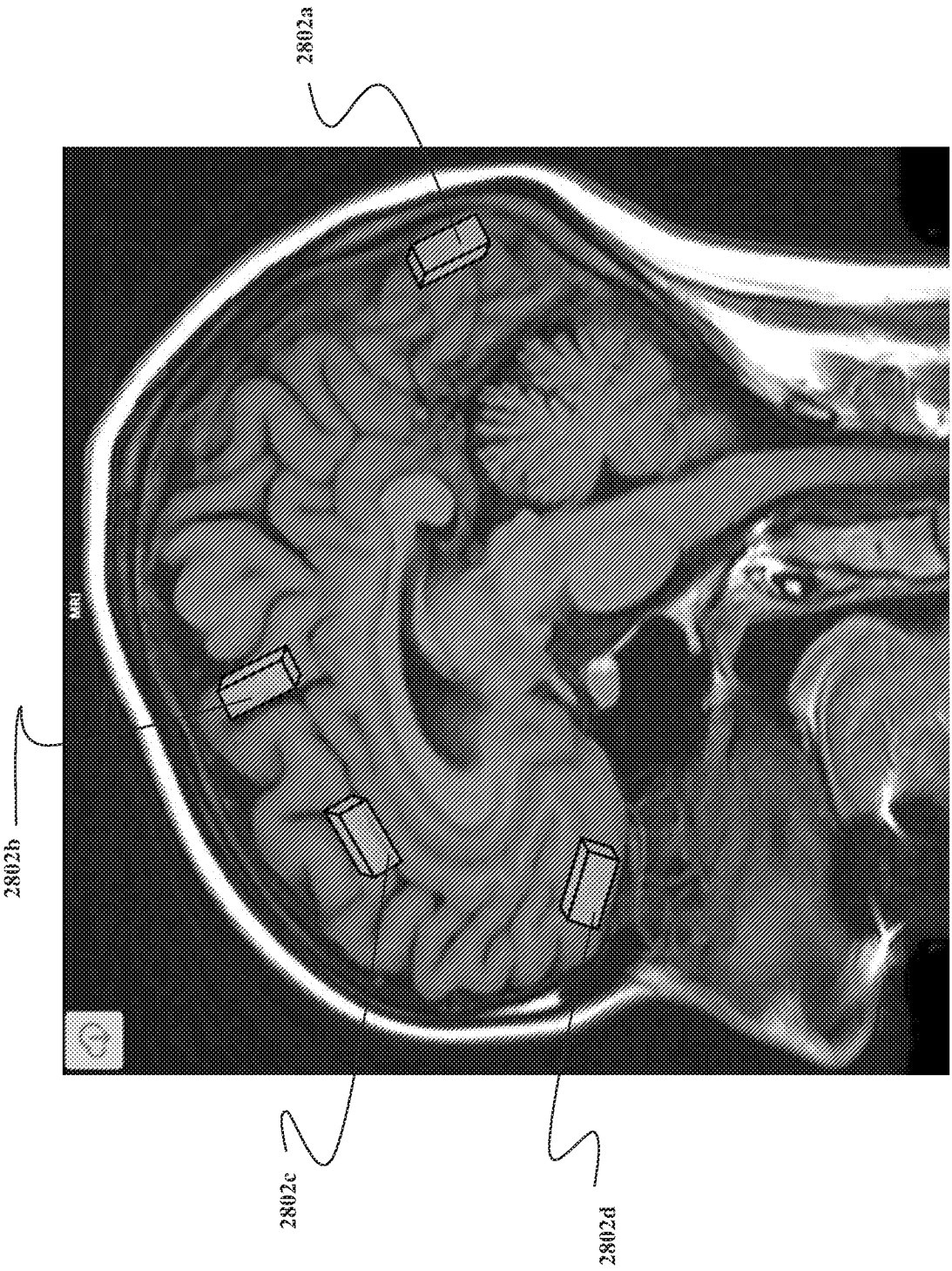

FIG. 28

FIG. 29A

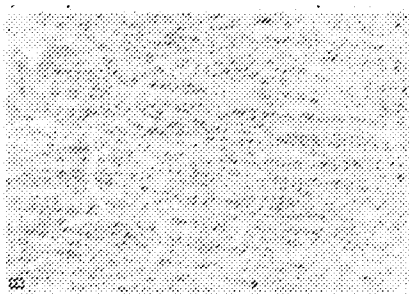

FIG. 29B

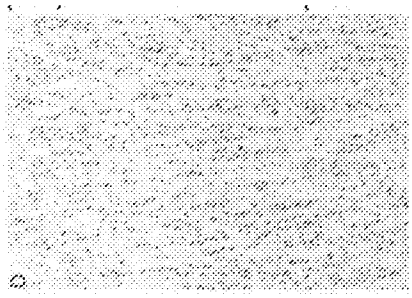

FIG. 29C

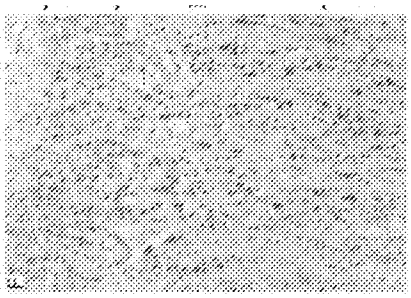

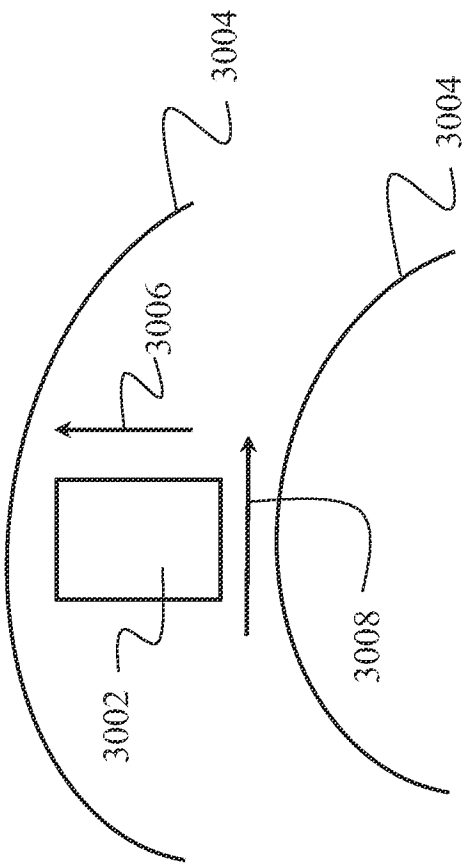

FIG. 30